DEVELOPMENT AND OPTIMIZATION OF NANOPARTICLE BASED FORMULATION(S) OF NATURALLY OCCURRING SMALL MOLECULE(S) TO GLORIFY THERAPEUTIC EFFICACY

Thesis submitted
by
PRATIK CHAKRABORTY

Doctor of Philosophy (Pharmacy)

Department of Pharmaceutical Technology
Faculty Council of Engineering & Technology
Jadavpur University
Kolkata, India
2025

JADAVPUR UNIVERSITY

KOLKATA 700032

WEST BENGAL, INDIA

INDEX NO: 292/20/Ph
REGISTRATION NO: 1022013002

1. Title of the thesis:

Development and optimization of nanoparticle based formulation(s) of naturally occurring small molecule(s) to glorify therapeutic efficacy.

2. Name, Designation & Institution of the supervisor:

Dr. Saikat Dewanjee
Professor
Department of Pharmaceutical Technology
Jadavpur University
188, Raja S C Mallick Road, Kolkata 700032
West Bengal, India.
Tel.: +91-33-2457-2043, E mail: saikat.dewanjee@jadavpuruniversity.in

3. List of Publications:

A. Related to the thesis work (1)

i. Chakraborty P, Das A, Chatterjee S, Bairagi A, Bhattacharya H, Bhattacharyya C, Chatterjee N, Sil PC, Dewanjee S. Formulation and evaluation of polymeric nanoparticles to improve in vivo chemotherapeutic efficacy of mangiferin against breast cancer. Naunyn Schmiedebergs Arch Pharmacol. 2025. doi: 10.1007/s00210-025-04068-0.. (**Impact factor: 3.1**).

B. Other publications obtained during the period of doctoral research (20)

i. Zuo T, Dewanjee S, Zhang C, **Chakraborty P**, Lu W, Jha NK, Bhattacharya H, Gangopadhyay M, Fleishman J, Jha SK, Chen J-S. Biopiezoelectric-based nanomaterials; a promising strategy in cancer therapy. J Exp Clin Cancer Res. 2025 Accepted. [**Impact factor: 11.4**].

ii. Dewanjee S, Bhattacharya H, Bhattacharyya C, **Chakraborty P**, Fleishman J, Alexiou A, Papadakis M, Jha SK. Nrf2/Keap1/ARE regulation by plant secondary metabolites: a new horizon in brain tumor management. Cell Commun Signal. 2024;22(1):497. doi: 10.1186/s12964-024-01878-2. (**Impact factor: 8.2**).

iii. **Chakraborty P**, Dewanjee S. Unrevealing the mechanisms behind the cardioprotective effect of wheat polyphenolics. Arch Toxicol. 2024;98(11):3543-3567. doi: 10.1007/s00204-024-03850-y.. (**Impact factor: 4.8**).

iv. Chatterjee S*, **Chakraborty P***, Dutta S, Karak S, Mahalanobis S, Ghosh N, Dewanjee S, Sil PC. Formulation of Carnosic-Acid-Loaded Polymeric Nanoparticles: An Attempt to Endorse the Bioavailability and Anticancer Efficacy of Carnosic Acid against Triple-Negative Breast Cancer. ACS Appl Bio Mater. 2024;7(3):1656-1670. doi: 10.1021/acsabm.3c01087. (**Impact factor: 4.6**).

v.Zhang C, Qin C, Dewanjee S, Bhattacharya H, **Chakraborty P**, Jha NK, Gangopadhyay M, Jha SK, Liu Q. Tumor-derived small extracellular vesicles in cancer invasion and metastasis: molecular mechanisms, and clinical significance. Mol Cancer. 2024;23(1):18. doi: 10.1186/s12943-024-01932-0. (**Impact factor: 27.7**).

vi. Chakraborty P, Bhattacharyya C, Sahu R, Dua TK, Kandimalla R, Dewanjee S. Polymeric nanotherapeutics: An emerging therapeutic approach for the management of neurodegenerative disorders. J Drug Deliv Sci Technol. 2023:105267. doi: 10.1016/j.jddst.2023.105267. (**Impact factor: 4.5**).

vii. Paul P, Chacko L, Dua TK, **Chakraborty P**, Paul U, Phulchand VV, Jha NK, Jha SK, Kandimalla R, Dewanjee S. Nanomedicines for the management of diabetic nephropathy: present progress and prospects. Front Endocrinol (Lausanne). 2023;14:1236686. doi: 10.3389/fendo.2023.1236686. (**Impact factor: 3.9**).

viii. Huang Z, Dewanjee S, **Chakraborty P**, Jha NK, Dey A, Gangopadhyay M, Chen XY, Wang J, Jha SK. CAR T cells: engineered immune cells to treat brain cancers and beyond. Mol Cancer. 2023;22(1):22. doi: 10.1186/s12943-022-01712-8. (**Impact factor: 27.7**).

ix. Chakraborty P, Dey A, Gopalakrishnan AV, Swati K, Ojha S, Prakash A, Kumar D, Ambasta RK, Jha NK, Jha SK, Dewanjee S. Glutamatergic neurotransmission: A potential pharmacotherapeutic target for the treatment of cognitive disorders. Ageing Res Rev. 2023;85:101838. doi: 10.1016/j.arr.2022.101838. (**Impact factor: 12.5**).

x.Yadav P*, **Chakraborty P**, Jha NK, Dewanjee S, Jha AK, Panda SP, Mishra PC, Dey A, Jha SK. Molecular Mechanism and Role of Japanese Encephalitis Virus Infection in Central Nervous System-Mediated Diseases. Viruses. 2022;14(12):2686. doi: 10.3390/v14122686. (**Impact factor: 3.8**).

xi. Agrawal K*, **Chakraborty P**, Dewanjee S, Arfin S, Das SS, Dey A, Moustafa M, Mishra PC, Jafari SM, Jha NK, Jha SK, Kumar D. Neuropharmacological interventions of quercetin and its derivatives in neurological and psychological disorders. Neurosci Biobehav Rev. 2022;144:104955. doi: 10.1016/j.neubiorev.2022.104955. (**Impact factor: 12.5**).

xii. Dewanjee S*, **Chakraborty P***, Bhattacharya H, Kumar Singh S, Dua K, Dey A, Kumar Jha N. Recent advances in flavonoid-based nanocarriers as an emerging drug delivery approach for cancer chemotherapy. Drug Discov Today. 2022:103409. doi: 10.1016/j.drudis.2022.103409. (**Impact factor: 6.5**).

xiii. Dewanjee S, **Chakraborty P**, Bhattacharya H, Chacko L, Singh B, Chaudhary A, Javvaji K, Pradhan SR, Vallamkondu J, Dey A, Kalra RS, Jha NK, Jha SK, Reddy PH, Kandimalla R. Altered glucose metabolism in Alzheimer's disease: Role of mitochondrial dysfunction and oxidative stress. Free Radic Biol Med. 2022:S0891-5849(22)00622-0. doi: 10.1016/j.freeradbiomed.2022.09.032. (**Impact factor: 7.1**).

xiv. Chakraborty P, Das SS, Dey A, Chakraborty A, Bhattacharyya C, Kandimalla R, Mukherjee B, Gopalakrishnan AV, Singh SK, Kant S, Nand P, Ojha S, Kumar P, Jha NK, Jha SK, Dewanjee S. Quantum dots: The cutting-edge nanotheranostics in brain cancer management. J Control Release. 2022;350:698-715. doi: 10.1016/j.jconrel.2022.08.047. (**Impact factor: 10.5**).

xv. Dutta S, **Chakraborty P***, Basak S*, Ghosh S*, Ghosh N*, Chatterjee S, Dewanjee S, Sil PC. Synthesis, characterization, and evaluation of in vitro cytotoxicity and in vivo antitumor activity of asiatic acid-loaded poly lactic-co-glycolic acid nanoparticles: A strategy of treating breast cancer. Life Sci. 2022;307:120876. doi: 10.1016/j.lfs.2022.120876. (**Impact factor: 5.2**).

xvi. Manna P, Dewanjee S, Joardar S, **Chakraborty P**, Bhattacharya H, Bhanja S, Bhattacharyya C, Bhowmik M, Bhowmick S, Saha A, Das J, Sil PC. Carnosic acid attenuates doxorubicin-induced cardiotoxicity by decreasing oxidative stress and its concomitant pathological consequences. Food Chem Toxicol. 2022;166:113205. doi: 10.1016/j.fct.2022.113205. (**Impact factor: 3.9**).

xvii. Kandimalla R*, **Chakraborty P***, Vallamkondu J, Chaudhary A, Samanta S, Reddy PH, De Feo V, Dewanjee S. Counting on COVID-19 Vaccine: Insights into the Current Strategies, Progress and Future Challenges. Biomedicines. 2021;9(11):1740. doi: 10.3390/biomedicines9111740. (**Impact factor: 3.9**).

xviii. Ogunmokun G, Dewanjee S, **Chakraborty P**, Valupadas C, Chaudhary A, Kolli V, Anand U, Vallamkondu J, Goel P, Paluru HPR, Gill KD, Reddy PH, De Feo V, Kandimalla R.

The Potential Role of Cytokines and Growth Factors in the Pathogenesis of Alzheimer's Disease. Cells. 2021;10(10):2790. doi: 10.3390/cells10102790. (**Impact factor: 5.1**).

xix. Dewanjee S, Vallamkondu J, Kalra RS, **Chakraborty P**, Gangopadhyay M, Sahu R, Medala V, John A, Reddy PH, De Feo V, Kandimalla R. The Emerging Role of HDACs: Pathology and Therapeutic Targets in Diabetes Mellitus. Cells. 2021;10(6):1340. doi: 10.3390/cells10061340. (**Impact factor: 5.1**).

xx. Dewanjee S, **Chakraborty P**, Mukherjee B, De Feo V. Plant-Based Antidiabetic Nanoformulations: The Emerging Paradigm for Effective Therapy. Int J Mol Sci. 2020;21(6):2217. doi: 10.3390/ijms21062217. (**Impact factor: 4.9**).

C. Book chapters (4):

i. Dewanjee S*, **Chakraborty P***, Dey A, Bhattacharya H, Bhattacharyya C, Sanyal R, Bhowmik M. Plant polysaccharides for colon-targeting drug delivery. In: Plant Polysaccharides as Pharmaceutical Excipients. Nayak A, Hasnain MS, Pal D (Eds). Elsevier, Netherland. 2022. 1st edition, Chapter 14; *pp.* 329-368. doi: 10.1016/B978-0-323-90780-4.00012-7.

ii. Dewanjee S, Zia-Ul-Haq M, Sarkhel S, **Chakraborty P**. Carotenoids as antiparkinson agent. In: Carotenoids: Structure and Function in the Human Body. M. Zia-Ul-Haq, S. Dewanjee, M. Riaz. (Eds.). Springer, 2021. Chapter 15; *pp.* 533-554. doi: 10.1007/978-3-030-46459-2_15.

iii. Dewanjee S**,** Das S, Joardar S, Bhattacharjee S, **Chakraborty P**. Carotenoids as anticancer agents. In: Carotenoids: Structure and Function in the Human Body. M. Zia-Ul-Haq, S. Dewanjee, M. Riaz. (Eds.). Springer, 2021. Chapter 13; *pp.* 475-512. doi: 10.1007/978-3-030-46459-2_13.

iv. Dewanjee S, Bhattacharjee N, **Chakraborty P**, Bhattacharjee S. Carotenoids as antioxidants. In: Carotenoids: Structure and Function in the Human Body. M. Zia-Ul-Haq, S. Dewanjee, M. Riaz. (Eds.). Springer, 2021. Chapter 12; *pp.* 447-474. doi: 10.1007/978-3-030-46459-2_12.

* Equal contributors

4. List of patents: Nil

5. List of presentations in national/international seminar/conferences: (3)

i. Chakraborty P, Dewanjee S. Formulation of Polymeric Nanoparticles with Nature-derived Small Molecule Improves Therapeutic Efficacy against Breast Cancer. 8th International Conference on Recent Advances in Science, Invertis University, Bareilly, India, March 2024.

ii. Chakraborty P, Bhattacharya H, Dewanjee S. Polymeric Nanoformulation Loaded with Natural Polyphenol Shows Promise against Hepatocellular Carcinoma. 2nd International Conference on Healthy Ageing & Research, Association of Pharmaceutical Scientists and Educators, Mysuru, India, March 2022.

iii. Chakraborty P, Bhattacharya H, Dewanjee S. Formulation and characterization of nano-carrier based delivery system with mangiferin, an attempt to glorify its therapeutic usefulness. 2nd International Conference on Transforming Ripples in Healthcare Research: Obstacle, Sustenance & Cutting Edge Innovations, Adamas Universiy, Kolkata, India, February 2022.

STATEMENT OF ORIGINALITY

I, **Pratik Chakraborty** registered on **24 January 2020** do hereby declare that this thesis entitled "**Development and optimization of nanoparticle based formulation(s) of naturally occurring small molecule(s) to glorify therapeutic efficacy**" contains literature survey and original research work done by the undersigned candidate as part of Doctoral studies.

All information in this thesis have been obtained and presented in accordance with existing academic rules and ethical conduct. I declare that, as required by these rules and conduct, I have fully cited and referred all materials and results that are not original to this work. I also declare that I have checked this thesis as per the "Policy on Anti Plagiarism, Jadavpur University, 2019", and the level of similarity as checked by iThenticate software is **4%** (checked on 21 May 2025).

Pratik Chakraborty

(Pratik Chakraborty)

Certified by Supervisor

Saikat Dewanjee

(Dr. Saikat Dewanjee)
Professor
Department of Pharmaceutical Technology
Jadavpur University
Kolkata, India

Prof. Saikat Dewanjee
Dept. of Pharmaceutical Technology
Jadavpur University
Kolkata - 700 032

CERTIFICATE FROM THE SUPERVISOR

This is to certify that the thesis entitled "**Development and optimization of nanoparticle based formulation(s) of naturally occurring small molecule(s) to glorify therapeutic efficacy**" submitted by **Shri. Pratik Chakraborty** who got his name registered on **24 January 2020** for the award of **Ph.D. (Pharmacy)** degree of Jadavpur University is absolutely based upon his own work under the supervision of **Prof. Saikat Dewanjee** and that neither his thesis nor any part of the thesis has been submitted for any degree/diploma or any other academic award anywhere before.

Saikat Dewanjee

.....

(Dr. Saikat Dewanjee)
Professor
Department of Pharmaceutical Technology
Jadavpur University
Kolkata, India

Prof. Saikat Dewanjee
Dept. of Pharmaceutical Technology
Jadavpur University
Kolkata - 700 032

Acknowledgements

Standing on the verge of accomplishing my Ph.D. curriculum, it is high time to acknowledge those persons of help to complete this huge task. I am not only delighted but also grateful to place on record the co-operation of those who not only helped me to complete this work but also kept me motivated throughout this journey. I would like to express my appreciation for all the efforts, of every individual who have directly or indirectly contributed their ideas and suggestions for the successful completion of this grand task.

First, I would wish to express my sincere gratitude to my supervisor, ***Prof. Saikat Dewanjee****, Department of Pharmaceutical Technology, Jadavpur University, Kolkata 700032, India, for his insightful and compassionate guidance, for shaping my career, giving directions to my dreams, and achieving them. It was a privilege for me to share the same workplace with him.*

I sincerely acknowledge the ***Council of Scientific & Industrial Research,*** *New Delhi, India, and* ***State Government Research Fellowship Scheme*** *of Jadavpur University, Kolkata, India for financial support (reference no. R-11/327/19 dated 18.03.2019 and R-11/13/20 dated 22.01.2020, respectively) through the Senior Research Fellowships to pursue research work.*

I am extremely thankful to the authorities of ***Jadavpur University,*** *Kolkata, India for providing the necessary facilities for the research work. It has been a fantastic experience working at Jadavpur University.*

I also express my profound gratitude towards ***Prof. Parames C. Sil,*** *Bose Institute, Kolkata, India and* ***Dr. Nabanita Chatterjee****, Chittaranjan National Cancer Institute, Kolkata, India for their cooperation during my research work.*

I would like to convey my forlorn mind for the soul of innocent experimental animals. Without their immolation, it would have been impossible to accomplish this research work.

I take this opportunity to convey my thanks to all of my ***labmates****, especially to* ***Dr. Swarnalata Joardar, Mr. Hiranmoy Bhattacharya, and Mr. Chiranjib Bhattacharyya*** *who always extended their hands for help whenever I needed. It has been a pleasure working alongside them through the ups and downs of the research journey.*

I would like to acknowlwdge the staff-members of ***School of Pharmacy, Techno India University, West Bengal****, India for their support.*

It would be unfair if I do not mention ***Dr. Rajesh Banik, Dr. Ashique Al-Haque, Dr. Sk Abdul Amin, Dr. Pratik Adhya, Dr. Chandan Kumar Malik, Dr. Sandipan Paul, Dr. Paramita Paul, Dr. Sanjit Kumar Roy, Mr. Anuran Bhattacharya, Mr. Saswata Banerjee, and Ms. Sharmistha Chatterjee*** *whose constant support helped me to stay motivated.*

*I would like to express my profound gratitude towards my **family members and well-wishers** who kept their calm and always inspired me for betterment. Without their support, it would not have been possible to reach at this juncture.*

*Finally, I am grateful to the **Almighty**, for blessings without which this journey could not have been possible, and for this beautiful gift called life.*

Pratik Chakraborty

*(**Pratik** Chakraborty)*

Place: Jadavpur, Kolkata.

Date:

29.05.25

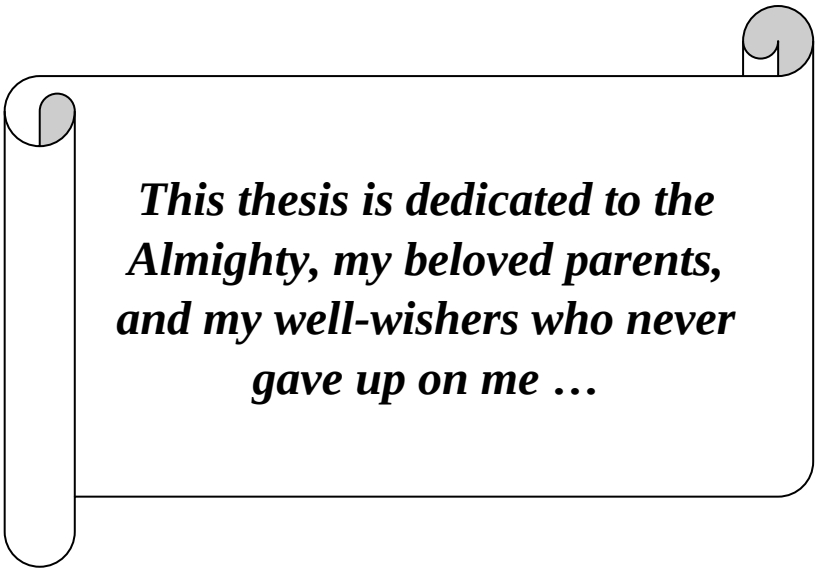
This thesis is dedicated to the Almighty, my beloved parents, and my well-wishers who never gave up on me …

Preface

Cancer is one of the most fatal diseases worldwide, and the incidence of new cancer cases is increasing alarmingly. Chemotherapy is a classical perioperative therapeutic strategy to deliver drugs for destroying cancer cells. However, non-selective toxicity is a serious concern in chemotherapy. Several clinically useful chemotherapeutic agents exhibit profound organ toxicity that compromises the perioperative care of patients with cancer, with life-threatening results. Many nature-derived small molecules exhibit promising results in killing cancer cells. Conversely, the in vitro promise fails to match their in vivo activity profiles owing to poor pharmacokinetics and biopharmaceutical attributes. Poor solubility in aqueous media, fast and extensive metabolism and poor systemic absorption are prime factors to limit their therapeutic effectiveness. Thus, formulating them with nanoscale delivery systems might potentially be a promising attribute to overcome the pharmaceutical incompatibility and maximize their therapeutic effects in biological systems. Polymeric nanoparticles, with their easy moldability, low toxicity, acceptable tissue penetrability, and sustained release effect, have emerged as one of the desirable tools in cancer therapeutics. Further, specifically engineered nanoplatforms enable delivery of cargo to a specific target site to attain maximum chemotherapeutic effects with negligible off-target toxicity. PLGA-based nanoparticles can extravasate through tumor vasculature by the enhanced permeability and retention (EPR) effect. They can even be decorated by ligand attachment via surface modifications for site-specific delivery. The approach practically integrates bioactive moieties on the surface of polymeric nanoparticles to allow target-specific, favorable biological interactions.

Breast cancer and liver cancer are considered among the most common cancer types worldwide. Interestingly, mangiferin, a naturally derived polyphenol, shows promise to act against breast cancer cells. On the contrary, it suffers from poor biopharmaceutical attributes, affecting its clinical usefulness. Polymeric nanoparticles may potentially be utilized to improve the chemotherapeutic efficacy of naturally occurring polyphenolic molecules. Further, galactose-conjugation of the same bears promise to selectively target liver carcinoma by recognizing asialoglycoprotein receptors. This thesis comprises the following chapters:

Chapter 1 is the introductory section that deals with the anticancer promise and concerns of nature-derived small molecules. It also discusses the possibilities of

nanostructured carriers to potentially improve the chemotherapeutic potential of the same. Finally, this chapter outlines the objectives of the presented research.

Chapter 2 deals with an in-depth literature review of the selected molecule and polymer, i.e. mangiferin (Mgf) and poly lactic-co-glycolic acid (PLGA), along with the anticancer promise of polymeric nanoparticles via passive and active targeting.

Chapter 3 depicts the development of PLGA nanoparticles carrying Mgf and evaluates the efficacy of the same against breast cancer via substantial preclinical assays. Stable and sphere-shaped Mgf-loaded PLGA nanoshells (MNPs) were formulated using the nanoprecipitation technique. MNPs exhibited satisfactory drug loading and release profiles. The Mgf-loaded nanoformulation exhibited better cytotoxic potential against breast cancer cells compared to native Mgf, owing to its better penetrability into cancer cells. MNPs were also found to confer superior in vivo chemotherapeutic efficacy in breast cancer-bearing mice, evidenced by the reduction of tumor load. Moreover, MNPs did not confer systemic toxicity at levels of concern. To conclude, the current study pleads for MNPs as a safe and efficacious tool in the fight against breast cancer for future translations.

Chapter 4 deals with the development of galactose-tailored PLGA nanoparticles loaded with Mgf, for active liver targeting, and evaluates the efficacy against hepatocellular carcinoma employing appropriate in vitro and in vivo preclinical experiments. The emulsion solvent evaporation method yielded stable and sphere-shaped nanoparticles with satisfactory loading capacity. Nanoparticles prepared using native PLGA (MPNPs) and galactose-conjugated PLGA (MGNPs), both depicted sustained Mgf release following more or less similar manners. However, MGNPs exhibited better cytotoxic potential on hepatocellular carcinoma cells compared to free Mgf and MPNPs. The interaction of asialoglycoprotein receptors present on liver cells with the galactose moiety may be attributed to the same. Moreover, MGNPs imparted superior chemotherapeutic activity in a mouse model of hepatocellular carcinoma, evinced by better tumor suppression. In addition, they did not inflict systemic toxicity at levels of

concern. To summarize, the study utilizes nanoencapsulation to improve the chemotherapeutic efficacy of naturally derived small molecule. Further, it brings up galactose-tailoring of polymeric nanoparticles as an efficacious and safe strategy to fight hepatocellular carcinoma via active targeting.

Chapter 5 comprises the list of references.

List of Abbreviations

Abbreviations	Full forms
AFM	Atomic force microscope
ALP	Alkaline phosphatase
ALT	Alanine transaminase
AST	Aspartate aminotransferase
ANOVA	One-way analysis of variance
Apaf-1	Apoptotic protease-activating factor 1
Bad	Bcl2-associated agonist of cell death
BBB	Blood-brain barrier
Bcl2	B-cell lymphoma 2
BUN	Blood urea nitrogen
CAT	Catalase
CNS	Central nervous system
CYP3A4	Cytochrome P450 3A4
DAB	Diaminobenzidine
DENA	N-nitrosodiethylamine
DLS	Dynamic light scattering
DMSA	Dimercaptosuccinic acid
DMSO	Dimethyl sulfoxide
DSC	Differential scanning calorimetry
EAC	Ehrlich ascites carcinoma
EPR	Enhanced permeability and retention
FBS	Fetal bovine serum
FESEM	Field emission scanning electron microscope
FTIR	Fourier transform infrared
Gal PLGA	Galactosylated PLGA
GSH	Reduced glutathione
H&E	Hematoxylin and eosin
HIF	Hypoxia-inducible factor
HPLC	High performance liquid chromatography
HPMC	Hydroxy propyl methyl cellulose
IAEC	Institutional animal ethics committee

IC_{50}	Half maximal inhibitory concentration
IκBα	Nuclear factor-kappa B inhibitor alpha
Keap1	Kelch-like ECH-associated protein 1
Mgf	Mangiferin
MGNPs	Galactose-decorated PLGA nanoparticles carrying Mgf
MMP	Mitochondrial membrane potential
MNPs	Mgf-containing PLGA(L/G=50:50)-based nanoparticles
MPNPs	Mgf-loaded nanoparticles using plain PLGA (L/G=85:15)
MTT	3-[4,5-dimethylthiazol-2-yl]−2,5 diphenyl tetrazolium bromide
MW	Molecular weight
NF-κB	Nuclear factor kappa-light-chain-enhancer of activated B cells
NMR	Nuclear magnetic resonance
Nrf2	Nuclear factor erythroid 2-related factor 2
PBS	Phosphate-buffered saline
PDI	Polydispersity index
P-gp	P-glycoprotein
PI	Propidium iodide
PI3K	Phosphoinositide 3-kinase
PKC	Protein kinase C
PLGA	Poly(lactic-co-glycolic) acid
PVP	Polyvinyl pyrrolidone
RGD	Arginyl-glycyl-aspartic acid
ROS	Reactive oxygen species
RPMI	Roswell Park memorial institute
SD	Standard deviation
siRNA	Small interfering RNA
SOD	Superoxide dismutase
TEM	Transmission electron microscope
Vitamin E-TPGS	Vitamin E tocopheryl polyethylene glycol succinate
XRD	X-ray diffraction

Index

Figure Index

Enhanced permeability and retention; Mgf, Mangiferin. PLGA, Poly(lactic-co-glycolic) acid.

Table Index

Chapter 1

Introduction

1.1. Background

Human dreams and imagination often give rise to new avenues in science and technology. Nanotechnology was also born with such dreams, defined as the understanding and control of matter on nanoscale dimensions, whereby unique phenomena enable novel applications. Nanotechnology encompasses the design, characterization, production and application of structures, devices and systems by controlling shape and size at the nanometer range. Nanoscience is the study of phenomena and manipulation of atomic, molecular and macromolecular scales where properties differ significantly compared to larger scales.

Nanoscience and nanotechnology have progressed rapidly over the years, with the scope of diverse applications. The applications of nanotechnology encompass many fields, including biomedical and health sciences. In the field of medical science, nanosized formulations have demonstrated unprecedented success in drug delivery systems compared to conventional formulations, enhancing the efficacy of therapeutic agents by improving their biopharmaceutical attributes, pharmacokinetic profiles and target specificity (Ioele et al., 2022; Haripriyaa and Suthindhiran, 2023). The development of nanocarrier-based drug delivery systems exhibits promise in terms of effectiveness, stability, bioavailability, biodistribution and sustained release patterns. Combinations of nanocarriers with ligands make them more target-specific (Javia et al., 2021). A further advantage conferred by nanoparticles is the protection of entrapped agents against degradation (Pinto et al., 2022). The increased success of nanostructured drug delivery systems has gained the interest of researchers in developing novel formulations against different diseases. Nanoscience and nanotechnology refer to structures, technologies and systems that possess novel features and functionalities as a result of the arrangement of their constituting units on the nanometer scale (Bayda et al., 2019). The prefix 'nano' refers to 'dwarf' or ‘very little'. Therapeutic nanoparticles are an emerging field of research, as they can meet the criterion of appropriate bioavailability and site-specific activity. Researchers have developed several physicochemical methods for framing different types of nanoformulations that can be used to design a well-defined nanocarrier system. Table 1.1 enlists noteworthy nanoformulations available for biomedical utilization.

T**able 1.1.** USFDA-approved nanopharmaceuticals for clinical utilization.

Names	Drugs	Nanoformulations involved	Indications	Years of approval
Abelcet	Amphotericin B	Liposomes	Fungal infection	1995
Doxil	Doxorubicin	Liposomes	Ovarian cancer,	1995

			multiple myeloma and Kaposi's sarcoma	
Eligard	Leuprolide acetate	Polymeric matrix system	Prostate cancer	2002
Macugen	Pegaptanib	Aptamer	Macular degeneration	2004
Abraxane	Paclitaxel	Albumin-bound particles	Pancreatic cancer and metastatic breast cancer	2005
Marqibo	Vincristine	Liposomes	Acute lymphoblastic leukemia	2012
Ryanodex	Dantrolene sodium	Nanocrystals	Malignant hypothermia	2014
Onivyde	Irinotecan	Liposomes	Pancreatic cancer	2015
Comirnaty	mRNA	Lipid nanoparticles	COVID-19 vaccine	2021
mRNA-1273	mRNA	Lipid nanoparticles	COVID-19 vaccine	2021

Over the years, research has yielded multiple small molecules from natural resources to be effective against different diseases. Many of them exhibit exciting activity in vitro. However, a gap persists between the in vitro findings and the in vivo results, apprehending their usefulness. Low bioavailability, poor water solubility, fast metabolism and P-glycoprotein (P-gp) efflux can be accountable for the lack of in vivo efficacy (Khurana et al., 2018; Dewanjee et al., 2023). To overcome the mentioned incompetence and to utilize their beneficial effects in therapeutics, different pharmaceutical approaches have been proposed. Interestingly, nanocarrier-mediated drug delivery systems have emerged with remarkable prospects to deliver naturally derived agents to improve the biopharmaceutical profile (Sharma et al., 2016). Nanoscale drug delivery systems are progressively gaining attention to improve therapeutic efficacy by lowering dosing frequency, increasing bioavailability, attaining sustained-release behavior and enhancing selectivity (Taghipour et al., 2019; Dewanjee et al., 2020).

1.2. Concerns regarding nature-derived small molecules

The majority of the naturally occurring molecules with promising bioactivity are hydrophobic in nature. In vitro, many of them display intriguing activity. Nevertheless, there still exists a discrepancy between the in vitro and in vivo outcomes, which somewhat disables the

probability of rampant clinical utilization. The poor biopharmaceutical properties may be attributed to different physico-chemical, physiological and anatomical barriers (Figure 1.1).

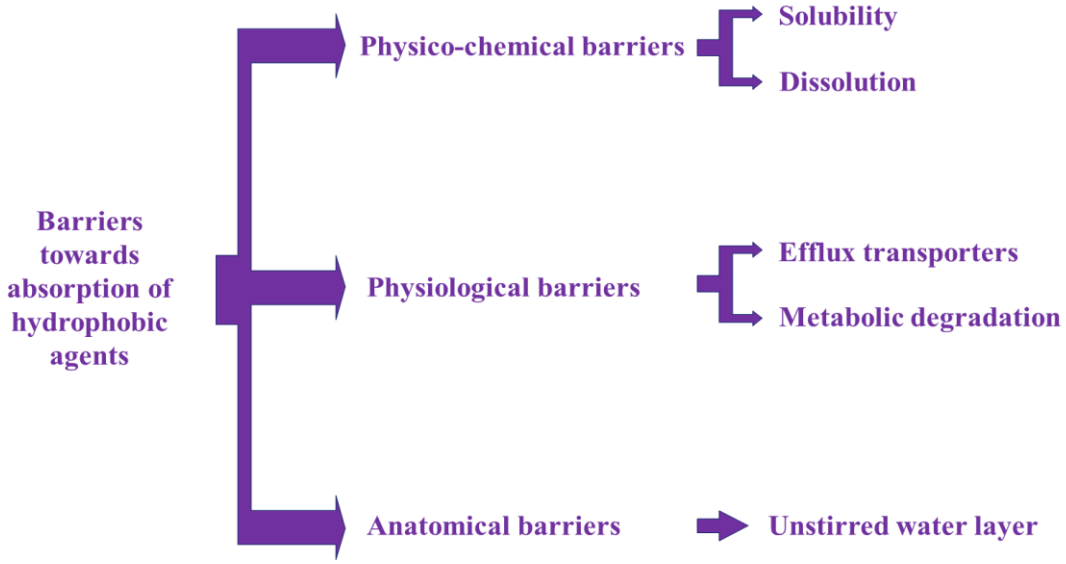

Figure 1.1. Absorption barriers for lipophilic moieties derived from natural resources.

1.2.1. Solubility

Many plant metabolites are significant sources of physiologically active chemicals, hence, they are frequently employed as research tools and leads for drug discovery. The effective delivery of therapeutic agents is limited by poor aqueous solubility, intrinsic dissolution rate and mass of the drug dissolved per unit time and area.

1.2.2. Rate of dissolution

Drug dissolution and drug release are key processes because they are prerequisites for absorption and consequently influence bioavailability (Talevi and Ruiz, 2022). Dissolution is the rate-limiting step regarding the absorption of hydrophobic drugs, such as agents belonging to class II and IV of the biopharmaceutical classification system (BCS), which exhibit low bioavailability.

1.2.3. P-gp efflux

Some transporters facilitate absorption, while others act as efflux transporters. P-gp plays an important role in the active transport of substrates out of the cells, leading to restricted bioavailability (Nguyen et al., 2021). Efflux transporters such as P-gp effectively minimize the magnitude of absorption, thus becoming accountable for the poor bioavailability of naturally derived small molecules. P-gp relentlessly pumps out a wide spectrum of substances, including therapeutic agents, from cells, leading to lower efficacy and resistance.

1.2.4. Chemical and enzymatic degradation

Different chemotherapeutic agents with lipidic structures are digested in vivo by lipase/co-lipase enzymes to produce short-chain fatty acids, thereby losing the active pharmacophore of the molecule. In addition, in the case of oral administration, when a lipophilic agent enters the enterocytes, it encounters biochemical hindrance in the form of metabolic enzymes such as cytochrome P450 3A4 (CYP3A4).

1.2.5. Unstirred water layer

The unstirred water layer is one of the major diffusional barriers towards the absorption of hydrophobic agents. Lipophilic moieties tend to diffuse across the unstirred water layer at a very slow pace (Khan et al., 2015). Drug molecules in the bulk phase must cross the unstirred water layer to get absorbed. In addition, owing to hydrophilicity, the unstirred water layer, in some cases, acts as a permeability barrier to the absorption of lipophilic compounds. Table 1.2 represents the pharmaceutical challenges of some promising nature-derived molecules.

Table 1.2. Concerns over nature-derived small molecules.

Sl No.	Compounds	Limiting concerns	References
1	Apigenin	High metabolic transformation, low oral bioavailability and high inter-individual variability.	Alshehri et al., 2019
2	Asiatic acid	Low aqueous solubility and poor bioavailability.	Lingling et al., 2016
3	Astaxanthin	High lipophilicity and low bioavailability.	Rodriguez-Ruiz et al., 2018
4	Baicalin	Low absorption, high metabolic conversion and poor bioavailability.	Huang et al., 2019
5	Carnosic acid	Hydrophobicity and poor dissolution.	Zheng et al., 2020
6	Chrysin	Extensive metabolism and high efflux.	Gao et al., 2021
7	Curcumin	Poor chemical stability, low absorption, poor penetrability, rapid metabolism and high faecal excretion.	Metzler et al., 2013; Tabanelli et al., 2021
8	Ferulic acid	Low water solubility, poor gastrointestinal stability, fast metabolism and poor bioavailability.	Panwar et al., 2018
9	Fisetin	Rapid first pass metabolism, high P-gp	Kadari et al., 2017

		efflux and low bioavailability.	
10	Fucoxanthin	Poor aqueous solubility and poor physico-chemical stability.	Sun et al., 2018
11	Lutein	Low water solubility, poor physico-chemical stability and poor oral bioavailability.	Toragall et al., 2021
12	Luteolin	Poor absorption and first-pass effect.	Xu et al., 2023
13	Mangiferin	Low water solubility and high P-gp efflux.	Khurana et al., 2017
14	Myricitrin	Low gastrointestinal stability, fast conversion to lower soluble myricetin by colonic microflora, low absorption and low bioavailability.	Man et al., 2019
15	Naringenin	Poor absorption, rapid metabolic transformation enzymes, P-gp efflux, fast metabolism by CYP450, low absorption and poor bioavailability.	Gera et al., 2017
16	Phloretin	Low water solubility and poor bioavailability.	Chhimwal et al., 2023
17	Quercetin	Poor chemicobiological stability, low absorption, rapid metabolism and fast elimination.	Kandemir et al., 2022
18	Resveratrol	Rapid elimination, low physico-chemical stability and limited systemic distribution.	Peñalva et al., 2018
19	Rhein	Low hydrophilicity and rapid metabolic degradation.	Luo et al., 2019
20	Rosmarinic acid	Low biological stability, poor absorption and fast metabolic transformation.	Madureira et al., 2016
21	Rutin	Low aqueous solubility, metabolic conversion and poor absorption from the gastrointestinal tract.	Semwal et al., 2021
22	Silibinin	Poor water solubility and low bioavailability.	Selc et al., 2024

1.3. Nanoscale carriers: trump cards in the biomedicinal field

The development of nanosized drug carriers is a promising approach to overcome the low bioavailability of naturally derived small molecules. They potentially improve the absorption profile of the loaded cargo. Particle size, shape and surface properties play crucial roles in this process. Nanoparticles improve the absorption owing to enhanced solubilization and dissolution, mucoadhesion, interaction with proteins in tight junctions, receptor-mediated endocytosis and transcytosis, phagocytosis via specialized microfold cells (M cells) of the Peyer's patches and other mucosa-associated lymphoid tissue (MALT) and lymphatic uptake via chylomicron uptake mechanisms. By manipulating structural characteristics, hydrophobicity and hydrophilicity to accommodate a wide variety of drug molecules and modulating the release profiles, nanoparticles can facilitate preferential uptake by cells (Sabourian et al., 2020; De et al., 2022). Nanocarrier-based delivery systems (Table 1.3) present with multiple advantages in the field of biomedicines, such as higher surface area leading to improved dissolution profile, lower dose and dosing frequency potentially resulting in improved patient compliance, protection from premature degradation in the biological system, improved bioavailability, controllable release profile, low undesired effects etc. Figure 1.2 depicts the key advantages of nanoformulations regarding biomedicinal aspects.

Table 1.3. Important nanocarriers belonging to diverse classes.

Classes	Nanoscale carriers
Polymer-based nanocarriers	Polymeric nanoparticles
	Dendrimers
Lipidic nanocarriers	Liposomes
	Solid lipid nanoparticles
	Nanostructured lipid carriers
Inorganic nanoparticles	Mesoporous silica nanoparticles
	Metal-based nanoparticles
	Quantum dots
	Carbon nanotubes
Biomimetic nanocarriers	Protein-based nanoparticles
	Small extracellular vesicles
Others	Black phosphorus nanoparticles
	Metal-organic framework nanoparticles

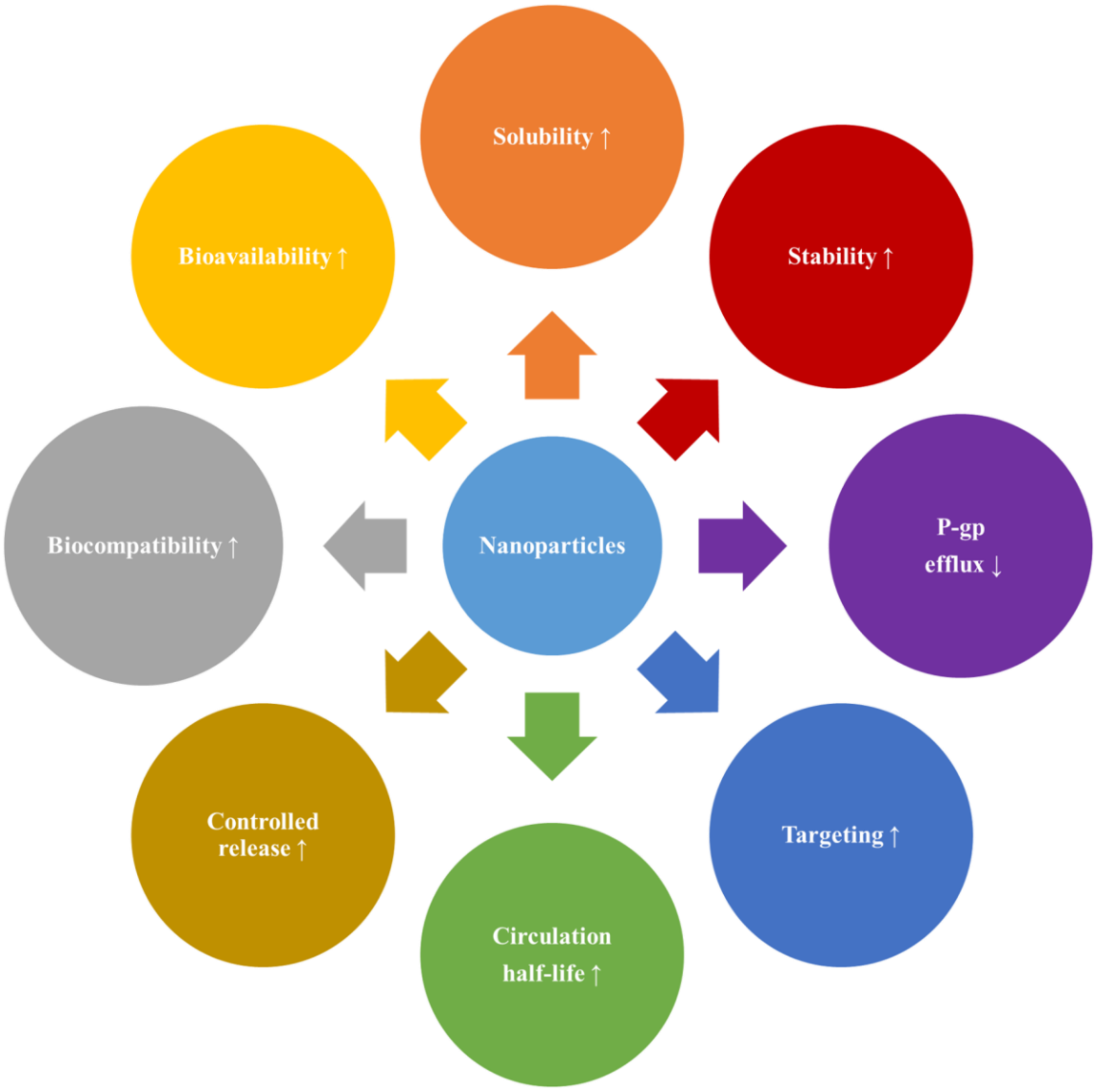

Figure 1.2. Characteristic advantages offered by nanoformulations for biomedicinal applications. '↑' represents improvement and '↓' represents suppression.

1.3.1. Improved solubility and dissolution rate

Development of nanoformulation is an exciting strategy to increase the dissolution rate and bioavailability of molecules with poor aqueous solubility by reducing the particle size and/or transforming drug(s) from a crystalline to an amorphous state. Owing to their small dimensions, nanoparticles offer a large effective surface area, leading to a high concentration gradient of poorly water soluble molecules, regulated pharmacokinetic features, and a faster dissolution rate of the loaded molecule (Dibaei et al., 2019). When hydrophobic agents are combined with

nanoparticles, they can attain a higher degree of bioavailability compared to conventional drug delivery methods. (Hogarth et al., 2021).

1.3.2. Improved bioavailability

Since nanoparticles offer improved solubility compared to free drugs, they provide greater systemic exposure and a faster and higher peak plasma concentration (Din et al., 2017). Biodegradable nanoparticles offer prolonged drug release, leading to improved bioavailability for a long period (Su and Kang, 2020). In the majority of cases, the hike in bioavailability appears to be due to the direct uptake of the nanoparticles. Interestingly, the size and surface chemistry of the nanoparticulate system regulate the direct uptake of nanoparticles (Acosta, 2009). Even a small alteration in the physico-chemical characteristics of nanoparticles can leave a significant impact on how they interact with biological processes and alter the bioavailability (Wang et al., 2020).

1.3.3. Duration of action

Nanocarriers have been explored for their ability to carry therapeutic agents and other bioactive compounds. The majority of these products take advantage of the smaller size of the nanoparticles to achieve a favorable distribution in the biological system (Natarajan et al., 2014). In general, such carriers sustain drug release over a few days. The incorporation of stimuli-responsive features and prolonged release properties has been recognized as an effective way to boost therapeutic efficacy and duration of action. Of late, smart sustained-release nanoparticles have been successfully developed for safe and efficacious delivery of therapeutic cargo with diverse kinetic characteristics, making them promising candidates for several applications (Bai et al., 2022).

1.3.4. Delivery of chemotherapeutic agents, proteins and peptides

Emerging evidence triggers the hope for the application of nanotechnology in important improvements regarding the diagnosis and treatment of various diseases (Dewanjee et al., 2020; Bai et al., 2022). Drug(s) encapsulated within or combined with nanoparticles either improve delivery to or uptake by target cells or minimize the unwanted effects of the native molecule in non-target areas. Conceptually, the delivery of loaded cargo has been transformed by nanotechnology. Nowadays, the generation of nanoparticles containing active moieties has made it feasible to improve the activity and reduce the toxicity of many compounds while also increasing their therapeutic value (Yetisgin et al., 2020). Mostly intravenous and subcutaneous injections are available for the delivery of proteins and peptides, and these procedures sometimes necessitate long-term repeated administration, which tends to reduce patient compliance. In

recent years, the clinical utilization of novel peptide drugs has been aided by nanotechnology (Cao et al., 2019).

1.3.5. Site-specific delivery

Nanoparticles offer targeted drug delivery to a specific site of action while reducing unwanted toxicity (Patra et al., 2018). It could be either a passive or an active targeted delivery method. The therapeutic agent is incorporated into a nanoscale formulation that is passively delivered to the target organ or tissue (Attia et al., 2019). The therapeutic cargo is coupled to a tissue or cell-specific ligand in active targeting (Yoo et al., 2019). Furthermore, as nanocarriers can be engineered to cross the blood-brain barrier (BBB) to transport desired pharmaceuticals into the central nervous system (CNS) (Dong, 2018).

1.3.6. Potential role in cancer therapeutics

Therapies against cancer need to be highly efficacious and lead to fewer undesirable effects. Desirable features of a chemotherapeutic agent include decreased viability of cancer cells, lower dose, and reduction in undesirable side effects (Senapati et al., 2018). Nanoparticles, by the enhanced permeability and retention (EPR) effect, and ligand-based active targeting have emerged as a favorable strategic tool for drug delivery in cancer therapeutics (Figure 1.3).

1.4. Nature-derived small molecules in cancer therapeutics: promises and challenges

Cancer has become a significant public health concern with a high rate of incidence and mortality globally, leading to nearly 10 million deaths per year (Sun et al., 2023). Lack of specificity, advent of resistance, and non-specific cytotoxicity give rise to substantial challenges towards effective cancer treatment. Emerging evidence suggests the anticancer effect of nature-derived small molecules with favorable safety profiles (Kopustinskiene et al., 2020; Aljabali et al., 2025). They inhibit cancer progression by blocking survival, proliferation, invasion, migration and inflammation of neoplastic cells, and angiogenesis through regulating diverse biological pathways They also exhibit chemotherapeutic effects based on dose and structural characteristics that ensure the killing of cancerous cells via production of free radicals as a result of pro-oxidant effect (Fernando et al., 2019; Kopustinskiene et al., 2020). On the contrary, the in vitro promise of such compounds fails to match their in vivo activity profiles. Poor pharmacokinetic and biopharmaceutical features may be attributed to the same (Khurana et al., 2018; Ratan et al., 2023). Low water solubility, rapid and extensive metabolism, and poor systemic absorption seem to lower their therapeutic potential in vivo (Table 1.2).

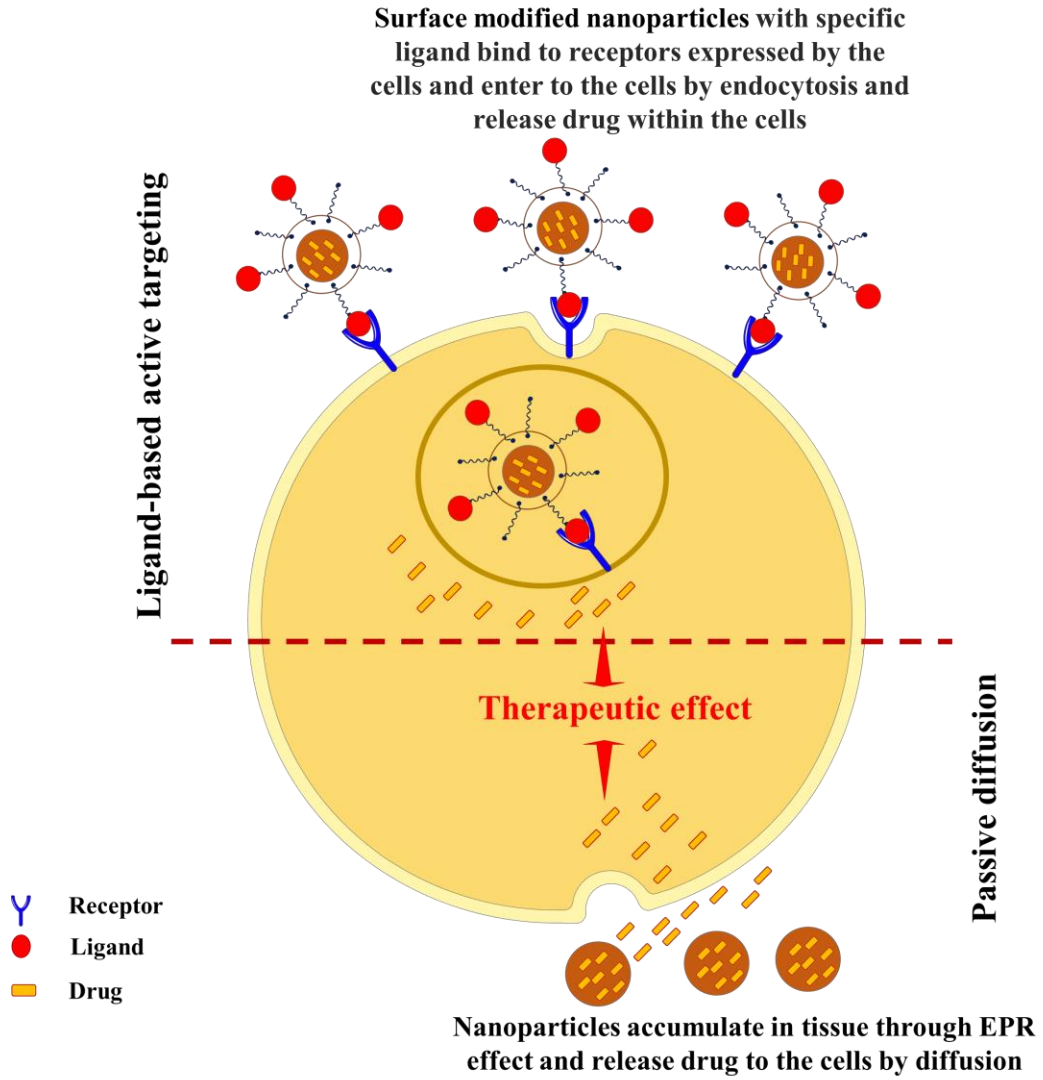

Figure 1.3. An impression of active and passive drug targeting by nanoparticles.

In cancer chemotherapeutics, conventional small molecules derived from natural sources act by destroying rapidly dividing neoplastic cells. In the process, they also pose the risk of damaging normal cells that divide rapidly, such as cells in the bone marrow, macrophages, digestive tract and hair follicles. A major concern over conventional chemotherapy is the lack of selective action against neoplastic cells (Sutradhar et al., 2014). This results in common side effects, which include myelosuppression, mucositis, alopecia, organ dysfunction, anaemia, thrombocytopenia, etc. These unwanted effects might impose dose reduction, treatment delay, and/or discontinuation. Thus, rampant clinical utilization of the nature-derived chemotherapeutic agents is yet to be practised. Chemotherapeutic agents often fail to penetrate the core of solid tumors, unable to kill the cancerous cells. Furthermore, in case of solid tumors, cell division

might effectively be ceased near the centre, making the cells located there somewhat insensitive to such agents. Nature-derived chemotherapeutic agents might get washed out from the circulation due to poor pharmacokinetic attributes and/or rapid metabolism (Haripriyaa and Suthindhiran, 2023). Thus, they remain in the circulation for a very short period and cannot interact with the cancerous cells sufficiently, rendering the chemotherapy rather ineffective. The poor aqueous solubility of most of the agents is another major concern. Another problem is associated with P-gp, an efflux transporter protein overexpressed on the surface of the cells. It effectively prevents drug accumulation inside tumor cells, acting as the efflux pump, and often mediates the development of resistance to anticancer agents.

1.5. Nanoformulations in cancer therapy: A contemporary promise

For effective chemotherapeutic outcomes, formulating nature-derived small molecules within a suitable drug delivery system could be a potential strategy to prevail over biopharmaceutical incompetence. Nanostructured drug carriers exhibit the potential to overcome biopharmaceutical and pharmacokinetic restrictions in potential therapeutic candidates to recover the efficacy of nature-derived small molecules in vivo (Khan and Gurav, 2018; Khurana et al., 2018). Nanosized delivery systems have exhibited remarkable success over the past few years compared to conventional anticancer drug delivery (Maghsoudnia et al., 2020; Sohail et al., 2021). Nanocarriers not only enhance the biopharmaceutical properties of therapeutic agents but also allow for targeted delivery to maximize therapeutic effects, simultaneously minimizing non-specific organ damage. Nanocarriers promote stability and regulate the release of chemotherapeutic drugs, possibly leading to better patient compliance. Further, Nanosized delivery systems can be generated for diverse routes of administration. Nanocarrier-based delivery can effectively overcome cancer-related chemoresistance (Yao et al., 2020). A growing body of evidence suggests that naturally occurring small molecules loaded onto suitable nanocarriers could offer greater absorption, better targeting, and improved therapeutic impact compared to the molecules in native form to uplift overall therapeutic compliance regarding management of diverse types of cancers (Wei et al., 2019; Khan et al., 2021). Over the past years, different classes of nanocarriers, carrying nature-derived small molecules, have displayed preclinical success in cancer therapeutics (Zhu and Liao, 2015; Dobrzynska et al., 2020).

Nanoparticles offer a large surface area, allowing a significant advantage in drug delivery. As such, it allows for increased functionalities of the nanoparticles. In addition to a large surface area, the particles can be controlled about how they release the loaded therapeutic agent(s). Nanoformulations, in addition to incorporating stability, lower wastage of the loaded

agent, given that sufficient amounts are delivered to the target region (Chenthamara et al., 2019). As discussed earlier, one of the concerns regarding conventional chemotherapy is that the anticancer agent undergoes some degree of metabolic degradation before reaching the target tissue. However, with nanotherapy, this can be circumvented. In cancer therapeutics, this has been particularly beneficial when expensive bioactive materials are being utilized. This helps improve efficiency as well as the cost-effectiveness of the treatment. Since most of the nature-derived small molecules tend to be hydrophobic, they are poorly dispersed in aqueous-based biological milieu (Pan et al., 2024). As a result, they are not completely absorbed by the tissue vasculature. As a consequence, a large fraction of the administered dose does not reach the target region. Nanoparticle-based delivery can potentially minimize this concern as the surface of the nanoparticle can be modified in a manner that enhances solubility. Further, nanotherapy tends to improve specificity regarding drug delivery by increasing the concentration of the therapeutic molecule at the target site while reducing damage to healthy tissues.

Passive targeting with nanoformulations relies mainly upon the EPR effect (Upponi and Torchilin, 2014). As tumorous cells continue to grow in neoplasia, new blood vessels are formed to supply nutrients. However, these new vessels are somewhat poorly formed, with leaky walls allowing therapeutic moieties to pass through. On the contrary, fast-growing solid tumor masses lack intra-tumor functional lymphatic vessels, thus altering flow to draining lymph nodes (Padera et al., 2016). Thus, tumor cells tend to retain the molecules inside. These features enable the retention of nanoparticles that enter the tumor cells, allowing therapeutic agents to accumulate for effective treatment. Active targeting is used to ensure the accumulation of nanoparticles into the tumor cells and intracellular spaces (Yameen et al., 2014). This is made possible by the incorporation of certain ligand molecules, viz. aptamers, antibodies, peptides, etc., to the surface of the nanoparticles. These combined moieties are crucial for active targeting since they improve site-specific delivery by recognizing certain receptors on the target cells (Kunjiappan et al., 2021).

1.6. Anticancer nanoparticles: peeking into mechanistic insights

The nanoparticles come in a variety of architectures. Techniques utilized to accomplish the synthesis of nanoparticles can broadly be divided into two categories, viz. top-down approach and bottom-up approach. For efficacious cancer therapy, it is essential to fabricate delivery systems bearing exceptional capability to target tumor cells selectively, sparing normal cells. Besides enhancing therapeutic efficacy, it would also protect normal cells from undesirable effects arising from cytotoxicity (Rahim et al., 2021). It can be accomplished by delivering

nanoparticles into the tumor microenvironment in a systematic manner. Nanoformulations should be able to cross diverse physiological and biological obstacles. These barriers are multi-layered systems made up of multiple components. Thus, certain constraints are imposed regarding the size, biocompatibility and surface chemistry of nanoparticles to minimize non-specific delivery (Gavas et al., 2021). Nanoparticles must be stable inside the body until they reach the tumor microenvironment. They should also escape the reticuloendothelial system as far as possible to reach tumor microenvironment through tumor vasculatures. Surface functionalization, physicochemical features, and pathophysiological factors play important roles in the process of nanoparticle-mediated delivery of anticancer chemotherapeutic agents.

1.6.1. Passive targeting

Different tumor biology (vascularity, leakiness) and carrier properties (size and circulation half-life) are the primary determinants of passive targeting. No particular ligand is utilized for targeting tumor cells in the case of passive targeting. Fenestrations on the tumor blood vessels, accompanied by poor lymphatic drainage, primarily give rise to the EPR effect. To cope with hypoxia, rapidly dividing tumor cells may form new blood vessels or engulf existing ones by neovascularization. Newly formed blood vessels are leaky and present with low permeability for tumors compared to normal blood vessels. This fast and faulty angiogenesis offers minimal barrier to extravasation, allowing nanoparticles carrying therapeutic cargo (often, nature-derived small molecules) to diffuse from such blood vessels and eventually gather at the tumor site (Figure 1.4; Subhan et al., 2021). Compromised lymphatic drainage in the tumor vicinity further contributes to the retention of the nanoparticles. Interestingly, the remarkable EPR effect does not apply to moieties with short circulation half-lives, as they get washed out rapidly. Hence, encapsulating small molecules within nanosized carriers improves their pharmacokinetics and tumor selectivity (Padera et al., 2004). In addition to the EPR effect, characteristic features of the tumor microenvironment, like lower pH can also be utilized for passive targeting (Pelicano et al., 2006).

However, tumor cells grow irregularly, owing to the heterogeneous blood supply. Cells near blood vessels divide more quickly than cells far from them or deep within the core, forming hypoxic or necrotic regions within the tumor (Hompland et al., 2021). Thus, irregular leaking raises interstitial pressure, and subsequently slows down the neovascularization process, impairing the transport and accumulation of nanoparticles.

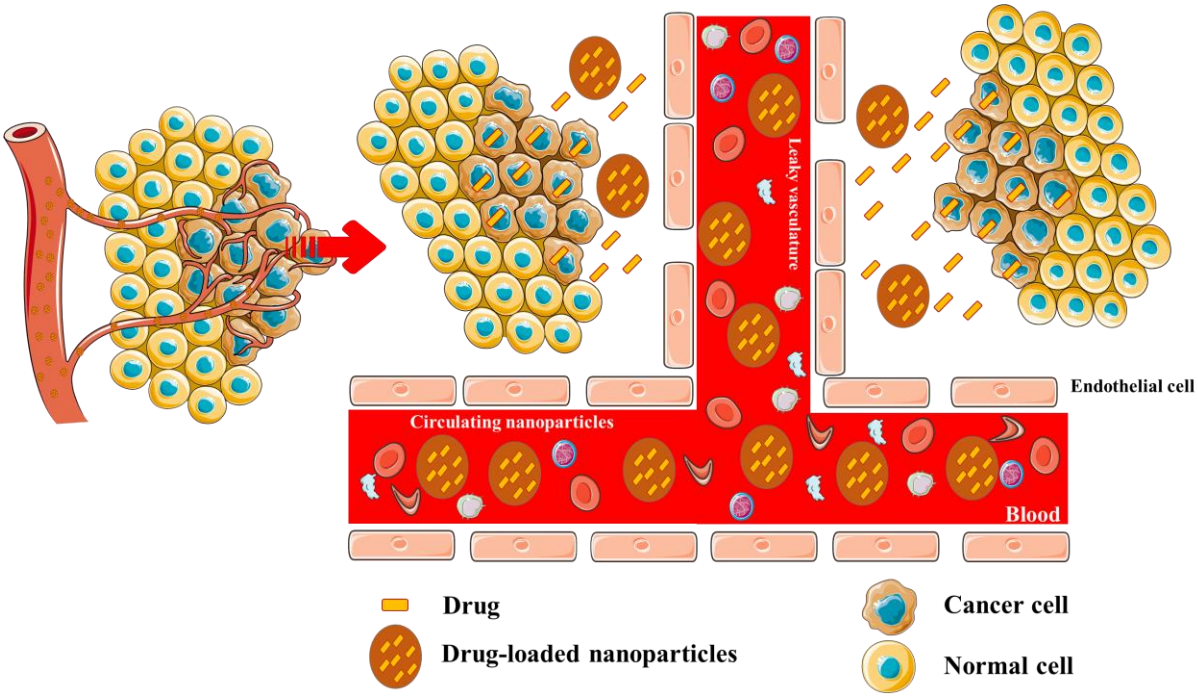

Figure 1.4. Schematic representation of the principle of passive targeting.

1.6.2. Active targeting

The main aim of active targeting is to enhance the crosstalk between nanoparticles and target cells without disturbing the distribution achieved by passive targeting. Active targeting relies upon specific ligand(s) that bind to receptor(s), exhibiting specific expression on the target tumor cells (Figure 1.5). This strategy enhances the binding of functionalized nanoparticles to cancer cells, increasing the accumulation of the therapeutic cargo. The recognition of ligands by target substrate receptors is an important step in ligand-mediated active targeting (Kunjiappan et al., 2021). Ligand-target interactions lead to the infolding of the membrane and internalization of nanosized carriers through receptor-mediated endocytosis. The multivalent nature of the nanoparticles enhances the interaction of ligand-functionalized nanoparticles with target cells. The production of such nanocarriers is complicated since architecture and ligand-target chemistry affect the overall efficacy of the approach (Gavas et al., 2021). Other elements that influence the performance include the route of administration, physicochemical features like ligand density, size and surface charge of nanoparticles, etc.

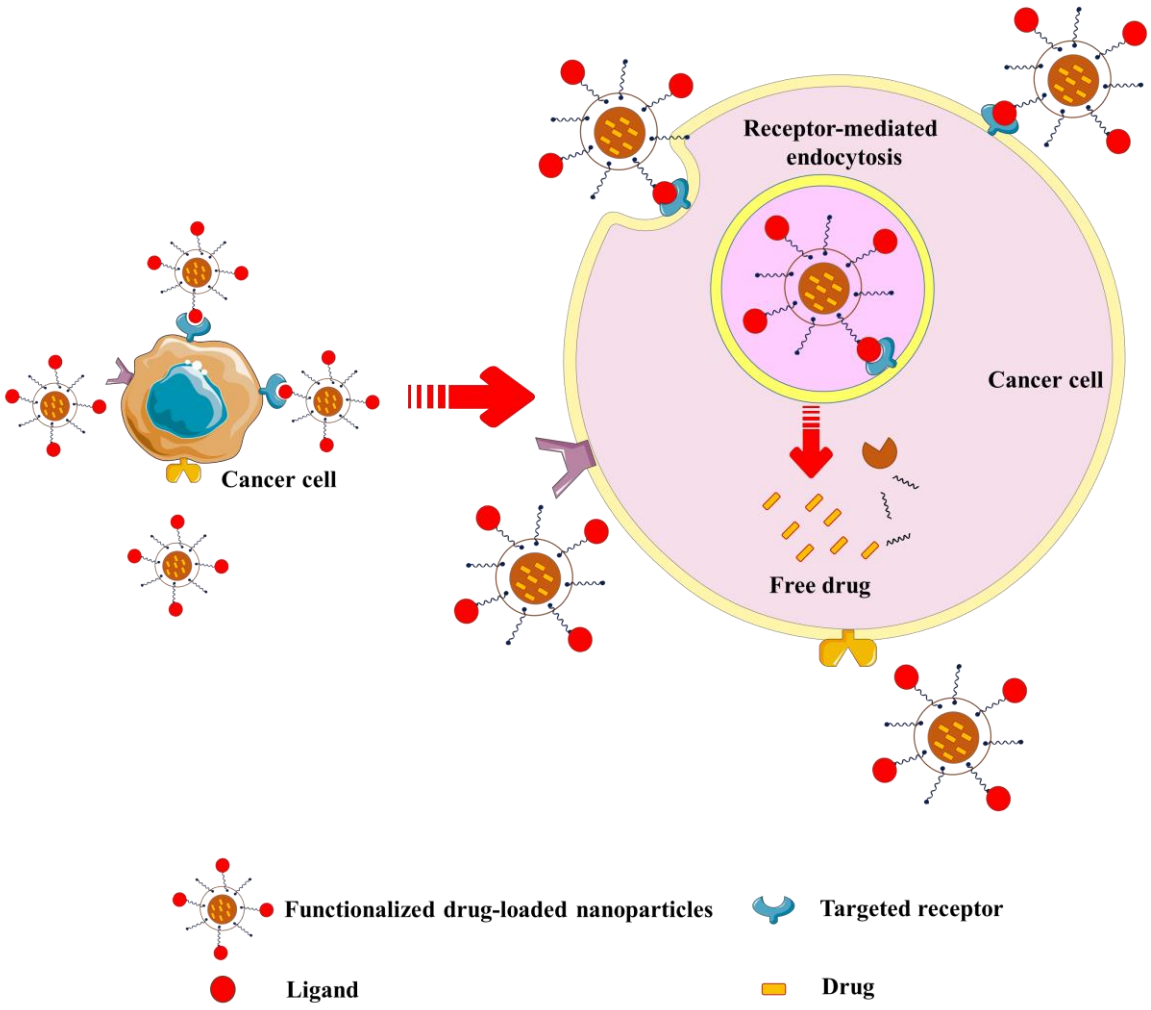

Figure 1.5. Schematic representation of the principle of active targeting.

1.6.3. Interaction with efflux transporters

The primary function of efflux transporters, such as P-gp (overexpressed in drug-resistant cancer cells), is to pump out therapeutic agents from the cell, thus lowering the intracellular concentration of the drugs. P-gp overexpression has been connected to malignancies that do not respond well to treatment (Allen et al., 2000; Chintamani et al., 2005). Nanoparticles get internalized by the cells mostly through endocytosis, and release the chemotherapeutic agent at the perinuclear site, distant from active efflux pumps. Nanocarriers can somewhat dodge the efflux pumps. In addition, by modulating drug release, e.g. by using acidic pH level as a trigger, nanoparticles may effectively bypass efflux transporters (Yuan et al., 2016). Another attractive technique is to co-deliver efflux pump inhibitor along with chemotherapeutic agent(s) loaded nanocarriers (Dey et al., 2022).

1.6.4. Nanocarriers and drug resistance

Drug resistance occurs when diseases develop a tolerance to treatments. It is a major issue in cancer management. Nanoparticles, with their remarkable ability to co-encapsulate several therapeutic cargos, can be employed to overcome cancer-related resistance. Some nanosized delivery systems act by inhibiting efflux pumps and promoting apoptosis (Prabha and Labhasetwar, 2004). Nanoparticles carrying hypoxia-inducible factor 1-alpha small interfering ribonucleic acid (HIF-1α siRNA) can be utilized to minimize hypoxia-related resistance in the tumor microenvironment (Liu et al., 2012).

1.6.5. Smart nanocarriers

Nanoscale drug carriers play a crucial role in smart nanomaterials. To qualify as desirable smart nanoparticles, the nanostructured delivery system(s) must meet certain characteristics, including stimuli-response materials or structures, stable nanoscale size, acceptable surface charge, high encapsulation capacity, biocompatibility, biodegradability, low toxicity, etc. In response to internal and external stimuli, smart nanoparticles can alter their solubility and self-association or dissociation behaviors and consequently lead to payload release, boost endosomal escape, and/or promote cellular internalization (Li et al., 2020; Sun et al., 2023).

1.7. Objectives

This research aims to develop and optimize effective nanoscale drug delivery systems to improve the chemotherapeutic efficacy of a nature-derived small molecule, mangiferin (Mgf), against two different types of cancer (breast cancer and hepatocellular carcinoma). The principal objective of the research is to formulate and characterize nanocarrier-assembled drug delivery systems of Mgf to improve therapeutic efficacy via enhancing the bioavailability, cell permeability and sustained-release property, as well as endorsing target specificity. The development and characterization of nanoformulations, followed by preclinical assays, would provide insights regarding therapeutic efficacy and safety profile.

In summary, the current research has aimed at developing Mgf-loaded polymeric nanoformulations to intensify bioavailability and chemotherapeutic efficacy of Mgf to treat breast cancer (via passive targeting) and hepatocellular carcinoma (via active targeting).

Chapter 2

Literature review

2.1. Background

Before initiating experimental research, a thorough literature review is necessary. Collecting relevant literature and research procedures from prior art is part of the literature review process. A comprehensive literature review aids in identifying untapped areas that would be addressed. It also helps in providing a more accurate definition of a research hypothesis. An extensive literature review contributes a novel research output, instead of reiterating earlier research. In addition, a thorough literature review guides us to implement the best protocol, sparing the pitfalls of earlier investigations, referencing the corresponding studies. Finally, it strengthens the argument regarding the impact of the research in present perspectives. This chapter presents excerpts from existing literature relevant to the research topic.

2.2. Mgf

Mgf (1,3,6,7-Tetrahydroxyxanthone C2-β-D-glucoside) is a bioactive polyphenol obtained from *Mangifera indica* L. and some other plants. Mgf exhibits poor solubility in water, and is practically insoluble in acetone, diethyl ether and n-hexane. It is freely soluble in DMSO and dimethyl formamide (Acosta et al., 2016; Tessiri et al., 2021). It exhibits a broad spectrum of pharmacological effects, including anti-tumor, cardioprotective, anti-hyperuricemic, antidiabetic, neuroprotective, anti-inflammatory, antipyretic and analgesic activities (Du et al., 2018). However, the progress of Mgf as a clinical therapeutic option is restricted by low aqueous solubility, poor bioavailability, considerable extent of P-gp efflux, and fast metabolism (Nguyen et al. 2021; Iqbal et al. 2023; Mei et al. 2023; Baghel et al. 2024).

Structural formula: $C_{19}H_{18}O_{11}$

Molecular weight (MW): 422.34

IUPAC name: 1,3,6,7-tetrahydroxy-2-[(2*S*,3*R*,4*R*,5*S*,6*R*)-3,4,5-trihydroxy-6-(hydroxymethyl) oxan-2-yl]xanthen-9-one. The molecular structure of Mgf is depicted in Figure 2.1.

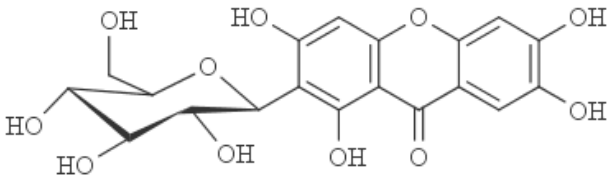

Figure 2.1. The molecular structure of Mgf.

Since this research has focused utilizing chemotherapeutic potential of Mgf through abasing its pharmaceutical incompetence by developing its polymeric nanoformulations, relevant

literature review of its chemotherapeutic potential of Mgf has been executed before initiation of the research.

2.2.1. Anticancer potential of Mgf

Mgf confers a wide range of pharmacological activities, including anticancer effects. Mgf displays a promising ability regarding apoptosis induction in tumor cells (Cuccioloni et al. 2016; Núñez Selles et al. 2016). Hence, Mgf holds potential to be a therapeutic agent in cancer chemotherapy. Mgf exhibits proapoptotic effect evidenced by the activation of Bax and caspases 3, 7, 8 and 9 and the suppression of anti-apoptotic, Bcl-2 (Figure 2.2; Pan et al., 2014; Kim et al.,

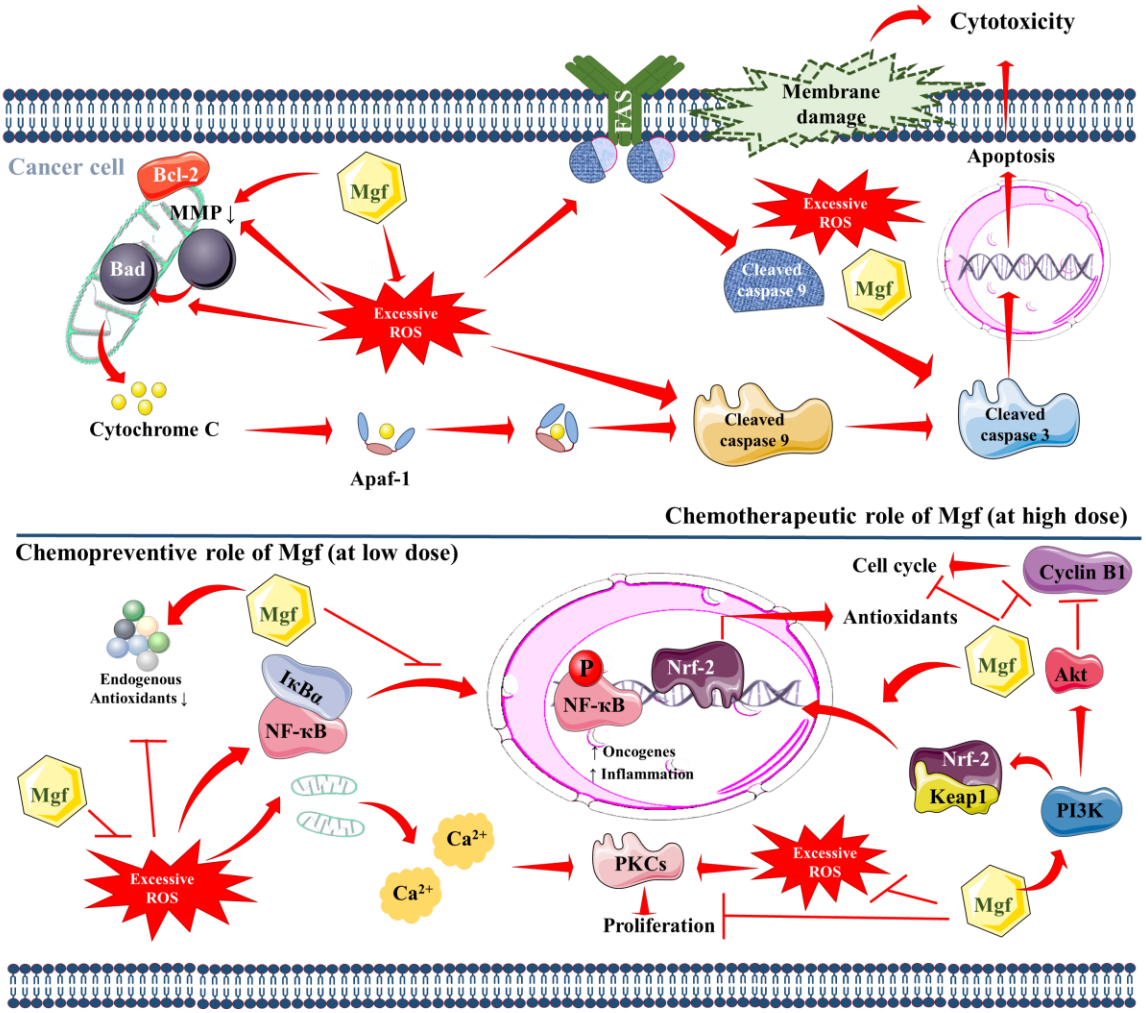

Figure 2.2. Chemotherapeutic and chemopreventive potential of Mfg. Red arrows indicate downstream events/activation, while red lines indicate inhibition/suppression. Akt, Ak strain transforming; Apaf-1, apoptotic protease-activating factor 1; Bad, Bcl2-associated agonist of cell death; BCl-2, B-cell lymphoma 2; FAS, Fas cell surface death receptor; IκBα, nuclear factor-kappa B inhibitor alpha; Keap1, Kelch-like ECH-associated protein 1; MMP, mitochondrial

membrane potential; NF-κB, nuclear factor kappa-light-chain-enhancer of activated B cells; Nrf-2, nuclear factor erythroid 2-related factor 2; PI3K, phosphoinositide 3-kinase; PKC, protein kinase C.

2012). In search of mechanisms, Mgf has been found to endorse oxidative stress via promoting reactive oxygen species (ROS) production, leading to apoptosis and modulating MMP (Dutta et al., 2017; Du et al., 2018). Interestingly, in the presence of Mgf, breast cancer cells display higher sensitivity to other chemotherapeutic drugs (Louisa et al., 2014; Iqbal et al., 2023). On the other hand, Mgf simultaneously exhibits chemopreventive effects at low concentrations through its antioxidant and anti-inflammatory effects (Figure 2.2). To confer chemopreventive effects, Mgf targets angiogenesis, tumor growth factors, cell proliferation and inflammation (Cuccioloni et al. 2016; Rahmani et al. 2023). Mgf leads to cell cycle arrest in the G2/M phase by regulating the CDK1-cyclin B1 signaling pathways (Peng et al., 2015; Gold-Smith et al., 2016). Mgf delays the S phase of the cell cycle by regulating NF-κB expression in cancer cells when combined with oxaliplatin (du Plessis-Stoman et al., 2011). Mgf can directly suppress inflammatory factors (Feng et al., 2022), which could significantly endorse the chemopreventive quality of the compound.

2.2.2. Pharmacokinetic constraints and perspectives

Although Mgf shows exciting pharmacological activities in vitro, its chemotherapeutic promise is somewhat limited in vivo, raising concerns about its potential clinical usefulness (Khurana et al., 2018). Poor water solubility, quick metabolism and significant P-gp efflux lead to low bioavailability of Mgf, contributing to its in vivo inadequacy (Nguyen et al. 2021; Baghel et al., 2024). This limited bioavailability may be attributed to inherent properties of Mgf, including hydrophobicity and a poor absorption profile. Interestingly, co-administration of Mgf with some other components, in the form of a polyherbal formulation, seems to enhance the residence time, delay elimination, consequently improving bioavailability (Kammalla et al., 2015).

Numerous methods have been attempted to address the concerns. To overcome the pharmacokinetic constraints and restore chemotherapeutic efficacy in vivo, Mgf may be formulated into an appropriate nanostructured delivery system. Nanoscale systems have come up with exciting potential to overcome pharmacokinetic and biopharmaceutical constraints of potential chemotherapeutic agents (Dewanjee et al., 2023). Mgf nanocrystals display improved pharmacokinetic profile, solubility, and stability, compared to free Mgf (Sarwar et al., 2023). Further, biopharmaceutical attributes of Mgf could be enhanced by Mgf-loaded self-assembled phospholipidic nanomicelles (Khurana et al., 2017). Nano-mixed micelles successfully improved

intestinal permeability and bioavailability of Mgf (Khurana et al., 2018). For oral administration of Mgf, β-lactoglobulin nanoparticles have been formulated to achieve sustained release and pepsin resistance (Samadarsi and Dutta, 2019). Regarding chemotherapeutic applications, solid-lipid nanoparticles delivering Mgf effectively inhibited the progression of lung cancer by targeting transferrin receptors for site-specific delivery (Zhou et al., 2022). Liposomal delivery of a combination of Mgf and curcumin confers impressive chemotherapeutic advancement in the case of ovarian cancer (Alharbi et al., 2024).

2.3. PLGA

The US Food and Drug Administration and the European Medical Association have approved the use of poly(lactic-co-glycolic) acid (PLGA) owing to biocompatibility and low toxicity. PLGA nanoshells can effectively encapsulate poorly soluble chemotherapeutic agents, and extravagate through tumor vasculature due to the EPR effect (Zi et al., 2022). The polymer is commonly employed in the formulation of polymeric nanoparticles owing to favourable safety, biocompatibility, and biodegradability. It serves as an efficient carrier for chemotherapeutic agents. For the production of micro and nano sized formulations, PLGA is one of the most popular polymers to date (Iureva et al., 2024). PLGA nanoshells present with lipophilic components on the inside and polar moieties on the exterior, allowing for effective encapsulation of chemotherapeutic agent(s), and release of the same in the desired medium. PLGA have gained immense popularity in anticancer drug delivery due to its biocompatibility, low toxicity, and sustained release characteristics. For target-specific delivery, certain ligand(s) may be attached to the polymer for surface modification.

Glycolic acid and lactic acid are two different monomer units primarily used to produce PLGA by copolymerization. Different forms of PLGA with varying MWs are manufactured based on the lactide: glycolide ratio. For biomedical applications, higher glycolide content results in faster degradation of the polymer and consequently, faster release of the accompanying therapeutic agent(s), indicating a more hydrophilic nature of glycolides, while higher lactide content leads to slower degradation (Figure 2.3; Singh and Singha, 2021). Metabolic biodegradation of PLGA yields lactic and glycolic acids. Lactate is finally eliminated from the body in the form of carbon dioxide and water upon further metabolic processing through the Krebs cycle. Glycolic acid is either excreted unaltered through urine or is converted to carbon dioxide and water by the Krebs cycle before elimination from the body (Makadia and Siegel, 2011).

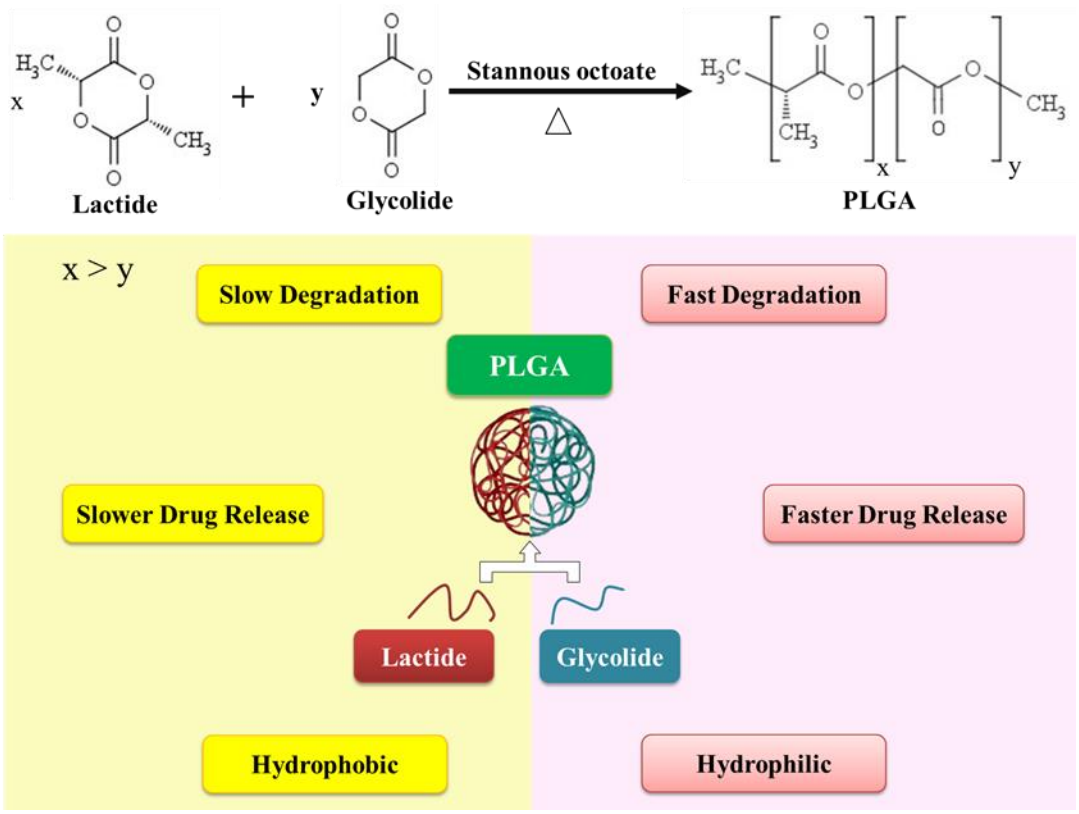

Figure 2.3. Effect of lactide and glycolide content on drug release pattern.

2.4. Polymeric nanoparticles in cancer therapeutics

Polymeric nanoparticles are nanostructures made of naturally occurring or synthetic polymers. They are expected to offer good stability, thus allowing sustained drug delivery for weeks, with low chances of leakage as an added benefit. In the polymeric nanostructures, the therapeutic agent(s) can either be linked covalently or may be adsorbed at the surface or entrapped within the nanoparticulate structure or encapsulated inside a polymeric shell (Elsabahy et al., 2015). Polymeric nanoparticles have attracted scientists in the domain of cancer therapeutics chiefly due to the ease of synthesis, biocompatibility, prolonged circulation time, low toxicity and capability to adsorb and/or encapsulate other molecules (Paul et al., 2021). Polymeric nanoparticles can carry and deliver different chemotherapeutic agents while offering a high surface-to-volume ratio. A wide range of polymers act as potential options due to their versatility and flexibility in meeting the needs of nanotechnology-based drug delivery systems.

Polymeric nanoparticles have emerged as attractive candidates in cancer therapeutics as carrier structures, especially for nature-derived small molecules to somewhat overcome their biopharmaceutical concerns (Singh and Singh, 2025). Gold-PLGA nanoparticles carrying quercetin exhibited promising activity against liver cancer (Ren et al., 2017). The polymeric-

metallic structure produced a slow, gradual release of quercetin over time. Naringenin-loaded polymeric nanoparticles made up of eudragit E100 exhibited much higher bioavailability and chemotherapeutic activity in a mouse model of colorectal cancer, compared to free naringenin (Chaurasia et al., 2018). The increased bioavailability is thought to be due to an electrostatic interaction of the polymeric surface with the cell membrane. When compared to free quercetin, quercetin-loaded gelatin-grafted pluronic-based nanogel demonstrated better activity against cervical cancer and breast cancer (Van Thoai et al., 2020). The gelatin backbone presented with an RGD (Arg-Gly-Asp) motif, whereby the net positive charge allows for greater internalization of the delivery system into tumor cells. Amphiphilic polymer chitosan has been utilized to improve chemotherapeutic efficacy of quercetin against breast cancer, by pH-responsive delivery (de Oliveira et al., 2018). Kaempferol-loaded polymeric nanoemulsion improved the chemotherapeutic efficacy of the flavonoid against glioma by enhancing transport to the brain (Colombo et al., 2018). The inclusion of chitosan served to improve the mucoadhesive qualities. PLGA nanoparticles displayed promise to enhance the therapeutic efficiency of apigenin against hepatocellular carcinoma (Bhattacharya et al., 2018). Polymeric nanoparticles carrying fisetin displayed exciting promise regarding cancer therapeutics, both in vitro and in vivo (Feng et al., 2019). PLGA nanoparticles also improved the cytotoxic potential of naringenin against pancreatic cancer (Akhter et al., 2020). Tang et al. (2019) achieved photothermal killing of breast cancer cells with polyvinyl pyrrolidone (PVP) nanoparticles of quercetin. Rutin-loaded PLGA nanoparticles exhibited promising activity against hepatocellular carcinoma (Pandey et al., 2018). ZnO and PLGA-matrix nanocarriers delivering lupeol and Mgf have displayed exciting anti-cancer promise in the case of hepatocellular carcinoma (Fabián et al. 2023). Table 2.1 enlists some promising polymeric nanoparticles carrying naturally occurring small molecules against cancer, in chronological order.

Table 2.1. Anticancer potential of polymeric nanoparticles.

Sl No.	Nanoformulations	Loaded drugs	Types of cancer	Anticancer promise	References
1	Gelatin-pluronic nanoparticles	Quercetin	Breast cancer, cervical cancer	Cytotoxicity.	Van Thoai et al., 2020
2	Eudragit-based nanoparticles	Naringenin	Colorectal cancer	Tumor suppression and improved survival rate.	Chaurasia et al., 2018
3	Chitosan-based nanoemulsion	Kaempferol	Glioma	Reduced cell viability and apoptosis induction.	Colombo et al., 2018

4	Chitosan-based pH-sensitive nanoparticles	Quercetin	Breast cancer	Cytotoxicity.	de Oliveira et al., 2018
5	PLGA nanoparticles	Apigenin	Hepatocellular carcinoma	Inhibition of tumor development and improved bioavailability.	Bhattacharya et al., 2018
6	PLGA nanoparticles	Rutin	Hepatocellular carcinoma	Reduced hepatic nodules and downregulation of proinflammatory cytokines.	Pandey et al., 2018
7	PLGA nanoparticles	Carnosic acid	Triple negative breast cancer	Improved anticancer effect.	Chatterjee et al., 2024
8	PLGA nanoparticles	Betulinic acid analog	Colorectal carcinoma	Improved chemotherapeutic efficacy (both in vitro and in vivo).	Dutta et al., 2019
9	PLGA nanoparticles	Naringenin	Pancreatic cancer	Cytotoxicity.	Akhter et al., 2020
10	PLGA nanoparticles	Asiatic acid	Breast cancer	Improved anticancer effect.	Dutta et al., 2022
11	ZnO-PLGA matrix nanoparticles	Lupeol and Mgf	Hepatocellular carcinoma	Reduced cell viability.	Fabián et al., 2023
12	Gold-PLGA nanoparticles	Quercetin	Hepatocellular carcinoma	Anti-proliferative effect and apoptosis induction.	Ren et al., 2017
13	PVP nanoparticles	Quercetin	Breast cancer	Photothermal killing of 4T1 cells.	Tang et al., 2019
14	PLA nanoparticles	Fisetin	Colon cancer, breast cancer	Cytotoxicity to colon cancer cells and in vivo anti-cancer effect opposing triple-negative breast cancer.	Feng et al., 2019

2.5. Surface-functionalization of polymeric nanocarriers for active targeting

Polymeric nanoparticles can either encapsulate or adsorb molecules of interest, delivering them to the target region. Polymeric nanoparticles can be engineered with desired features to improve their appeal, their ability to bear physiological stress and their high biological stability.

They can even be regulated by ligand attachment and/or functionalization by surface modifications for site-specific delivery (Beach et al., 2024). The approach practically integrates bioactive moieties on the surface of polymeric nanoparticles, with an aim to enable functionalities in order to allow target-specific, favorable biological interactions (Table 2.2). However, scalability and precise control over surface modifications are concerns to be fully addressed before rampant clinical utilization (Haidar et al., 2024).

Table 2.2. Key strategies to improve target-specificity.

Surface modifications	Target attributes
Aminoethyl anisamide functionalization	Sigma receptors
Antigen-mediated targeting	Surface antigens overexpressed on tumor cells
Aptamer functionalization	Oncoproteins
DMSA functionalization	Preferential distribution to the cancer region
Folate functionalization	Folate receptors
Galactosylation	Asialoglycoprotein receptors
Hyaluronic acid functionalization	CD44 receptors
Transferrin functionalization	Transferrin receptors
Triphenylphosphine functionalization	Mitochondriotropic ligand

Functionalization of the surface of polymeric nanostructures has gained considerable attention from researchers to improve target-specificity and reduce off-target effects (Dey et al., 2024). Functionalization of EGCG-loaded PLGA nanoparticles with small molecular entities improved chemotherapeutic activity by virtue of actively targeting prostate cancer cells (Sanna et al., 2017). The functionalized nanoformulation displayed greater therapeutic impact compared to its non-functionalized counterpart concerning antiproliferative actions and apoptosis induction. Tumor cells express sigma receptors, which can be actively targeted using nanoformulations modified with aminoethyl anisamide. The PEG-polycaprolactone nanoshells, surface modified with aminoethyl anisamide, resulted in effective targeting of breast cancer cells to improve the chemotherapeutic efficacy of silibinin (Jiang et al., 2020). The functionalized nanoformulation significantly inhibited fibrosis and angiogenesis while inducing anticancer immunity. Cancer cells often overexpress folate receptors, which can be explored as delivery targets. EGCG-loaded folate peptide conjugated PLGA nanoparticles exhibited promise to target breast cancer, resulting in higher treatment efficacy compared to non-targeted formulation (Kazi et al., 2020). In line with the findings, folic acid-conjugated polyamidoamine dendrimers have enhanced anticancer attributes of baicalin in the case of cervical cancer (Lv et al., 2017). Galactose-modified PLGA

nanoparticles carrying apigenin displayed promising potential to target asialoglycoprotein receptors on hepatocellular carcinoma cells (Ganguly et al., 2021). Galactosylation enhanced selectivity and therapeutic efficacy against hepatocellular cancer, both in vitro and in vivo. Similarly, dalbergin-loaded PLGA-galactose decorated nanoparticles also exhibited promising activity against hepatocellular carcinoma (Gautam et al., 2024). Aptamer-functionalized PLGA nanoparticles showed potential promise in the domain of targeted therapeutics to actively target hepatocellular carcinoma (Chakraborty et al., 2020). In another experiment, aptamer-conjugated PLGA nanoparticles displayed a promising efficacy and safety profile to improve the anticancer potential of apigenin in mouse model of colon cancer (Dutta et al., 2018). Apigenin-loaded PLGA nanoparticles outperformed free apigenin in terms of chemotherapeutic potential against melanoma lung metastasis (Sen et al., 2021). Surface modification by meso-2,3 dimercaptosuccinic acid (DMSA) enhanced therapeutic effect, evidenced by increased apoptosis and anti-metastatic effects. Improved accumulation of the functionalized nanoformulation within the lungs may lead to better chemotherapeutic activity (Sen et al., 2021). Naringenin-loaded polycaprolactone nanocarriers enhanced the chemotherapeutic prospect of the flavonoid (Parashar et al., 2018). Surface modification with hyaluronic acid specifically targeted CD44 receptors, overexpressed by lung cancer cells, to achieve site-specific delivery. Table 2.3 represents a summary of leading strategies for cancer-specific targeting via functionalization approach.

Table 2.3. Surface-functionalized polymeric nanoparticles exhibiting anticancer promise.

Sl No.	Surface modifications	Loaded drugs	Types of cancer	Outcomes	References
1	Antigen-specific targeting	EGCG	Prostate cancer	Lowered prostate-specific antigen level and reduced tumor volume.	Sanna et al., 2017
2	Folate decoration targeting folate receptors	Baicalin	Cervical cancer	Improved anticancer potential.	Lv et al., 2017
3	Folate-decoration	EGCG	Breast cancer	Improved target-specificity.	Kazi et al., 2020
4	Aptamer functionalization	Apigenin	Colon cancer	Improved chemotherapeutic efficacy and lowered off-target toxicity.	Dutta et al., 2018
5	Aptamer	Paclitaxel	Hepatocellular	Apoptosis induction	Chakraborty

	functionalization		carcinoma	selectively to neoplastic hepatocytes.	et al., 2020
6	Hyaluronic acid decoration targeting CD44 receptors	Naringenin	Lung cancer	Site-specific delivery to improve therapeutic efficacy.	Parashar et al., 2018
7	Aminoethyl anisamide targeting sigma receptors	Silibinin	Breast cancer	Inhibition of angiogenesis and fibrosis.	Jiang et al., 2020
8	Galactose conjugation targeting asialoglycoprotein receptors	Apigenin	Hepatocellular carcinoma	Higher selectivity and therapeutic efficacy.	Ganguly et al., 2021
9	Galactose conjugation	Dalbergin	Hepatocellular carcinoma	Suppression of cell growth and apoptosis induction.	Gautam et al., 2024
10	DMSA	Apigenin	Melanoma lung metastasis	Improved therapeutic impact.	Sen et al., 2021

Chapter 3

PLGA-based polymeric nanoformulation improved the chemotherapeutic efficacy of Mgf against breast cancer

3.1. Background

Breast cancer has become one of the most common types of malignancies in women across the globe (Lyu et al., 2023). Worldwide, incidences of breast cancer are projected to go past 3 million by 2040, leading to nearly 1 million fatalities per year (Arnold et al., 2022). Additional challenges in managing breast cancer therapeutically arise from the heterogeneity. Conventional chemotherapeutic methods confer troublesome non-specific effects, in most cases (Wu et al., 2022). Newer methods are therefore desperately required for the effective treatment of breast cancer. Mgf, a nature-derived polyphenol, is an apoptosis inducer in cancer cells (Pan et al., 2014; Cuccioloni et al., 2016; Li et al., 2016; Núñez Selles et al., 2016). Thus, it bears promise as a futuristic chemotherapeutic tool against breast cancer. Formulation of Mgf within a suitable drug delivery system can potentially eradicate the biological incompetence in vivo. Nanoscale carriers of Mgf are displaying promise as chemotherapeutic tools against cancers (Zhou et al., 2022; Fabián et al., 2023). The present study aimed to formulate Mgf-containing PLGA-based nanoparticles (MNPs) using vitamin E tocopheryl polyethylene glycol succinate (TPGS) as emulsifier, employing the nanoprecipitation technique to enhance pharmacokinetic attributes and, subsequently, improve chemotherapeutic effectiveness of Mgf against breast cancer. It aimed to assess the therapeutic efficacy and safety profile of developed MNPs and compared them with native Mgf employing substantial preclinical assays.

3.2. Materials and methods

3.2.1. Key materials

Mgf (CAS No. 4773–96-0), PLGA (L/G molar ratio 50:50, MW 38,000–54,000, acid-terminated), and vitamin E-TPGS were procured from Sigma-Aldrich, St. Louis, USA. MDA MB-231 cells and MCF-7 cells were obtained from the National Centre for Cell Science, Pune, India. Culture media and 3-[4,5-dimethylthiazol-2-yl]−2,5 diphenyl tetrazolium bromide (MTT) were procured from HiMedia Laboratories, Mumbai, India. Serum assay kits were obtained from Transasia Bio-medicals Limited, Solan, India, and Span Diagnostics Limited, Mumbai, India. Annexin V-FITC/PI Apoptosis Kit (E-CK-A211) was procured from Elabscience, Houston, USA. Primary antibody was obtained from Biobharati LifeScience, Kolkata, India (p53, #BB-AB0100). Immunohistochemistry kits were purchased from Abcam, MA, USA.

3.2.2. Preparation of nanoparticles

Mgf-loaded nanoparticles were formulated following the nanoprecipitation method (Fessi et al., 1989). In brief, Mgf and PLGA were first dissolved in a non-aqueous solvent system (acetone: ethanol; 4:1; v/v). A drug: polymer ratio of 1:10 has been chosen for the

nanoprecipitation technique based on earlier studies by our group, whereby this ratio exhibited best-suited results regarding drug encapsulation (Gaonkar et al., 2017; Chatterjee et al., 2024). The solution containing Mgf and PLGA was added dropwise to an aqueous solution of vitamin E-TPGS (0.03%; w/v), under continuous stirring. The resultant dispersion loses its transparency owing to the formation of nanoparticles. Evaporation of the non-aqueous solvent was allowed overnight. The aqueous dispersion underwent filtration to remove the unwanted particles. Nanoparticles were recovered by centrifugation (Hermle refrigerated centrifuge, Wehingen, Germany) at 16,000 rpm for 50 min at 4 °C. Upon centrifugation, the supernatant was disposed of, and the pellet was washed 2–3 times with water and lyophilized (LaboGene Scanvac Coolsafe, Bjarkesvej, Denmark) to obtain a free-flowing powder. Following a similar protocol, blank nanoparticles were also synthesized. For fluorescent nanoparticles, an alcoholic solution of FITC (0.4%; w/v) was included in the non-aqueous phase, and a similar protocol was followed for the rest of the steps. However, fluorescent nanoparticles were protected from light during preparation and storage.

3.2.3. Characterization of prepared nanoparticles

Mean particle size and polydispersity index (PDI) were determined using Malvern Zetasizer Nano-ZS (Malvern Instruments, Malvern, Worcestershire, UK), according to the concept of dynamic light scattering (DLS). Briefly, nanoparticle suspension (1 mg/mL) was prepared in MilliQ water. 10 µL of this dispersion was diluted to 1 mL with MilliQ water and analyzed. Using the same instrument, the zeta potential of properly diluted samples was measured at 25 °C. The shape and surface morphology of the prepared nanoparticles were examined in a field emission scanning electron microscope (FESEM, JEOL JSM-7600F, Tokyo, Japan). Particle structure was evaluated in a transmission electron microscope (TEM, JEOL JEM-2100Plus, Tokyo, Japan). Atomic force microscopy (AFM; MFP-3D Origin, Asylum Research, Oxford Instruments, CA, USA) was undertaken to observe the surface topography of the nanoparticles. The specific surface area was determined with a BET surface area analyzer (Micromeritics Gemini VII 2390t, GA, USA).

Physicochemical compatibility between Mgf and other formulation ingredients was evaluated using Fourier transform infrared (FTIR) spectroscopy (IR Prestige-21, Shimadzu, Kyoto, Japan), X-ray diffraction (XRD; Ultima III, Rigaku, Japan) analysis, and differential scanning calorimetry (DSC; DSC STARe System, Mettler Toledo, USA). Drug loading capacity and entrapment efficiency were determined utilizing a spectrophotometric technique with the help of a JASCO V-550 double beam UV–visible spectrophotometer (OK, USA).

To assess the long-term stability of prepared MNPs, lyophilized nanoparticles were preserved at ~4 °C for 90 days and evaluated for FTIR spectrum, drug loading, particle size, and surface charge.

3.2.4. In vitro drug release kinetics

In vitro release pattern of Mgf from the MNPs was evaluated in PBS (pH 7.4) as per the protocol described by Gaonkar et al. (2017). To elaborate, MNPs were dissolved in PBS (1 mg/mL) and stirred continuously at 100 rpm at a temperature of ~37 °C. At preselected intervals, 2 mL of release medium was taken out from the system and centrifuged, and the supernatant was collected for spectroscopic analysis. Meanwhile, the pellet (nanoparticles with unreleased Mgf) was redissolved in an equal volume of fresh PBS and was transferred back to continue the process, maintaining sink condition. The collected supernatant was analyzed spectrophotometrically (JASCO V-550 double beam UV–Visible spectrophotometer, OK, USA) at 258 nm to measure the released Mgf from the nanoshells. The procedure was performed in triplicate.

Diverse mathematical models were utilized to anticipate the manner/mechanism of release of Mgf from the nanoformulation. The obtained data were fitted into various kinetic equations to explore the mechanistic pattern regarding the release of Mgf from the polymeric matrix.

3.2.5. In vitro cytotoxicity assay

MDA-MB-231 cells were maintained in RPMI medium or RPMI 1640 fortified with 10% FBS and 1% penicillin–streptomycin, incubated at 37 °C under humidified conditions of 5% CO_2. To perform cytotoxicity assay, ~5000 cells/ well were seeded in a 96-well plate (Corning Costar, Fisher Scientific, NY, USA) and incubated for 24 h to allow the cells to adhere. The cells were then incubated with Mgf and MNPs in a concentration gradient of 0–50 µg/mL for 24 h. After the treatment, cells were subjected to 20 µL of MTT (5 mg/mL, in PBS) and incubated for 4 h. Finally, the insoluble formazan was solubilized in DMSO, and the absorbance was measured at 450 nm. Cytotoxicity of MNPs to MCF-7 cells and NKE cells was also assayed following a similar protocol.

3.2.6. In vitro cellular uptake

To evaluate the intracellular uptake, FITC-tagged nanoparticles were given to MDA-MB-231 cells, followed by incubation for 6 h. The cells were then trypsinized and uptake assessed by flow cytometry (BD LSRFortessa, BD Biosciences, NJ, USA), and the percentage of cellular uptake was calculated with control cells.

3.2.7. Assessment of the therapeutic effects of MNPs in vitro

To assess the apoptosis-inducing ability of Mgf and MNPs at their respective IC_{50} concentrations obtained from the MTT assay, MDA-MB-231 cells were seeded in 6-well plates (~15×10^4 cells/well) followed by overnight incubation. Treatments of Mgf and MNPs were given at respective IC_{50} doses calculated from the MTT assay for 24 h. Cells were then harvested, stained with FITC Annexin V, and incubated for 15 min. Finally, the cells were stained with PI. Cells were acquired in a flow cytometer (BD LSRFortessa, BD Biosciences, NJ, USA). To evaluate ROS production by MNPs at an effective concentration, MDA-MB-231 cells were plated in 35 mm culture plates (~2×10^5 cells/mL). After 24 h of incubation following treatment with Mgf and MNPs, respectively, the cells were washed and stained with diluted DCFDA solution at 37 °C for 45 min in the dark. Intracellular ROS was evaluated by flow cytometry (BD LSRFortessa, BD Biosciences, NJ, USA). To assess the effect of MNPs on MMP, MDA MB-231 cells were plated in 35 mm culture plates (~2×10^5 cells/mL). After incubation for 24 h following treatment with Mgf and MNPs, respectively, the medium was removed, followed by washing with PBS, and JC-1 solution was added further. The plates were incubated in the dark for 20 min, and expression was measured by flow cytometric technique (BD LSRFortessa, BD Biosciences, NJ, USA).

3.2.8. Experiments involving animals

In the study, 2–3-week-old female Balb/c mice were used. Animals were acclimatized for 14 days in a 12 h light/dark cycle and provided with water and food ad libitum. The study has been carried out according to the guidelines of the Institutional Animal Ethics Committee (IAEC) of Jadavpur University, Kolkata, India, vide certificate proposal no. JU/IAEC-22/31 dated 15.06.2023.

3.2.8.1. Hemolysis assay

Freshly collected mouse blood was taken in EDTA-coated tubes and centrifuged at 2000 rpm for 5 min, maintaining 4 °C. After discarding the supernatant, the erythrocyte pellet was washed with PBS. 200 µL aliquots were utilized for the hemolysis study. To determine the hemolytic effect and predict biocompatibility, 200 µL of MNPs dispersion (containing MNPs at the intended dose amount) was introduced to the PBS dispersion. The mixture thus obtained was incubated at 37 °C for 1 h under shaking conditions, followed by centrifugation at 2000 rpm for 5 min. To calculate the hemolysis percentage, the optical density of the supernatant was measured spectroscopically at 570 nm. Triton X-100 and PBS served as controls, positive and negative, respectively.

3.2.8.2. Evaluation of anti-tumor efficacy in vivo

To evaluate the in vivo effect of the developed MNPs, an Ehrlich ascites carcinoma (EAC)–based solid mammary tumor-bearing mouse model was undertaken (Badawi et al., 2022; Shehatta et al., 2022; El-Ashmawy et al., 2023; Shaker et al., 2023; El-Masry et al., 2024). Briefly, 15 Balb/c mice were randomly divided into five groups. Groups I and V received subcutaneous injections of PBS in mammary pads. The rest of the animals received subcutaneous injection of EAC cells (~10^7 cells/50 µL for each mouse; Kundu et al., 2019). Ehrlich tumor, a spontaneous murine mammary adenocarcinoma, is undifferentiated, rapidly proliferating, malignant, and easy to grow and transplant. Ehrlich tumors have been used in tumor biology for many years to study carcinogenesis and evaluate anti-tumor effects of different agents (Shehatta et al., 2022). After inoculation, animals were monitored for about 2 weeks to allow the growth of solid tumors. Then, the animals were treated with PBS (groups I and II), Mgf (5 mg/kg, group III) and nanoparticles (equivalent to 5 mg/kg of Mgf, group IV; and group V) through the intravenous route for 14 days every alternate day. After completion of the treatment period, animals were sacrificed after collecting blood samples, and tumors and organs were removed. After determining tumor mass and tumor volume (ellipsoidal volume equation), they were stored for further analyses (Bhattacharya et al., 2015).

The extent of accumulation of Mgf within tumor tissues was evaluated quantitatively by HPLC (Dionex Ultimate 3000, Dionex, Idstein, Germany) utilizing a C-18 column (250 × 4.6 mm, particle size 5 µm; Thermo Scientific™ Hypersil GOLD™, MA, USA) and UV detector. Accurately weighed tissue samples from each tumour-bearing group were homogenized individually in a solution containing methanol (75%) and DMSO (0.05%). The mixture was then centrifuged for 15 min at 10,000 rpm. Supernatant was collected, filtered and analyzed chromatographically. Aliquots of the filtrate (injection volume 20 µL) were eluted with an isocratic mobile phase comprising 0.1% formic acid and acetonitrile at a ratio of 87:13, with a flow rate of 1.5 mL/min and detection wavelength set at 258 nm (Naveen et al., 2017). The Mgf concentration in the tissues was determined following the standard curve method.

To measure the alterations in the enzymatic and non-enzymatic antioxidant activity levels in the tumor tissues upon different treatments, activities of catalase (CAT), superoxide dismutase (SOD), and reduced glutathione (GSH) were assessed following established protocols of our laboratory (Manna et al., 2022). The extent of protein carbonylation was assessed as an oxidative stress marker according to standard protocol.

For histological observations, tumor tissues isolated from experimental animals were fixed in 10% formalin and processed for paraffin sectioning. Subsequently, paraffin-embedded sections were stained with hematoxylin and eosin (H&E) to study the histological changes using a bright field light microscope (Leica Microsystems, Wetzlar, Germany).

Sections of tumor tissues were subjected to immunohistochemical staining to assess the localized expression profile of p53. Following standard protocol, tissue sections on charged slides were incubated with anti-p53 antibody (Biobharati LifeScience, Kolkata, India, #BB-AB0100) at an appropriate dilution. Slides were then exposed to HRP-conjugated secondary antibody. Diaminobenzidine (DAB) was introduced to serve as a substrate for HRP. Hematoxylin served as a counterstain in the experiment to aid in visualizing the nuclei. Slides were mounted in DPX before observing in a bright field light microscope (Leica Microsystems, Wetzlar, Germany).

3.2.8.3. Assessment of systemic toxicity in vivo

The levels of ALT and ALP in serum were evaluated as hepatic toxicity markers for all five groups. Further, levels of blood urea nitrogen (BUN) and creatinine in sera were examined as renal toxicity markers. All serum markers were analyzed using commercially available kits following the respective manufacturers' protocols. The histological sections (H&E-stained) of the liver, kidney, heart, and spleen of different experimental groups were also analyzed for the estimation of systemic toxicity using a bright field microscope (Leica Microsystems, Wetzlar, Germany).

3.2.9. Data analyses

Experiments were performed in triplicate, and data were expressed as mean ± SD. Statistical analyses of experimental data were conducted using GraphPad Prism 10.0.2. Statistical analyses involved one-way analysis of variance (ANOVA) followed by Dunnett's test and t-test; statistical significance was designated as $p\text{-value} < 0.05$.

3.3. Results and discussions

3.3.1. Preparation and characterization of nanoparticles

MNPs with an average hydrodynamic diameter of ~162.5 nm were produced (Figure 3.1A), exhibiting 5.08 ± 0.49% loading and encapsulation efficiency of 55.89 ± 5.39%. A low PDI value of 0.103 indicated narrow size distribution, i.e., nearly uniform-sized particles. surface charge of − 34.9 mV (Figure 3.1B) was satisfactory for stable nanoparticles with low chances of agglomeration with each other in the dispersed phase as well as for imparting acceptable effectiveness (Betancourt et al., 2007; Shavi et al., 2015; Markeb et al., 2016; Németh et al., 2022). Such monodisperse particles with a loading efficiency of about ~5% have been

evinced as potential candidates for good biological activity against cancer (Betancourt et al., 2007; Ganguly et al., 2021; Sen et al., 2021). The FESEM image (Figure 3.1C) exhibited a thick distribution of more or less uniform-sized nanospheres with smooth exteriors. TEM-based image (Figure 3.1D) revealed a discrete spherical delineation of the nanoparticles. Smooth, sphere-shaped particles devoid of aggregation were further ascertained by AFM images (Figure 3.1E). The three-dimensional view also revealed a more or less homogeneous size distribution of particles, with smooth topography (Figure 3.1F). BET analysis revealed a specific surface area of ~157.51 m^2/g.

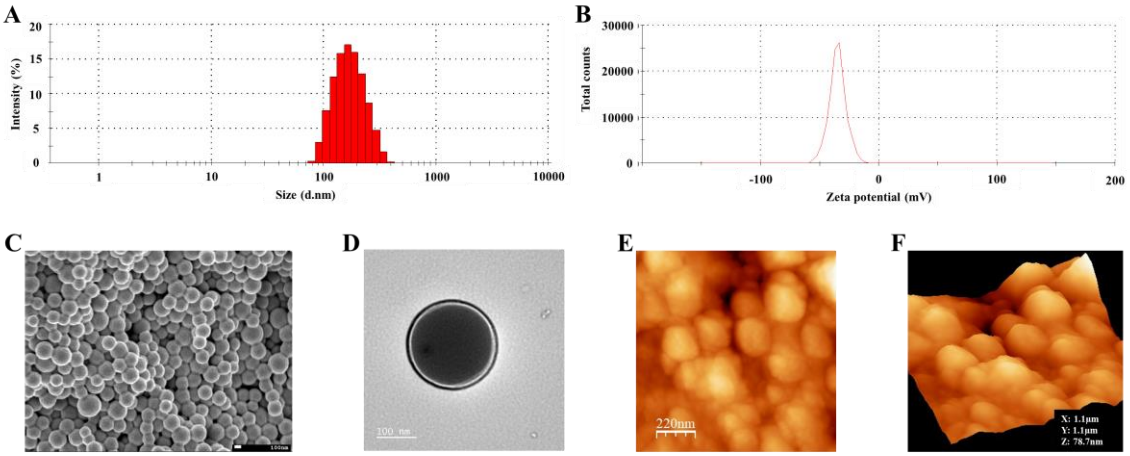

Figure 3.1. Characterization of MNPs in terms of particle size distribution (A), surface charge (B), FESEM image (C), TEM image (D) and AFM image, both 2D (E) and 3D (F) views.

FTIR spectroscopic investigations provided information regarding the compatibility and/or stability of Mgf with other formulation ingredients. FTIR spectra were documented for Mgf, PLGA, vitamin E-TPGS, their physical mixture, blank nanoparticles, and MNPs (Figure 3.2A). The spectra showed the characteristic peaks for Mgf at 3365 cm^{-1} due to OH-stretching of secondary hydroxyl groups, a peak at 2939 cm^{-1} due to C-H stretching, and the peak at 1651 cm^{-1} corresponding to conjugated carbonyl stretching. Peaks at 1620 cm^{-1}, 1492 cm^{-1}, and 1406 cm^{-1} indicate aromatic C=C ring-stretching; the peak at 1253 cm^{-1} correlates to ether-stretching, while the peak at 1097 cm^{-1} indicates C–O–C-stretching. FTIR spectrum of PLGA revealed the characteristic peaks at 3000–2947 cm^{-1} for C-H stretching bands. A peak at 1049 cm^{-1} corresponds to –OH bending vibrations. In the spectrum representing vitamin E-TPGS, peaks at 3415 cm^{-1} and 2868 cm^{-1} indicate terminal –OH function and –CH function stretching, respectively. The carbonyl band of vita min E-TPGS appears at 1732 cm^{-1}. Majority of the important peaks of Mgf, PLGA and vitamin E-TPGS are featured in the FTIR spectrum of the physical mixture, exhibiting only minor shifts. Certain physical interactions such as dipole–dipole

interaction, hydrogen bond formation and Vander-Waals force acting between the functional groups of Mgf and excipients might have led to the minor shifting of the peaks. The spectrum of blank nanoparticles exhibits major characteristic peaks of PLGA and vitamin E-TPGS. Similarly, the appearance of typical peaks of Mgf and excipients in the spectrum of prepared MNPs indicates the presence of Mgf without any major chemical interactions. XRD analysis detects the presence of crystalline properties of samples. Amorphous materials, like polymers, do not produce any sharp peaks, whereas sharp peaks with high intensity are observed with crystalline materials. XRD patterns of Mgf, PLGA, vitamin E-TPGS, their physical mixture, blank nanoparticles, and MNPs are depicted in Figure 3.2B. The XRD pattern for native Mgf displays distinct peaks free of distortions, indicating a crystalline nature. The absence of sharp peaks in the diffractogram of the polymer confirms its amorphous nature. Interestingly, the diffractogram corresponding to the physical mixture exhibited some distinct peaks; their positions suggested minimal to no interaction of Mgf with other components. The characteristic peaks of Mgf disappeared in the XRD pattern of MNPs, which might indicate transformation from crystalline to amorphous state while encapsulation during nanoparticle formation (Gaonkar et al., 2017). The DSC thermograms of Mgf, PLGA, vitamin E-TPGS, their physical mixture, excipient mixture (blank), and MNPs are depicted in Figure 3.2C. All of Mgf, polymer, and vitamin E-TPGS exhibited sharp endothermic peaks in their respective spectra at characteristic positions. The disappearance of the characteristic melting peak of Mgf in the DSC pattern of MNPs hints at the possibility of transformation of Mgf from crystalline to an amorphous disordered state during nanoencapsulation, thus promoting the stability of the formulation by inhibiting crystal growth (Ganguly et al., 2021). Findings from DSC studies in this regard conform to the observation from XRD analysis. Also, in the thermogram for MNPs, the endothermic peak is close to that of the native polymer, hinting that the polymer is not degraded during nanoparticulate structure formation.

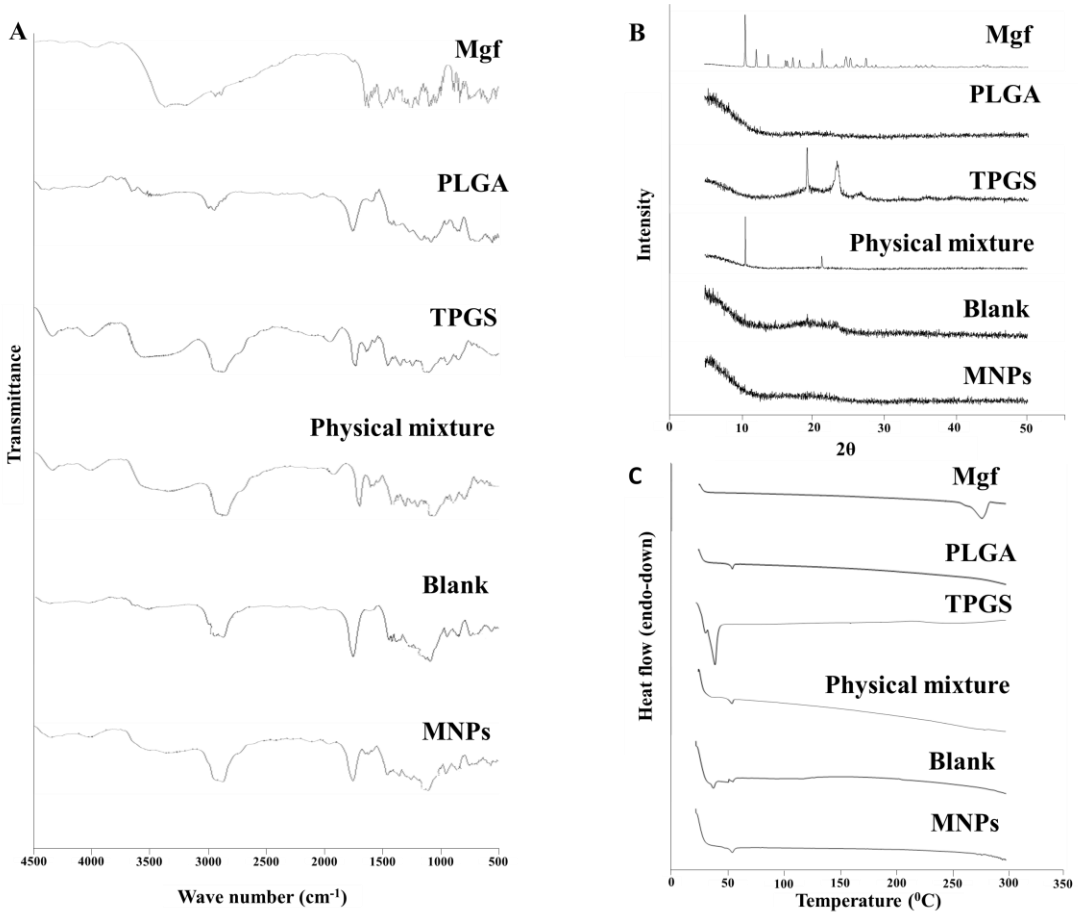

Figure 3.2. Physicochemical characterization of MNPs concerning FTIR spectra (A), XRD diffractograms (B) and DSC thermograms (C).

3.3.2. In vitro release kinetics

This study observed an initial rapid release of 38.13 ± 0.41% within the initial 6 h. The release rate was moderate up to 24 h, followed by a sustained release of Mgf up to 5 days, after which no noteworthy increment in the cumulative release of Mgf was noticed. Over a period of 5 days, 82.61 ± 1.51% Mgf was released (Figure 3.3A). The early burst might be attributed to Mgf loosely attached onto the surface and/or embedded within the surface layer of the polymeric matrix. Again, the persistent sustained release seems to result from diffusion of Mgf from the polymer shell possibly by virtue of either or more of erosion, swelling, and degradation of the polymer matrix (Gaonkar et al., 2017; Jabbari et al., 2018; Ghosh et al., 2023). Interestingly, the phasic behavior regarding release pattern potentially allows the formulated MNPs for fast onset of action besides serving as drug depot (Chatterjee et al., 2024).

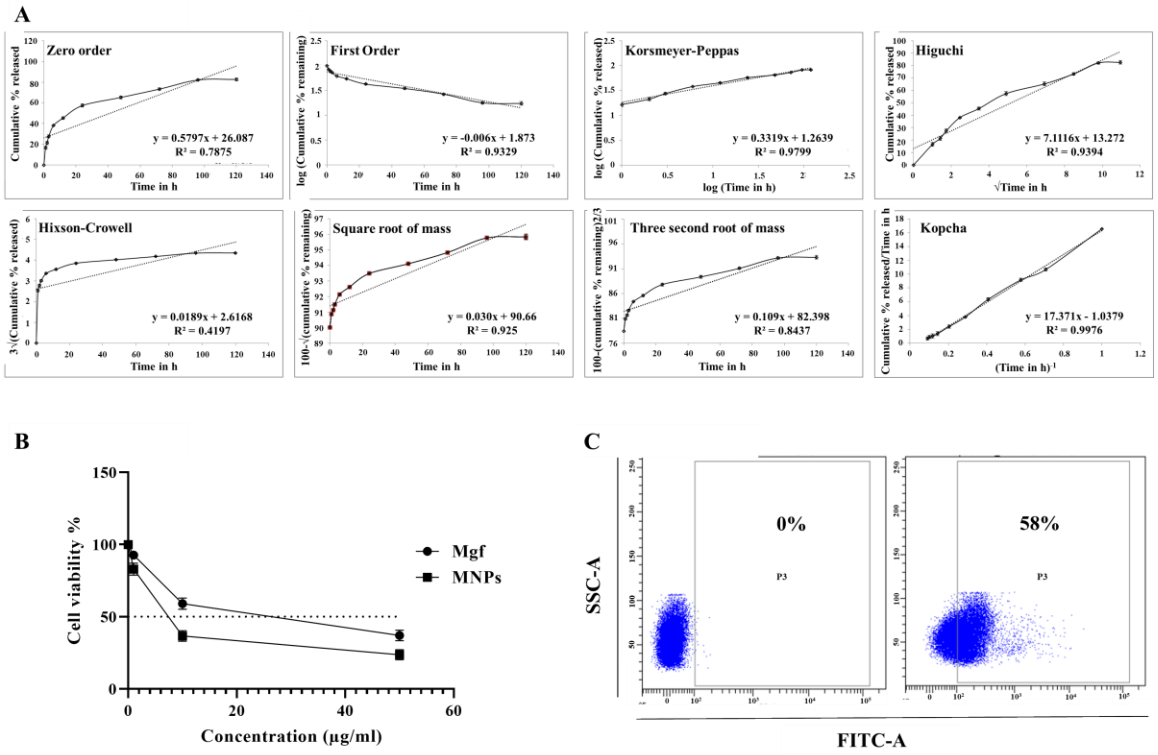

Figure 3.3. In vitro drug release pattern from MNPs (A), the effect of nanoencapsulation of Mgf on in vitro cell viability of MDA-MB-231 cells (B) and cellular uptake of MNPs by MDA-MB-231 cells (C). The values were expressed as mean ± SD (n = 3).

The in vitro release data obtained experimentally were fitted to mathematical models in order to examine the mechanistic pattern of Mgf release (Figure 3.3A). According to regression co-efficient (R^2) values, the Kopcha model emerged as the best fit, followed by Korsmeyer-Peppas release kinetics (Table 3.1). Kopcha plot computes the contribution of diffusion and erosion to the release pattern. Absolute values of diffusion and erosion constants suggested that diffusion dominates over erosion in the drug release (Rezk et al., 2019). Supporting this, the Korsmeyer-Peppas release exponent also hinted at Fickian diffusion to be the principal mechanism for Mgf release (Siepmann and Peppas 2001; Moodley and Singh 2020).

Table 3.1. In vitro pharmacokinetic modelling of MNPs.

Models	Equations	R^2 values
Zero order	y = 0.5797x + 26.087	0.7875
First order	y = -0.006x + 1.873	0.9329
Korsmeyer-Peppas	y = 0.3319x + 1.2639	0.9799
Higuchi	y = 7.1116x + 13.272	0.9394

Hixson-Crowel	y = 0.0189x + 2.6168	0.4197
Square root of mass	y = 0.030x + 90.66	0.9250
Three second root of mass	y = 0.109x + 82.398	0.8437
Kopcha	y = 17.371x - 1.0379	0.9976

3.3.3. Stability studies

The free-flowing powder of MNPs was stored at ~4 °C for 90 days. Prepared nanoparticles represented no major alterations in particle size and surface charge on storage (Table 3.2). Drug loading did not vary significantly (Table 3.2) between fresh and stored formulations, indicating stable nanoshells without leakage. Also, the FTIR spectrum (Figure 3.4A) did not exhibit any major changes from that of freshly prepared MNPs, hinting at decent stability of MNPs on storage.

Table 3.2. Parameters of MNPs regarding stability study.

Parameters	Freshly prepared	After 90 days at ~4 ºC
Particle size (nm)	162.5	164.2
Surface charge (mV)	-34.9	-33.4
Drug loading (%)	5.08 ± 0.49	5.03 ± 0.43

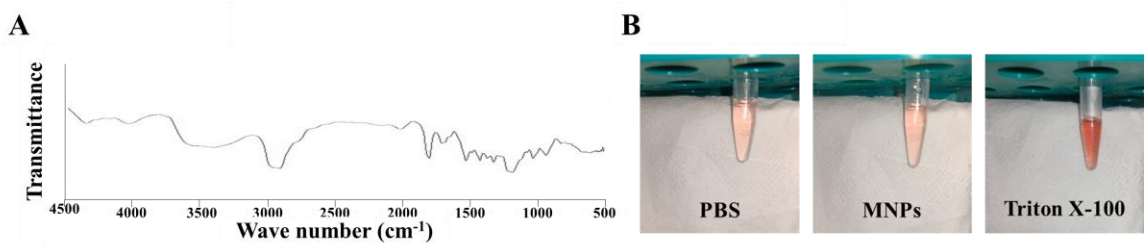

Figure 3.4. FTIR spectrum of MNPs after 90 days at ~4 ^{0}C (A) and photograph of one set of samples during hemolysis assay, captured just before spectroscopic measurement (B).

3.3.4. MNPs improve therapeutic efficacy in vitro

Cytotoxic potential is a primary feature of an anticancer candidate for chemotherapy. While evaluating the percentage viability of breast cancer cells, MTT assay discovered dose-dependent cytotoxicity on MDA-MB-231 cells. IC_{50} value of MNPs was found to be ~ 7.53 µg/mL while that of free Mgf was found to be ~ 27.03 µg/mL (Figure 3.3B). Clearly, MNPs exhibited better inhibition compared to free Mgf on cancer cells. Comparable IC_{50} values of MNPs were obtained for both types of breast cancer cells, i.e., MDA-MB-231 cells

(~7.53 µg/mL) and MCF-7 cells (~7.80 µg/mL). Cell viability of NKE cells remained above 50% at the experimental concentration range of MNPs, hinting at lower inhibition to normal cells.

Several studies claimed that Mgf induces the death of cancer cells by elevating oxidative stress and promoting apoptosis (Li et al., 2016; Du et al., 2018). The apoptotic potential of free Mgf and MNPs at equivalent effective concentrations was examined to reveal whether the nanoformulation development would impart any change in the cell death mechanism. MDA-MB-231 cells were treated with Mgf and MNPs at their respective IC_{50} concentrations. Cells exhibited a similar pattern of death induction (Figure 3.5A). However, the effectiveness of MNPs was achieved at much lower concentrations, which hints at improved apoptosis induction efficacy of nanoscale formulation containing Mgf. Treatment groups exhibited comparable intracellular ROS production in breast cancer cells (Figure 3.5B), indicating induction of oxidative stress as a primary mechanism for inducing cell death. Comparable intracellular ROS production achieved with nearly $1/4^{th}$ concentration of chemotherapeutic agent hints at superior efficacy of the nano scale delivery system. Regarding MMP, MNPs enhanced the FITC-positive cells which indicates increased depolarized mitochondria percentage and simultaneously decreased PE-positive cells (Figure 3.5C). Combining the observations, MNPs induce mitochondria-dependent apoptosis by virtue of elevating ROS production in breast cancer cells, which also conforms to earlier findings regarding the mechanism of action of Mgf (Li et al., 2016; Dutta et al., 2017). The superior efficacy of MNPs could well be associated with impressive cellular internalization of the nanoformulation (Figure 3.3C) such that an elevated amount of Mgf becomes available in the intracellular microenvironment to confer activities.

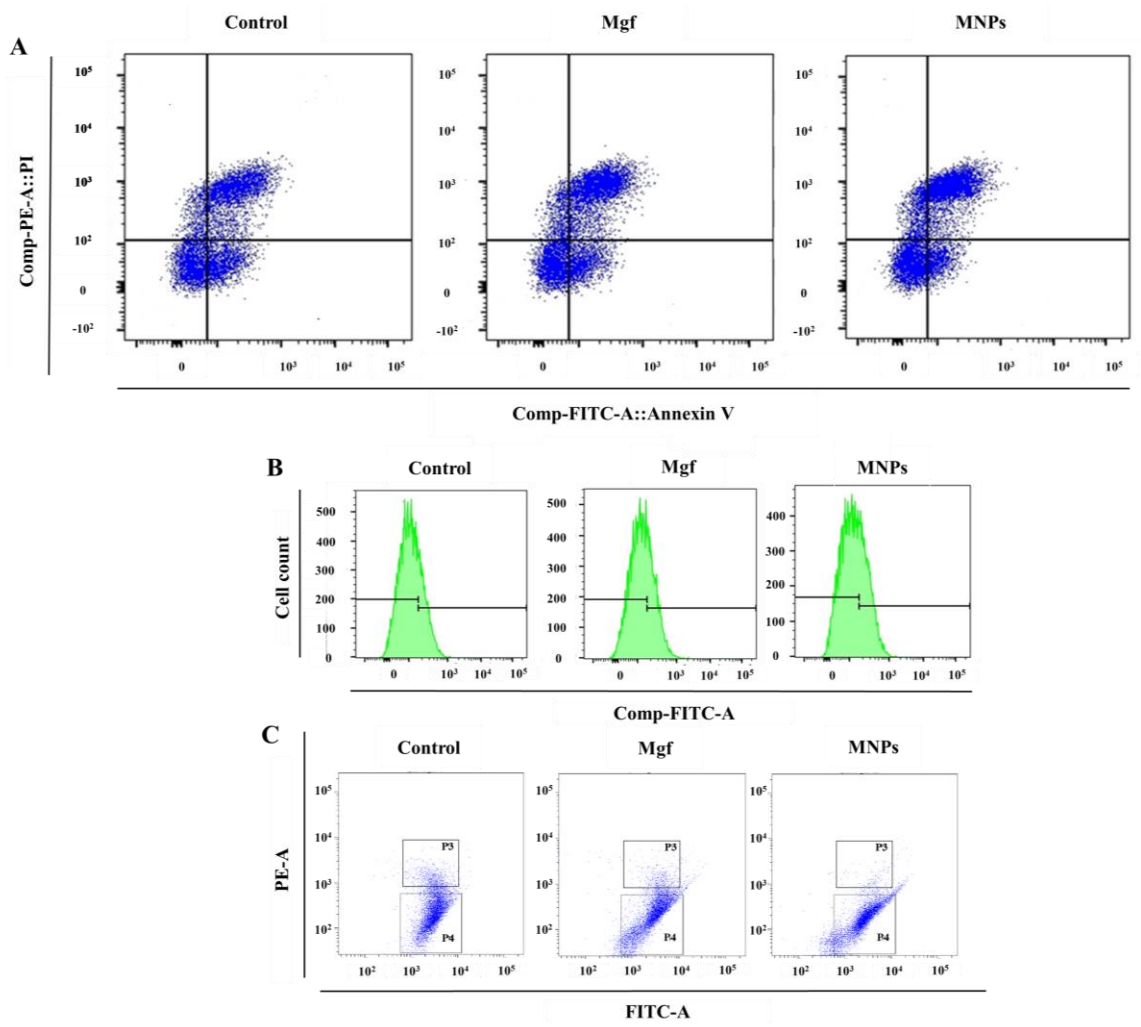

Figure 3.5. Effects of MNPs-treatment on the nature of cell death, accumulation of ROS, and MMP in MDA-MB-231 cells. (A) Analysis of apoptosis induced by Mgf and MNPs; (B) analysis of ROS accumulation; (C) effect on MMP.

3.3.5. Effect on hemolysis

Hematocompatibility is an important parameter for injectables, especially for intravenous route. In the present study, formulated MNPs exhibited negligible (Figure 3.4B) hemolytic activity (0.51 ± 0.03%) upon 1 h incubation. Results indicated that the formulated MNPs could be used safely in biological system (Mittal et al., 2019).

3.3.6. In vivo anti-tumor efficacy

MDA-MB-231 cells are considered among the most aggressive breast cancer cell lines (Azizi et al., 2017; Nirgude et al., 2020). Thus, it can be expected that a formulation displaying efficacy against these cells would be effective against breast cancer. In vitro assays served to gather some mechanistic insight regarding the efficacy of MNPs against breast cancer. The

undifferentiated EAC cells offer a rapid growth rate, good transplantation capability and high malignancy and virulence, making it suitable for chemotherapy-based in vivo assays (Ali et al., 2015).

Experimental mice belonging to diverse groups did not represent a notable variation regarding normal movement throughout. In tumor-bearing groups, induction of tumor was confirmed by visual inspection (Figure 3.6A). Throughout the treatment duration, the body weights of all the mice were observed every alternate day, whereby group II animals displayed the lowest body weight in contrast to higher body weights of other groups, especially groups I and V (Figure 3.7A). This difference might arise from lowered food intake as a consequence of tumor load in the body and allied discomfort. Upon sacrificing the animals, mammary pad tumors were isolated and examined for volume and mass. MNPs clearly exhibited superior anti-tumor activity evinced by the lowest tumor mass and volume in the animals of group IV among the tumor-bearing groups, followed by group III (free Mgf), whereas group II animals presented with the highest tumor load concerning mass and volume (Figure 3.6B; Figure 3.7B–D). Accumulation of Mgf in tumor tissues also corroborates the findings since group IV exhibits significantly higher accumulation from MNPs, compared to that in group III (Figure 3.7E). Thus, the lowest tumor load of group IV among tumor-bearing groups can be attributed to the highest accumulation of Mgf within tumor tissues (Figure 3.7E).

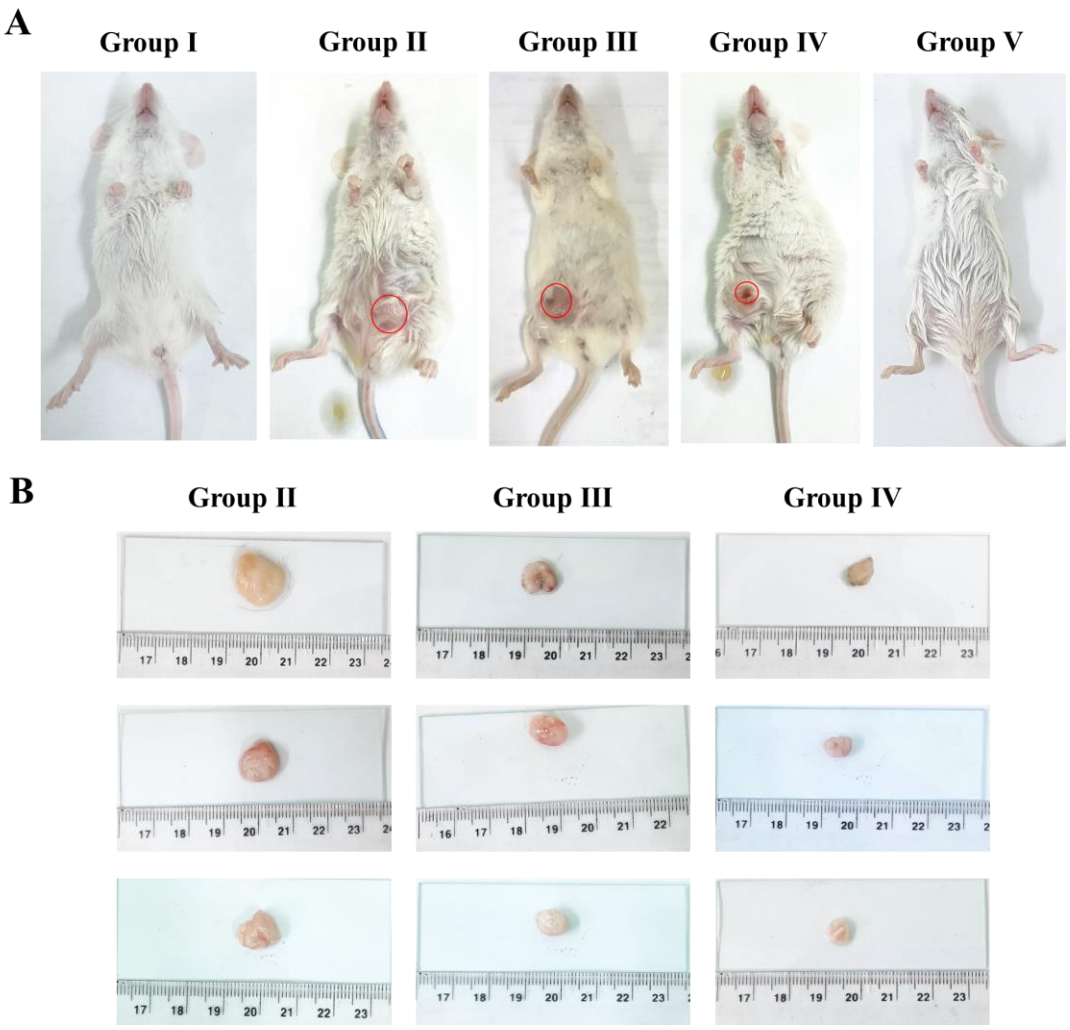

Figure 3.6. Representative images of tumor-bearing mice from each group (A, position of mammary-pad tumors are marked in red) and a full set of photographic images of mammary pad tumors dissected from tumor-bearing mice (B).

To further assess anti-tumor activity, dissected tumor tissues from tumor-bearing groups were stained with H&E and observed under a microscope (Figure 3.7F). In disease control mice (group II), high cellular intensity and compactness signify uncontrolled cell division, a typical characteristic of tumor tissue. In the Mgf treated group, void spaces indicative of cellular death have started to appear. In group IV (treated with MNPs), the packing density of cells loosened up further, aided by a higher abundance of void spaces. Cells in group IV showed more distinctive outlines compared to the disease-control group, and the tissue showed hints of regaining normalcy of breast tissue architecture. Immunohistochemical studies reassured the therapeutic impact of MNPs on tumors (Figure 3.7G). Group IV tumors exhibited the highest expression of

tumor suppressor protein p53, indicating superior therapeutic activity of MNPs. In line with the earlier findings, the immunohistochemical study also establishes the superior anti-tumor activity of MNPs. Infliction of oxidative stress is reassured by evaluating antioxidant markers in tumor tissues. MNPs significantly augmented the inhibitory effects on both SOD and CAT activities while downregulating GSH (Figure 3.7H–J), thereby indicating induction of oxidative stress (likely to lead to subsequent apoptotic cell death) in tumor tissues (Kannan and Jain 2000). In addition, the highest level of carbonylated protein was found in group IV tissues (Figure 3.7K), reinstating the previous findings regarding the infliction of oxidative stress. Thus, clearly, MNPs improve the in vivo efficacy of Mgf against breast cancer.

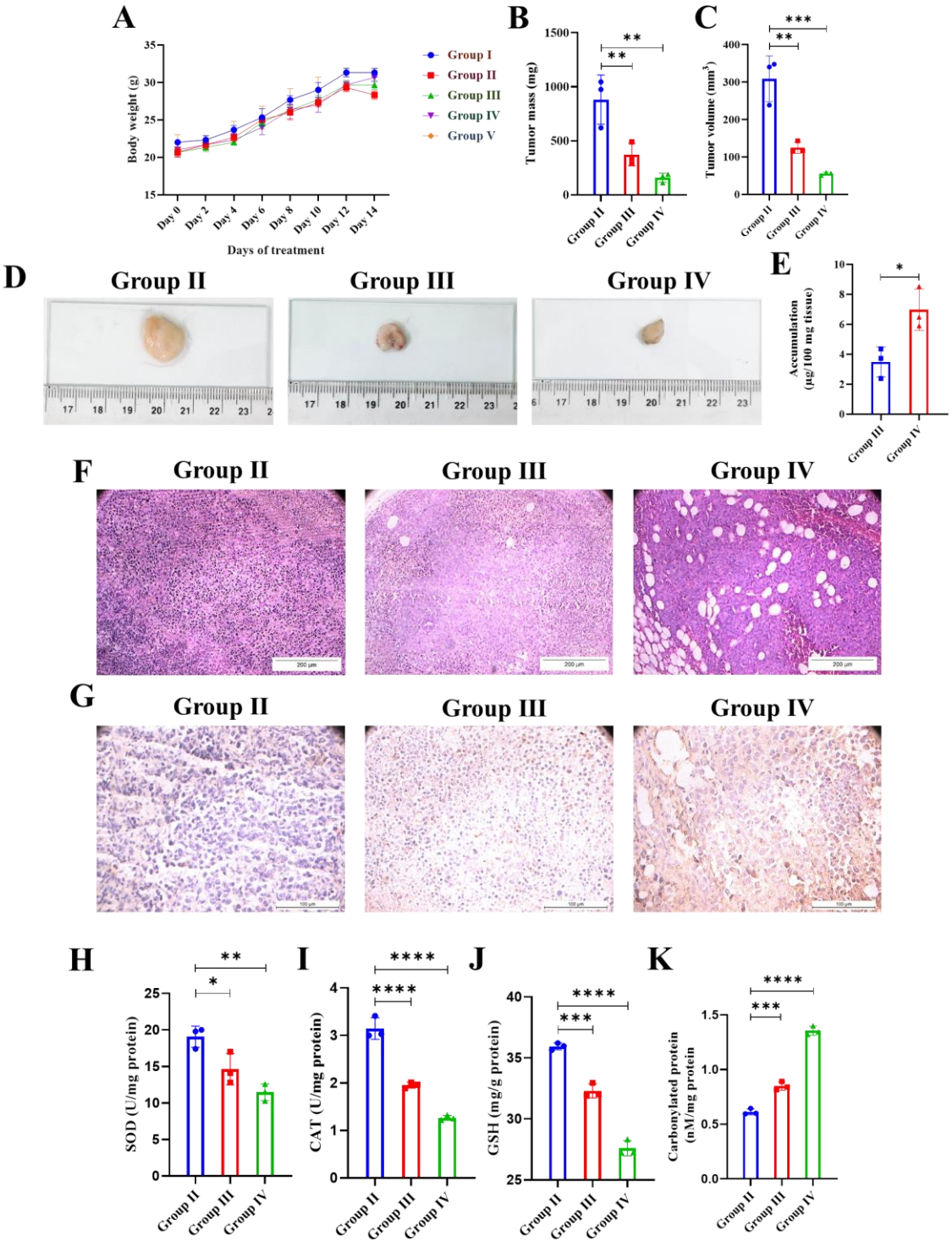

Figure 3.7. Anti-tumor effects of MNPs on breast tumor-bearing mice. (A) Body weight of mice belonging to different groups during treatment duration, (B) tumor mass and (C) tumor volume of different tumor-bearing groups, (D) Representative images of mammary pad tumors dissected

from experimental tumor-bearing mice, (E) tissue accumulation of Mgf in treatment groups, (F) H&E-stained histological sections of tumor tissues, (G) immunohistochemical detection of p53 expression in tumor tissue sections and the effects on tumor tissues receiving different treatments regarding endogenous antioxidant parameters, such as (H) SOD, (I) CAT and (J) GSH and (K) protein carbonylation. Graphical data were expressed as mean ± SD (n = 3). *Values signify $p < 0.05$; **values signify $p < 0.01$; ***values signify $p < 0.001$; ****values signify $p < 0.0001$.

3.3.7. Effects on systemic toxicity

A proper balance between therapeutic and toxicological outcomes of any treatment module is a crucial parameter to evaluate its applicability towards pharmacological utilization. To assess any probable systemic toxicities of the prepared nanoformulation at the applied dose, levels of renal and hepatic biomarkers in blood were examined, as well as H&E-stained tissue sections of vital organs from experimental animals were also analyzed. Figure 3.8A clearly indicates that induction of tumor leads to hepatic abnormality characterized by sharp increments in ALP and ALT values of group II animals compared to normal controls. The levels of hepatic biomarkers seem to reduce among different treatment groups, thus indicating no additional toxicity and/or side effects to the liver arising from experimental chemotherapeutic regimens (Guruswamy et al., 2020). Both hepatic and renal parameters, i.e., ALP, ALT, BUN, and creatinine (Figure 3.8A) did not differ significantly between group I and group V, hinting at the absence of hepatotoxicity and nephrotoxicity imposed by nanoparticles during the period of treatment. Tumor induction and progress seem to disrupt the normalcy of liver tissue, as indicated by the elongation of the portal vein and vacuolated cytoplasm in group II (Figure 3.8B). This is probably a result of the EAC-induced generation of ROS, as well as the downregulation of antioxidants. However, hepatic tissue gradually displays lower abnormality along with gradual reduction of tumor load among different experimental groups. Anti-tumor therapy might well have replenished the antioxidant defense system, consequently reducing ROS production and leading to hepatoprotection (Bhattacharyya et al., 2007). Renal tissues did not represent major alterations among experimental groups (Figure 3.8B). Cardiac tissues seem to remain unaffected by tumor induction and by nanoparticles treatment, retaining normal tissue characteristics across all the groups (Figure 3.8B). These observations are in line with earlier findings in this regard (Ali et al., 2015; El-Sisi et al., 2020; Alkhatib et al., 2021). Tumor load seems to affect splenic tissue to some extent; however, the spleen images represent reduced abnormality correlating with a reduction in tumor load by means of anti-tumor therapy in treatment groups (Figure 3.8B) (Sadhukhan et al., 2019; Guruswamy et al., 2020). The apparent absence of MNPs-induced

apoptotic cascade might also hint at insignificant localization in tissues other than tumor tissues. Interestingly, the fact that none of the organs exhibits any abnormality in tissue architecture of group V animals further supports the prepared nanoparticles somewhat as a safe choice for chemotherapy.

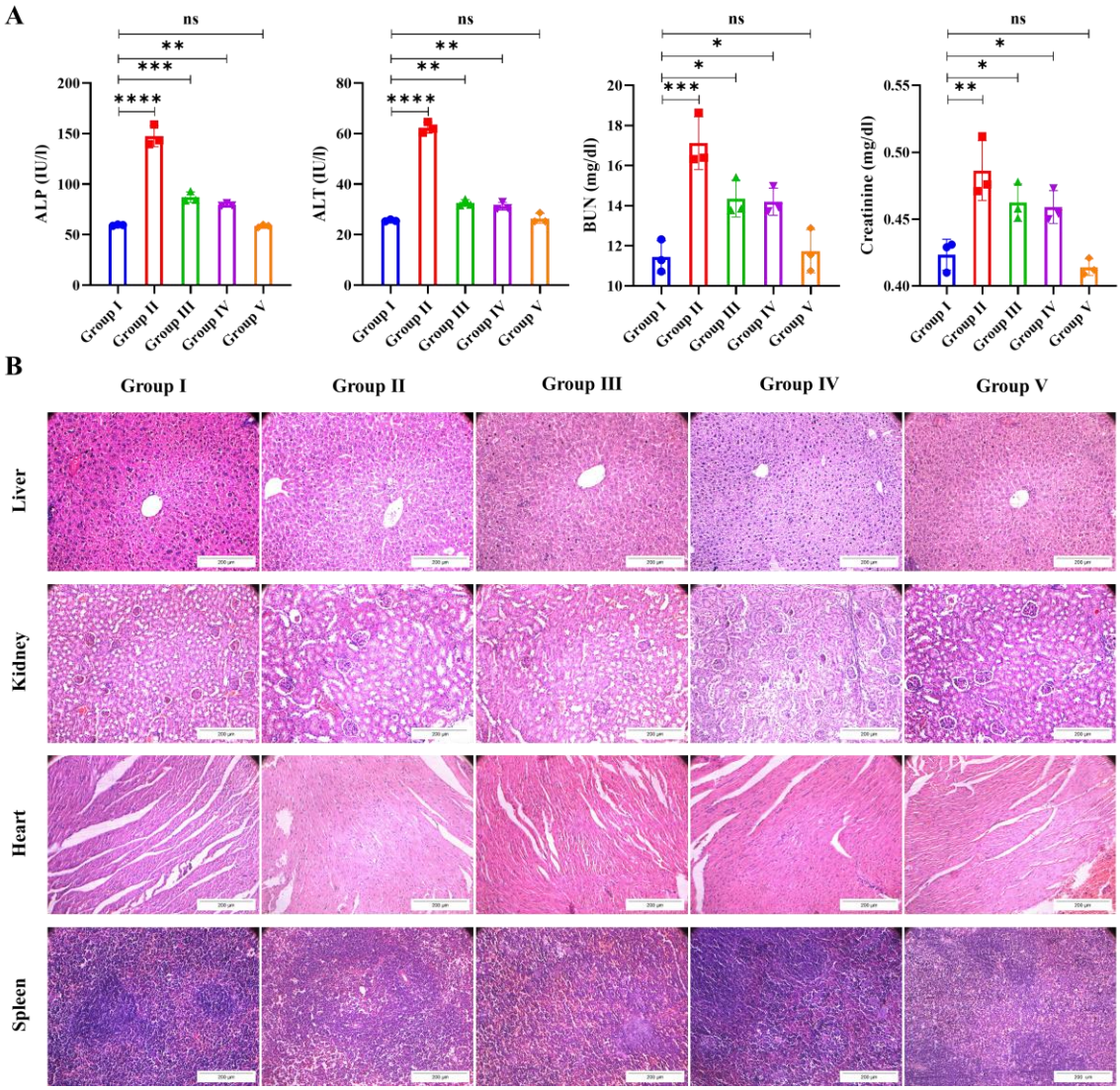

Figure 3.8. Safety profile of formulated MNPs. (A) Serum biochemical parameters regarding hepatic and renal biomarkers of different experimental groups and (B) H&E-stained histological sections of the liver, kidney, heart, and spleen of different experimental groups. Graphical data were expressed as mean ± SD (n = 3). *Values signify $p < 0.05$; **values signify $p < 0.01$; ***values signify $p < 0.001$; ****values signify $p < 0.0001$; ns, insignificant.

3.4. Concluding remarks

Current study produced stable, well-characterized nanoparticles with substantial loading and a satisfactory release profile of Mgf. MNPs conferred anticancer effects on breast cancer. Mgf imparts death to cancer cells by elevating pro-oxidative stress and endorsing apoptosis via modulating MMP. MNPs inflicted comparable anticancer effects in vitro at nearly 1/4th of the concentration of free Mgf. Hence, MNPs can be attributed to improving chemotherapeutic efficacy against breast cancer cells. PLGA nanoparticles tend to ensure improved cancer cell penetration, making it possible to achieve similar cytotoxic effects at much lower concentrations. In vivo observations ascertain that MNPs retain efficacy in animal systems, also, thus igniting the possibilities of utilization of Mgf in cancer therapeutics, overcoming its unfavorable biopharmaceutical attributes. EPR effect can be attributed to the localization of MNPs at tumor vicinity, upon cellular internalization, they release Mgf in the intracellular microenvironment (Figure 3.9).

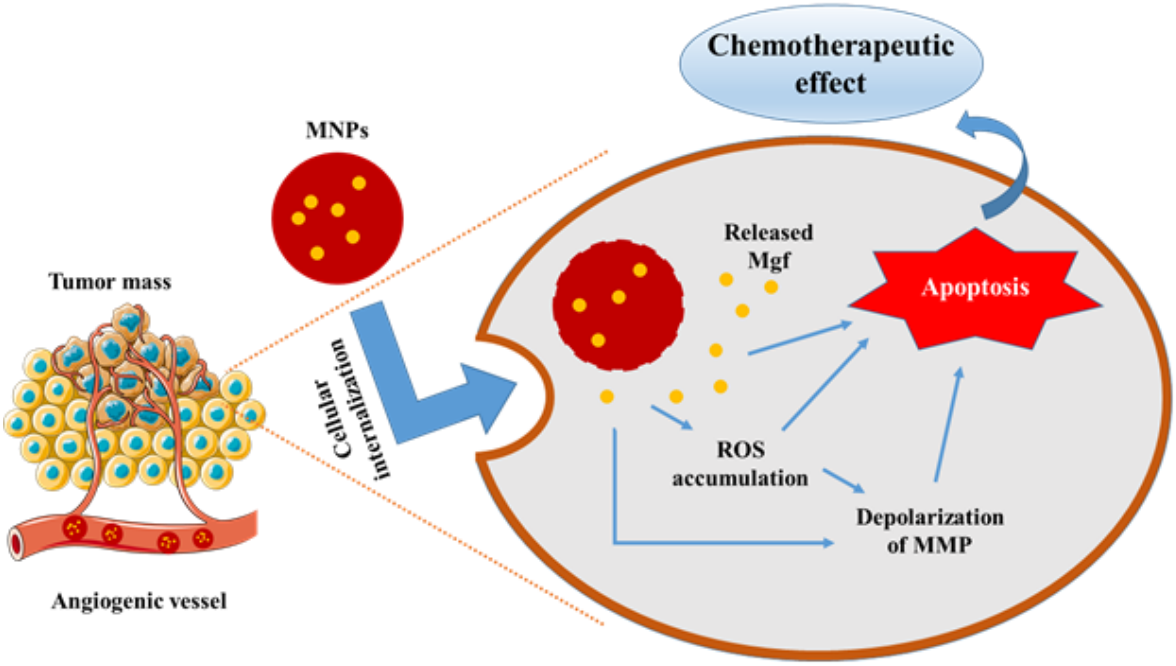

Fig 3.9. Schematic representation of anti-tumor potential of MNPs. Mgf, Mangiferin; MMP, mitochondrial membrane potential; MNPs, Mgf-containing PLGA-based nanoparticles; ROS, Reactive oxygen species.

MNPs significantly endorsed tumor reduction by improving the accumulation of Mgf within tumor tissue as well as by elevating the cellular uptake in breast cancer cells.

During in vivo preclinical assays, MNPs could significantly minimize tumor load compared to native Mgf along with a promising safety profile. Hence, MNPs might well lead to an answer to the limitations regarding futuristic therapeutic translation of plant-derived small molecule, i.e., Mgf, as well as to the search for a safe and efficacious chemo therapeutic modality against breast cancer. However, more detailed in vitro and in vivo correlation studies, such as in vivo pharmacokinetic profile in biological systems, comparative localization of Mgf in tumor tissue and other vital organs, etc., can be intriguing segments for research before probable translation from preclinical to clinical stage in future.

Chapter 4

Galactose-conjugated PLGA nanoparticles improve the therapeutic efficacy of Mgf against hepatocellular carcinoma by active targeting

4.1. Background

Incidence of hepatocellular carcinoma has emerged as a leading cause of cancer-associated fatalities worldwide (Li et al., 2016a). Several biochemical pathways are altered during the development of hepatocellular carcinoma, resulting in the sequential conversion of normal hepatocytes into malignant hepatocytes with the acquisition of numerous neoplastic traits including uncontrolled cell proliferation, dysfunction of the cellular death signaling mechanism, promotion of angiogenesis, metastasis and chemoresistance (Trachootham et al., 2009; Chakraborty et al., 2020). High recurrence and aggressive tumor growth result in a poor prognosis for the disease. Low survival rates further enhance the complexity regarding hepatocellular carcinoma. Life expectancy depends upon multiple factors such as tumor stage, overall liver health status and individual response to treatment attempts. Poor prognosis enhances the difficulty regarding recovery from the disease, often leaving chemotherapy as the sole treatment option. Hence, one of the main requirements for its therapeutic management is the delivery of chemotherapeutic agents in a target-specific manner. Mgf, a bioactive polyphenol, offers promise regarding anticancer chemotherapy, especially when delivered using a suitable formulation system (Pan et al., 2014; Zhou et al., 2022; Fabián et al., 2023). Polymeric nanoparticles have gained widespread attention for cancer therapeutics mainly due to their ease of synthesis, biocompatibility, prolonged, controllable circulation time, minimal toxicity and remarkable ability to adsorb and/or encapsulate therapeutic agents (Paul et al., 2021). They can deliver diverse chemotherapeutic agents while offering a high surface-to-volume ratio. PLGA, a copolymer of lactides and glycolides, is approved by multiple drug regulatory agencies. PLGA-based nanoparticles are capable of encapsulating poorly soluble agents. Galactose, a sugar moiety, can be recognized by asialolycoprotein receptors, which are abundantly expressed by hepatocytes. Since galactose can be detected by asialoglycoprotein receptors prevalent in liver cells (Figure 4.1), galactosylation of polymer can potentially enhance liver targeting efficiency (Ganguly et al., 2021). The present study aimed to formulate galactose-decorated PLGA nanoparticles carrying Mgf (MGNPs) and assess the efficacy of the same against hepatocellular carcinoma. Mgf-loaded nanoparticles using plain PLGA (MPNPs) were also prepared, and efficacy and safety profiles of MGNPs, MPNPs and free Mgf were compared through relevant preclinical assays.

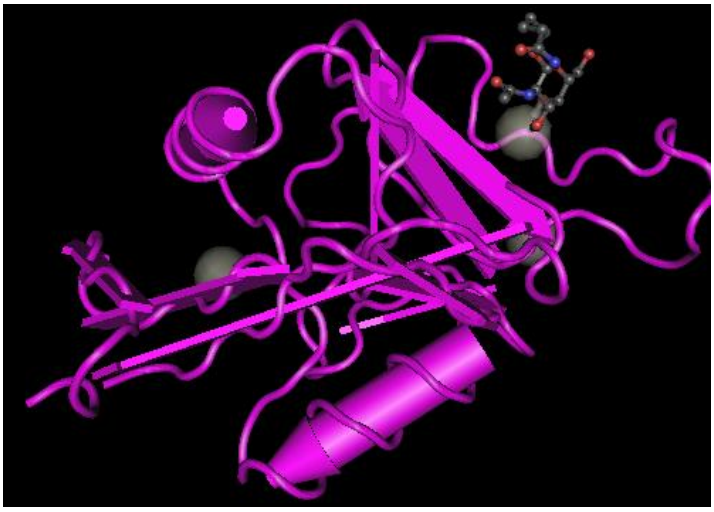

Figure 4.1. Crystal structure of asialoglycoprotein receptor 1 in complex with N-acetylgalactosamine azide unit. (Extracted from PDB ID 6YAU).

4.2. Materials and methods

4.2.1. Key materials

Mgf (CAS No. 4773–96-0), PLGA ((L/G molar ratio 85:15, MW 50,000–75,000), and N-Nitrosodiethylamine (DENA) were purchased from Sigma-Aldrich, St. Louis, USA. Hydroxypropyl methyl cellulose (HPMC) was obtained from HiMedia Laboratories, Mumbai, India. D-galactose was obtained from Sisco Research Laboratories, Mumbai, India. HepG2 cells were obtained from the National Centre for Cell Science, Pune, India. Culture medium and MTT were purchased from HiMedia Laboratories, Mumbai, India. Serum assay kits were obtained from Transasia Bio-medicals Limited, Solan, India, and Span Diagnostics Limited, Mumbai, India. Primary antibody was obtained from Biobharati Life Science, Kolkata, India (p53, #BB-AB0100). The immunohistochemistry kits were purchased from Abcam, MA, USA.

4.2.2. Galactose conjugation of PLGA

Synthesis of galactosylated PLGA (Gal PLGA) was conducted by the method described earlier (Ganguly et al., 2021). Initially, methane sulfonic acid (4 µL) was added to a solution of galactose in dimethylformamide (1 mg/mL, 10 mL) with continuous stirring for 5 min. Then, PLGA (200 mg) was added and stirred for 24 h, maintaining the temperature at ~60 °C. On the next day, ice-cold distilled water was introduced into the reaction mixture, and the synthesized polymer was separated by centrifugation (Hermle refrigerated centrifuge, Wehingen, Germany) at 12,000 rpm for 45 min. The obtained pellet was washed repeatedly using water before lyophilization (LaboGene Scanvac Coolsafe, Bjarkesvej, Denmark) to yield Gal PLGA. Further,

samples from the obtained product and native polymer were subjected to ^{1}H nuclear magnetic resonance (NMR) spectroscopic analysis (Bruker 400 MHz Avance NEO spectrometer, MA, USA) to assess galactosylation of PLGA.

4.2.3. Preparation of nanoparticles

Mgf-loaded nanoparticles were formulated by the means of the emulsion solvent evaporation technique. PLGA and Mgf were dissolved in dichloromethane and ethanol (3:1). Three different Mgf: PLGA ratios (1:5, 1:10 and 1:20) were used to prepare three batches of nanoformulations. In each case, the dispersion was added dropwise to aqueous HPMC (0.3% w/v) solution, and homogenized for 5 min at 20,000 rpm (IKA Ultra Turrax T-10 Basic, Staufen, Germany). After the addition of the organic phase, the aqueous phase immediately turned milky due to the formation of nanoparticles. To reduce particle size further, it was sonicated using bath sonication for 1 h, maintaining ice-cold temperature, followed by evaporation of organic solvents overnight. The colloidal dispersion was then centrifuged using a high-speed refrigerated centrifuge (Hermle refrigerated centrifuge, Wehingen, Germany) at 3000 rpm for 10 min to segregate larger particles, and the supernatant so obtained was again centrifuged at 16,000 rpm for 45 min. Finally, the pellet obtained was collected after repeated washing and lyophilized (LaboGene Scanvac Coolsafe, Bjarkesvej, Denmark). To formulate MGNPs, plain PLGA was replaced with Gal PLGA, followed by an identical procedure. Following a similar protocol, blank nanoparticles were also synthesized.

4.2.4. Characterization of prepared nanoparticles

Average particle size and PDI of both MPNPs and MGNPs were discovered utilizing Malvern Zetasizer Nano-ZS (Malvern Instruments, Malvern, Worcestershire, UK), as per the concept of DLS using dilutions of respective samples. Using the same instrument, the zeta potential of MPNPs and MGNPs was also measured at 25 °C. The shape and surface morphology of the two types of nanoparticles were examined using FESEM (JEOL JSM-7600F, Tokyo, Japan). Particle structures were evaluated by TEM (JEOL JEM-2100Plus, Tokyo, Japan).

Physicochemical compatibility of Mgf with other formulation components was examined using FTIR spectroscopy (IR Prestige-21, Shimadzu, Kyoto, Japan) and XRD (Ultima III, Rigaku, Japan). Drug loading percentage and entrapment efficiency were evaluated utilizing spectrophotoetric technique with the help of a JASCO V-550 double beam UV–visible spectrophotometer (OK, USA).

4.2.5. Stability study

To assess the long-term stability of MGNPs, lyophilized nanoparticles were preserved at ~4 ºC for 90 days. Upon completion of the stipulated period, the nanoparticles were evaluated for particle size distribution, surface charge, and drug loading.

4.2.6. In vitro drug release kinetics

In vitro release patterns of Mgf from MPNPs and MGNPs were evaluated individually in PBS (pH 7.4). PBS is an isotonic physiologic solution mimicking extracellular fluid. It imitates the pH, ionic concentration and osmolarity of blood to a large extent. Therefore, it is widely used to study release kinetics in vitro. Developed nanoparticles were dissolved in PBS (1 mg/mL) and stirred continuously at 100 rpm at a temperature of ~37 °C. At preselected time intervals, 2 mL release medium was taken out from the system and centrifuged, and the supernatant was collected for spectroscopic analysis. Meanwhile, the pellet was redissolved in an equal volume of fresh PBS and transferred back to continue the process, maintaining sink conditions. The collected supernatant was analyzed spectroscopically (JASCO V-550 double beam UV–visible spectrophotometer, OK, USA) at 258 nm to measure the released Mgf. The procedure was performed in triplicate.

Multiple mathematical models were utilized to anticipate the manner/mechanism of Mgf release from the nanoparticles. The obtained data were fitted into different kinetic equations to explore the mechanistic pattern regarding the release of Mgf from polymeric matrices.

4.2.7. Cell-based in vitro assays

HepG2 hepatocellular carcinoma cells were cultured in Eagle's minimum essential medium supplemented with 10 % FBS and antibiotic solution (Hi-Media, Mumbai, India). The cells were maintained at a condition of 90 % humidity, 5% CO_2 and 37 ºC temperature. HepG2 cells originate from liver cancer tissue of human. This immortal cell line is widely utilized in cancer research, among others, to study the biological aspects of hepatocellular carcinoma under an in vitro setup.

4.2.7.1. Cytotoxicity assay

To perform cytotoxicity assay, ~1 x 10^4 cells/well were seeded in a 96-well plate followed by 24 h incubation. The cells were then incubated with Mgf, MPNPs and MGNPs, separately, in a concentration gradient of 0-100 µg/mL for 24 h. After the treatment, cells were subjected to MTT and incubated for 4 h. Finally, the insoluble formazan was solubilized in DMSO, and the absorbance was measured at 450 nm.

4.2.7.2. In vitro cellular uptake

To evaluate intracellular uptake, HepG2 cells were incubated for 24 h and then treated with native Mgf, MPNPs and MGNPs (IC_{50} equivalent doses of Mgf). Subsequently, cells were lysed, followed by spectroscopic analysis of cell homogenates, to assess Mgf present in the cells. This study aims to provide a comparative idea of the localization of Mgf within cancer cells.

4.2.7.3. Hoechst nuclear staining

HepG2 cells (~2 x 10^3) were transferred to the wells of a 96-well culture plate and incubated at 37 ºC and 5 % CO_2. Cells were then treated with MGNPs, MPNPs and native Mgf. Following treatment, cells were incubated for 24 h under identical conditions. A set of untreated HepG2 cells served as a control. Finally, cells were stained using Hoechst 33258 (5 µg/mL in PBS) according to established protocol, and counts and patterns of nuclei were observed in a fluorescent microscope.

4.2.7.4. Intracellular levels of antioxidants

To assess the antioxidant enzyme activity levels in the cellular milieu following treatment with MGNPs, MPNPs and Mgf, intracellular levels of CAT, SOD and GSH were determined following established protocols (Murthy and Narsaiah, 2021).

4.2.8. Experiments involving animals

In the study, 2–3-week-old male Swiss albino mice were used. Animals were acclimatized for 14 days in a 12 h light/dark cycle while providing water and food ad libitum. The mice were kept under cautious monitoring throughout the entire study duration. The study has been carried out according to the guidelines of the IAEC of Jadavpur University, Kolkata, India, vide certificate proposal no. JU/IAEC-25/86 dated 16.01.2025.

4.2.8.1. Evaluation of anti-tumor efficacy in vivo

To assess the in vivo effect of the developed nanoparticles, i.e. MPNPs and MGNPs, a mouse model of hepatocellular carcinoma was utilized (Sur et al., 2016; Sarkar et al., 2023). Briefly, 12 mice were randomly arranged into four groups (n=3 in each group), and induced with hepatocellular carcinoma. Mice were injected intraperitoneally with CCl_4 (50 µL/kg body weight) thrice in a week, followed by intraperitoneal administration of DENA 75 mg/kg once weekly for three weeks and 100 mg/kg once weekly for another three consecutive weeks. The mice were not allowed to consume food or water for 1 h pre- and post-DENA administration. Animals were monitored undisturbed before initiating the chemotherapeutic regimen. The control group was treated with PBS while other groups received Mgf (10 mg/kg), MPNPS (equivalent to 10 mg/kg Mgf), and MGNPs (equivalent to 10 mg/kg Mgf) via the intraperitoneal route every alternate day

for two weeks. After completion of the treatment period, animals were sacrificed, blood samples were collected, and livers were excised and preserved for subsequent analyses.

The extent of accumulation of Mgf within liver tissues was evaluated quantitatively by HPLC (Dionex Ultimate 3000, Dionex, Idstein, Germany) utilizing a C-18 column (250 × 4.6 mm, particle size 5 µm; Thermo Scientific™ Hypersil GOLD™, MA, USA) and a UV detector. Accurately weighed tissue samples from each group were homogenized individually in a solution containing methanol (75%) and DMSO (0.05%). The mixture was then centrifuged at 10,000 rpm for 15 min. Supernatant was collected, filtered (0.45 µm) and analyzed chromatographically. Aliquots of the filtrate (injection volume 20 µL) were eluted with an isocratic mobile phase comprising formic acid (0.1%) and acetonitrile at a ratio of 87:13, flowing at 1.5 mL/min, and detection wavelength set at 258 nm (Naveen et al., 2017).

For histological observations, hepatic tissue sections from experimental animals were stained with H&E to study the histological changes using a bright field light microscope under 20x objective magnification (Leica Microsystems, Wetzlar, Germany).

Sections of liver tissues were subjected to immunohistochemical staining to assess the localized expression profile of p53. Following standard protocol, tissue sections on charged slides were incubated with anti-p53 antibody (Biobharati LifeScience, Kolkata, India, #BB-AB0100) at an appropriate dilution. Slides were then exposed to HRP-conjugated secondary antibody. DAB was introduced to serve as a substrate for HRP. Hematoxylin served as a counterstain in the experiment to aid in visualizing the nuclei. Slides were mounted in DPX prior to observing in a bright field light microscope at 40x objective magnification (Leica Microsystems, Wetzlar, Germany).

4.2.8.2. Assessment of systemic toxicity in vivo

For the simultaneous evaluation of systemic toxicity, 12 mice were randomly allocated to four groups (n = 3 in each group). The control group received PBS while other groups were treated with Mgf (10 mg/kg), MPNPS (equivalent to 10 mg/kg of Mgf), and MGNPs (equivalent to 10 mg/kg of Mgf), respectively, via the intraperitoneal route every alternate day for two weeks. After completion of the treatment period, mice were sacrificed, blood samples were collected to assess serum biochemical markers, and organs, namely the kidney, heart and liver, were excised and preserved for histological analysis. Serum markers were analyzed using commercially available kits following the respective manufacturers' protocols. The histological sections (H&E-stained) of the organs of different experimental groups were observed using a bright field microscope (Leica Microsystems, Wetzlar, Germany) at 20x objective magnification.

4.2.9. Data analyses

Experiments were carried out in triplicate, and resultant data were represented as mean ± SD. Statistical analyses of experimental data were conducted by the use of GraphPad Prism. Statistical analyses involved ANOVA, Dunnett's test and t-test; statistical significance was designated as p-value < 0.05.

4.3. Results and discussions

4.3.1. Galactosylation of PLGA

Native PLGA and Gal PLGA were subjected to proton NMR spectroscopy. The ^{1}H NMR spectrum of PLGA exhibited chemical shifts at 1.55, 4.82 and 5.22 ppm corresponding to $–CH_3$, $–CH_2$ and –CH groups, respectively, of the PLGA structure (Raposo et al., 2020). Galactosylation was confirmed with the appearance of an additional peak at 4.2 ppm due to the galactose moiety (Ganguly et al., 2021).

4.3.2. Physicochemical compatibility

FTIR spectroscopic investigations provided information regarding the compatibility and/or stability of Mgf with other formulation ingredients. FTIR spectra were documented for Mgf, PLGA, HPMC, their physical mixture, blank nanoparticles, Gal PLGA, MPNPs and MGNPs (Figure 4.2A). The spectrum of Mgf displayed the characteristic peaks at 3368 cm^{-1} due to OH-stretching of secondary hydroxyl groups, a peak at 2940 cm^{-1} due to C-H stretching and a peak at 1651 cm^{-1} corresponding to conjugated carbonyl stretching. Peaks at 1620 cm^{-1}, 1493 cm^{-1} and 1406 cm^{-1} indicate aromatic C=C ring-stretching; peak at 1254 cm^{-1} correlates to ether-stretching while peak at 1098 cm^{-1} indicates C–O–C-stretching. FTIR spectrum of PLGA revealed the characteristic peaks at 2992–2947 cm^{-1} for C-H stretching and 1749 cm^{-1} for the C–O stretching band of ester. A peak at 1051 cm^{-1} corresponds to –OH bending vibrations. Gal PLGA also represented such peaks with only minor shifts. The majority of the important peaks of Mgf, PLGA and HPMC featured in the FTIR spectrum of the physical mixture, exhibiting only minor shifts. Certain physical interactions, such as dipole–dipole interaction, hydrogen bond formation, and van der Waals force acting between the functional groups of Mgf and excipients, might have led to the minor shifting of the peaks. Similarly, the appearance of typical peaks of Mgf without major changes, in the spectra of prepared MPNPs and MGNPs, ensures the presence of Mgf without any major chemical interactions. XRD analysis detects the presence of crystalline properties of samples. Amorphous materials, like polymers, do not produce any sharp peaks, whereas sharp peaks with high intensity are observed with crystalline materials. XRD patterns of Mgf, PLGA, HPMC, their physical mixture, blank nanoparticles, Gal PLGA, MPNPs and

MGNPs are shown in Figure 4.2B. The XRD pattern for native Mgf displays distinct peaks free of distortions, indicating a crystalline nature. The absence of sharp peaks in the diffractograms of polymers confirms their amorphous nature. The diffractogram corresponding to the physical mixture exhibited few distinct peaks; their positions suggested minimal to no interaction of Mgf with other components. The characteristic peaks of Mgf almost disappeared in the XRD pattern of nanoparticles, hinting at transformation from crystalline to amorphous state during encapsulation.

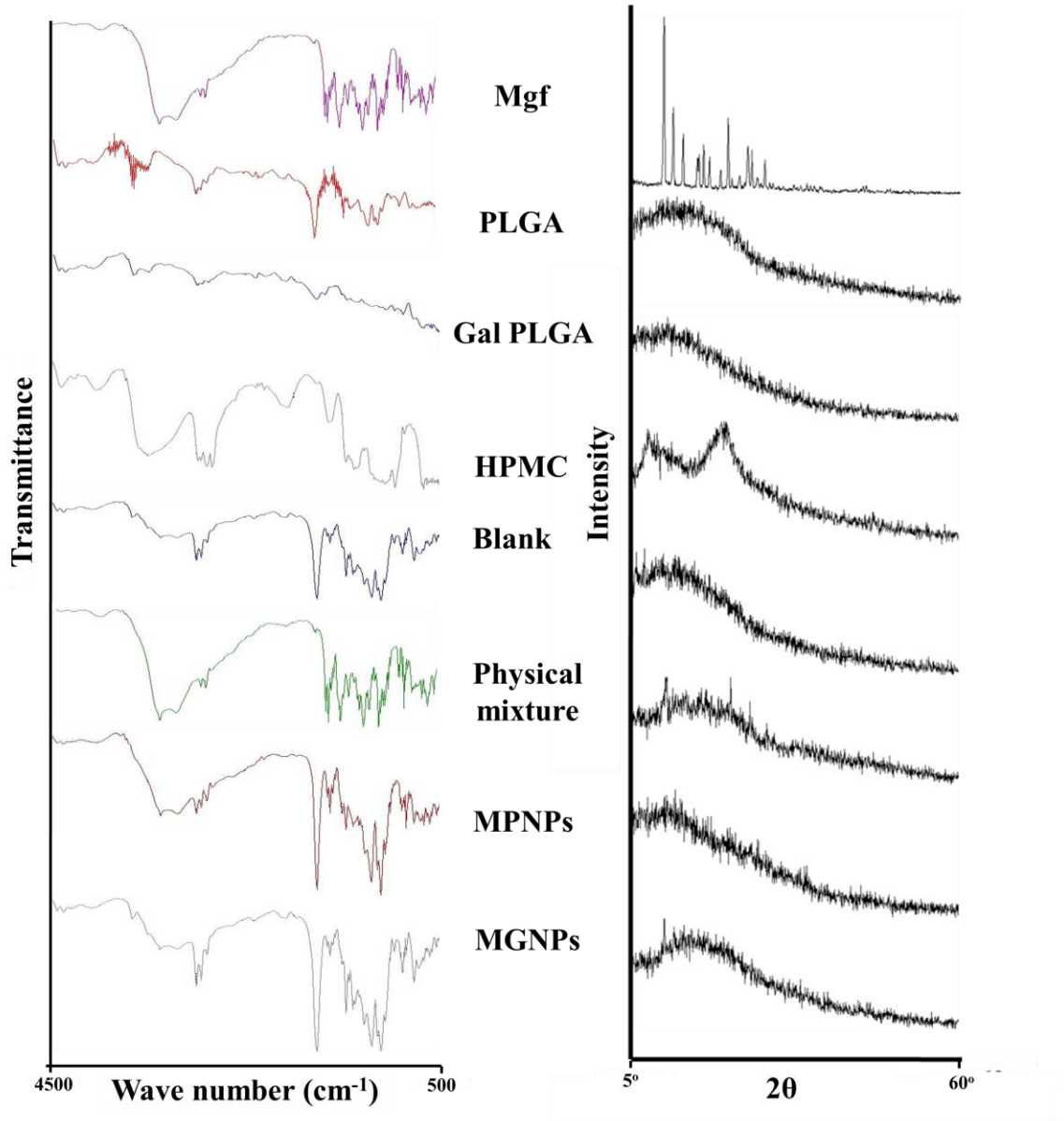

Figure 4.2. Evaluation of physicochemical compatibility of formulation components. (A) FTIR spectra and (B) XRD diffractograms.

4.3.3. Characterization of nanoparticles

Both MPNPs and MGNPs were prepared by an emulsion solvent evaporation process and characterized subsequently. A Mgf: PLGA ratio of 1:10 was optimized for further nanoparticle development (Table 4.1). MPNPs and MGNPs formulated with the selected ratio represented satisfactory entrapment efficiency of 67.77 ± 4.1% and 66.12 ± 3.63%, respectively. Optimized MPNPs presented with a hydrodynamic diameter of ~296.2 nm and surface charge of about -16.4 mV, while prepared MGNPs displayed a hydrodynamic diameter of ~326.8 nm and surface charge of about -8.2 mV (Figure 4.3A-B). PDI values on the lower side (0.234 and 0.128 for MPNPs and MGNPs, respectively) indicated narrow size distribution. Surface charge values were indicative of stable, non-aggregating nanoparticles. The lowering of the absolute value of zeta potential in MGNPs might have arisen from galactosylation of PLGA. Further, negative zeta potential supports reticuloendothelial system uptake by the liver (Kaminskas and Boyd, 2011). Earlier evidence suggests that a drug loading capacity of ~6 % can be considered acceptable for anticancer attributes (Chakraborty et al., 2020). FESEM images (Figure 4.3C) of both MPNPs and MGNPs exhibited a thick distribution of sphere-shaped nanoparticles with smooth exterior surfaces. TEM-based images (Figure 4.3D) revealed discrete spherical delineation of both types of nanoparticles.

Table 4.1. Composition and features of nanoparticles.

Types of polymer	Mgf: polymer ratio	Drug loading %
Plain PLGA	1:5	3.41 ± 0.29
Plain PLGA	1:10	6.16 ± 0.38
Plain PLGA	1:20	2.23 ± 0.18
Gal PLGA	1:10	6.01 ± 0.33

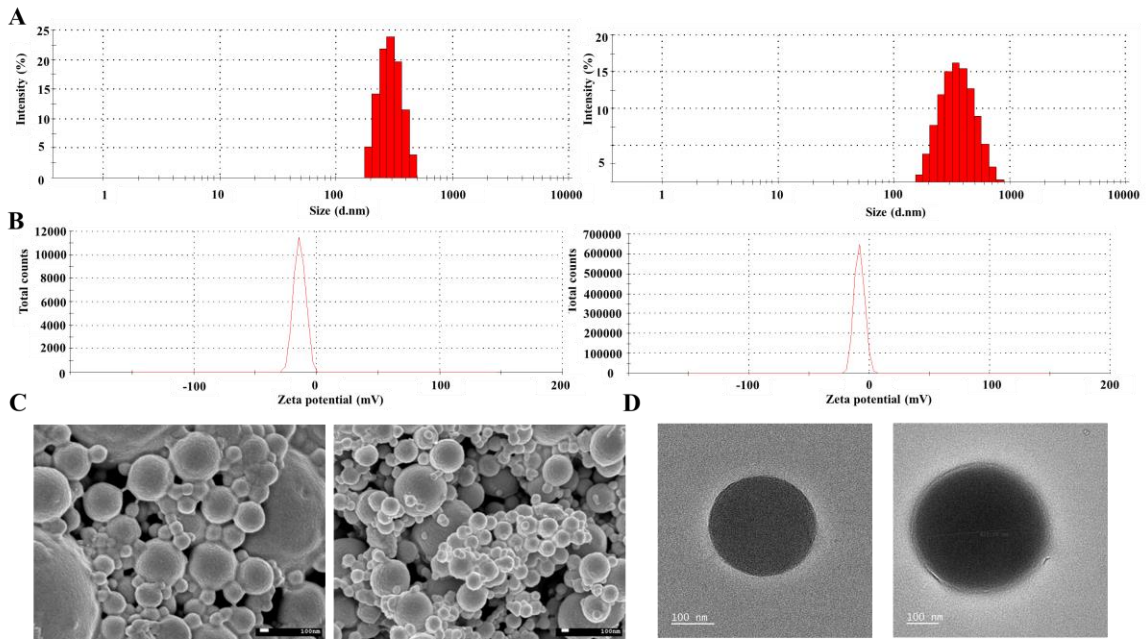

Figure 4.3. Characterization of MPNPs and MGNPs. Particle size distribution (A), surface charge (B), FESEM image (C) and TEM image (D) of MPNPs (left) and MGNPs (right), respectively.

4.3.4. In vitro release kinetics

Both MPNPs and MGNPs were assessed for in vitro release performance in PBS. In case of MPNPs**, t**he study observed an initial rapid release of 19.96 ± 0.12% within the initial 6 h. The release rate was moderate up to 24 h, subsequently followed by sustained release of Mgf up to 9 days, after which no noteworthy increase regarding the cumulative release of Mgf was noticed. Over the timespan of 216 h, 89.92 ± 0.41% Mgf was released (Figure 4.4A). The early burst might be attributed to Mgf loosely attached onto the surface and/or embedded within the surface layer of the polymeric matrix. Again, the persistent sustained release seems to result from diffusion of Mgf from the polymer shell, possibly by either or more of erosion, swelling, and degradation of the polymer matrix (Gaonkar et al., 2017; Jabbari et al., 2018; Ghosh et al., 2023). MGNPs also followed a similar pattern of Mgf release over 9 days. An initial burst release of 19.43 ± 0.60 % was observed for the initial 6 h, followed by moderate to slow sustained release. Over 9 days, 88.03 ± 1.39 % Mgf was released (Figure 4.4B). Release of Mgf from MGNPs was slightly slower compared to the release from MPNPs; however almost similar pattern regarding release behavior indicates almost no effect of galactose conjugation on release pattern. Interestingly, the phasic behavior regarding the release profile of Mgf potentially allows the

formulated nanoparticles, both MPNPs and MGNPs, to have a fast onset of action besides serving as a drug depot.

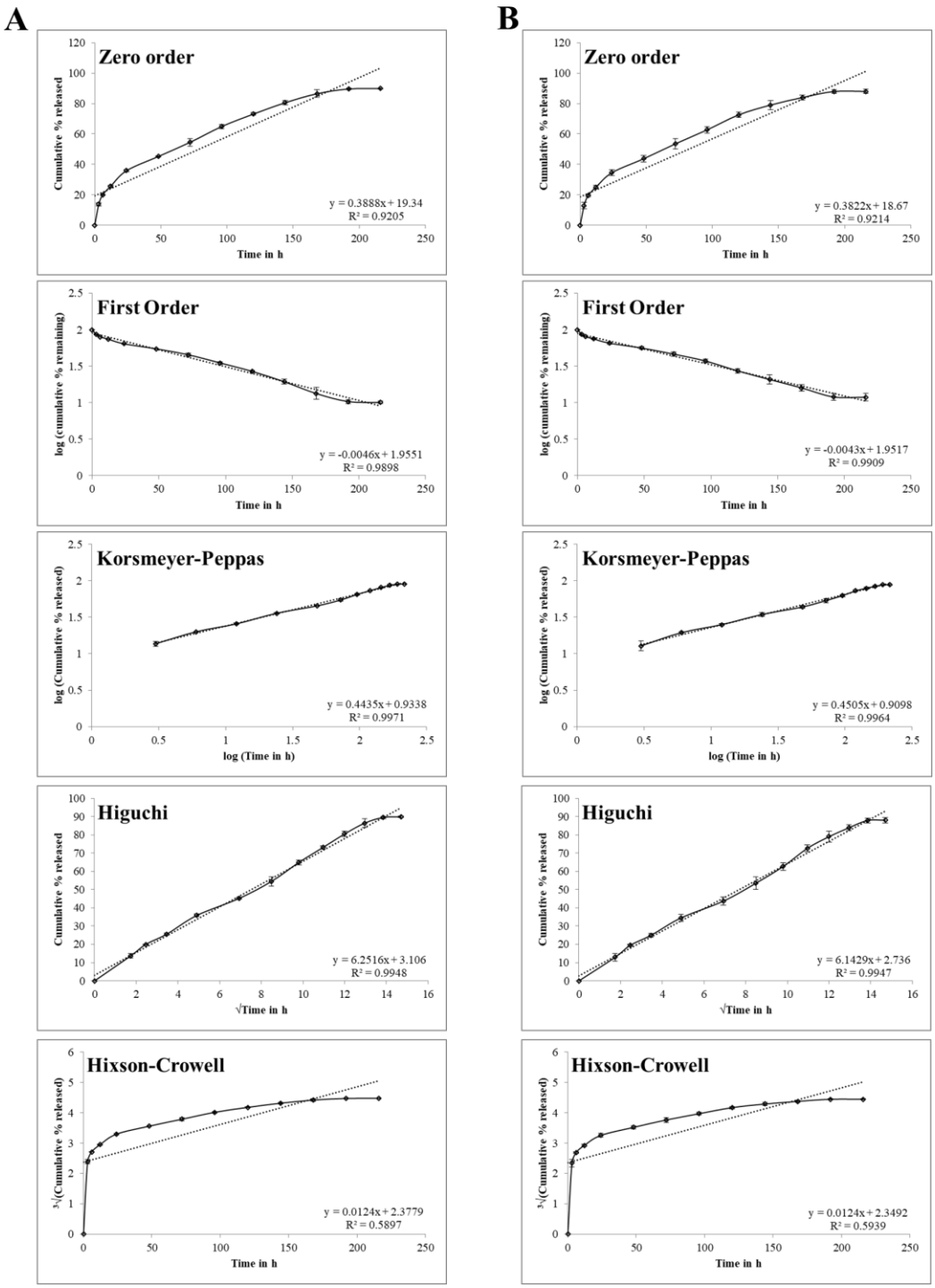

Figure 4.4. In vitro release patterns of MPNPs (A) and MGNPs (B). Data were represented as mean ± SD (n = 3).

The in vitro release data obtained experimentally were fitted to mathematical models to examine the mechanistic pattern of Mgf release (Table 4.2). According to regression coefficient (R^2) values, the Korsmeyer-Peppas model emerged as the best fit. This semiempirical model links exponential release with time elapsed (Figure 4.4A-B), which is a characteristic feature of many polymeric matrix-based formulations (Chatterjee et al., 2024; Ray et al., 2025). The Korsmeyer-Peppas release exponent indicated that swelling plays the principal role during drug release (Moodley and Singh 2020).

Table 4.2. In vitro pharmacokinetic modelling of nanoparticles.

Models	**MPNPs**		**MGNPs**	
	Equations	**R^2 values**	**Equations**	**R^2 values**
Zero order	y = 0.3888x + 19.34	0.9205	y = 0.3822x + 18.67	0.9214
First order	y = –0.0046x + 1.9551	0.9898	y = –0.0043x + 1.9517	0.9909
Korsmeyer-Peppas	y = 0.4435x + 0.9338	0.9971	y = 0.4505x + 0.9098	0.9964
Higuchi	y = 6.2516x + 3.106	0.9948	y = 6.1429x + 2.736	0.9947
Hixson-Crowel	y = 0.0124x + 2.3779	0.5897	y = 0.0124x + 2.3492	0.5939

4.3.5. Stability of MGNPs

The developed MGNPs were stored at ~4 ºC for 90 days. Prepared nanoparticles represented no major alterations in particle size and size distribution on storage (Table 4.3). Surface charge still maintains a negative value after 90 days. Drug loading did not vary significantly (Table 4.3) between freshly prepared nanoparticles and nanoparticles stored at ~4 ºC for 90 days, indicating a stable nanoparticulate structure without leakage. Therefore, MGNPs seem to retain stable characteristics upon storage.

Table 4.3. Parameters of MGNPS regarding the stability study.

Parameters	**Freshly prepared**	**After 90 days at ~4 ºC**
Particle size (nm)	326.8	333.8
Surface charge (mV)	–8.20	–3.97
PDI	0.128	0.117
Drug loading (%)	6.01 ± 0.33	5.98 ± 0.31

4.3.6. Effects on hepatocellular carcinoma cells

Cytotoxic potential is a primary characteristic of any anticancer candidate for chemotherapy. While evaluating the percentage viability of hepatocellular carcinoma cells, MTT analysis revealed dose-dependent cytotoxicity on HepG2 cells (Figure 4.5A). IC_{50} values of free

Mgf, MPNPs and MGNPs against HepG2 cells were observed to be ~56.92 μg/mL, ~15.67 μg/mL and ~10.25 μg/mL, respectively. Obviously, MPNPs imparted better inhibition compared to native Mgf, while MGNPs exhibited the best inhibition among the three, on hepatocellular carcinoma cells. The superior activity of MGNPs could well be correlated with impressive internalization by hepatocellular carcinoma cells **(**Figure 4.5B**).** A significantly higher amount of Mgf becomes available in the intracellular microenvironment of HepG2 cells from MGNPs compared to MPNPs, which might be a result of actively targeting hepatocellular carcinoma cells. In the Hoechst staining assay (Figure 4.5C), the control group retained nuclear morphology and showed the highest nuclear count. The nuclear count decreased gradually in Mgf-treated, MPNPs-treated and MGNPs-treated groups, in the order. The MGNPs-treated group exhibited significant alterations in nuclear patterns in the form of condensed dots and fragmentations, hinting at apoptosis. Chemotherapeutic regimens often induce apoptosis by upregulating oxidative stress. In this study, MGNPs significantly augmented the inhibitory effects on both SOD and CAT activities while downregulating GSH activity in HepG2 cells (Figure 4.5D–F), thereby indicating pro-oxidant functions, and inducing oxidative stress. Induction of oxidative stress within cancer cells is a criterion in cancer chemotherapy to trigger the cell death process via apoptosis induction. Endogenous antioxidant enzymes and metabolites are important players in the redox defense system to reduce ROS. Hence, suppression of the antioxidant moieties would promote the accumulation of ROS in the intracellular milieu.

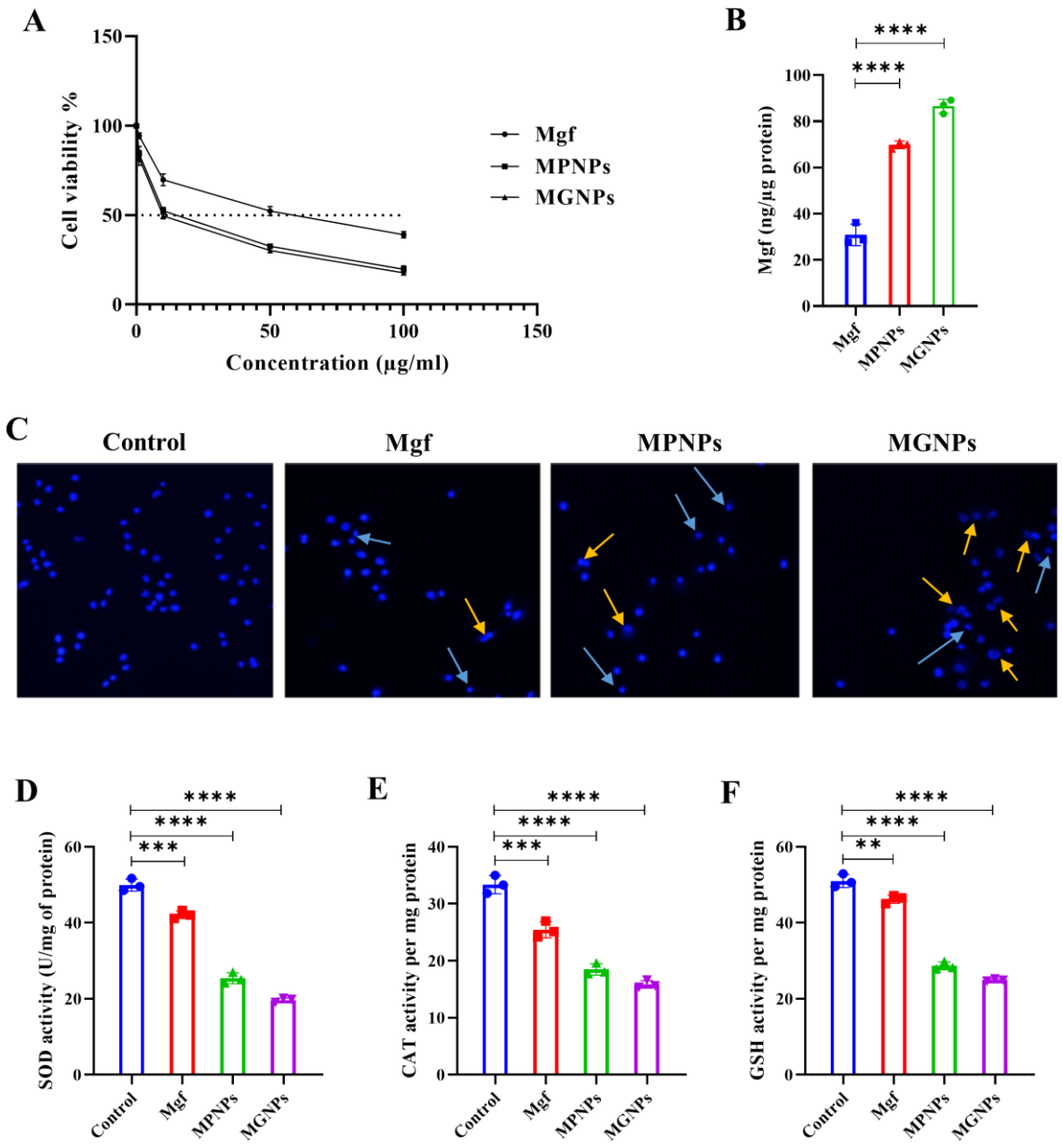

Figure 4.5. Effect of treatment with Mgf, MPNPs and MGNPs on HepG2 cells in vitro. (A) Effect of free drug and nanoparticles on in vitro cell viability of HepG2 cells, (B) cellular uptake of Mgf from different formulations by HepG2 cells, (C) Effect on Hoechst staining upon different treatments, and effects on HepG2 cells receiving different treatments regarding endogenous antioxidant parameters i,e, SOD (D), CAT (E) and GSH (F). Light blue arrows indicate nuclear condensation, and yellow arrows indicate nuclear fragmentation. Graphical data were expressed as mean ± SD (n = 3). **values signify $p < 0.01$; ***values signify $p < 0.001$; ****values signify $p < 0.0001$.

4.3.7. In vivo anti-tumor efficacy

Experimental mice were induced with hepatocellular carcinoma using the CCl_4 + DENA model. During DENA administration, the movement of mice slowed down over time, which might be attributed to discomfort associated with the progressing disease. During treatment, the body weights of experimental mice were recorded every alternate day. The MGNPs-treated group represented the lowest body weight towards the end, though the differences across the groups were not very pronounced (Figure 4.6A). Upon sacrifice, excised livers were also weighed. The liver weight to body weight ratio exhibited a trend of high to low values for the control, Mgf-treated, MPNPs-treated and MGNPs-treated groups, respectively (Figure 4.6B). Significantly low ratio in the MGNPs-treated group might hint at the highest alleviation of tumor burden (Assar et al., 2021; Sarkar et al., 2023). Levels of hepatic biomarkers in blood were examined in experimental animals to gain an idea of liver function. Figure 4.6C indicates that the control group represents the highest values of ALP, AST and ALT, followed by Mgf-treated, MPNPs-treated and MGNPs-treated groups, in order. Induction of hepatocellular carcinoma leads to hepatic abnormality characterized by high ALP, AST and ALT values, however, the gradual decrease across the groups hints at a reduction in tumor load and associated abnormality, groupwise. Accumulation of Mgf in hepatic tissues also corroborates the findings since the MGNPs-treated group exhibits the highest accumulation, compared to the other groups (Figure 4.6D). The significantly higher accumulation of Mgf in hepatic tissues from MGNPs, compared to MPNPs, also indicates the supremacy of galactosylated polymer for liver-specific delivery.

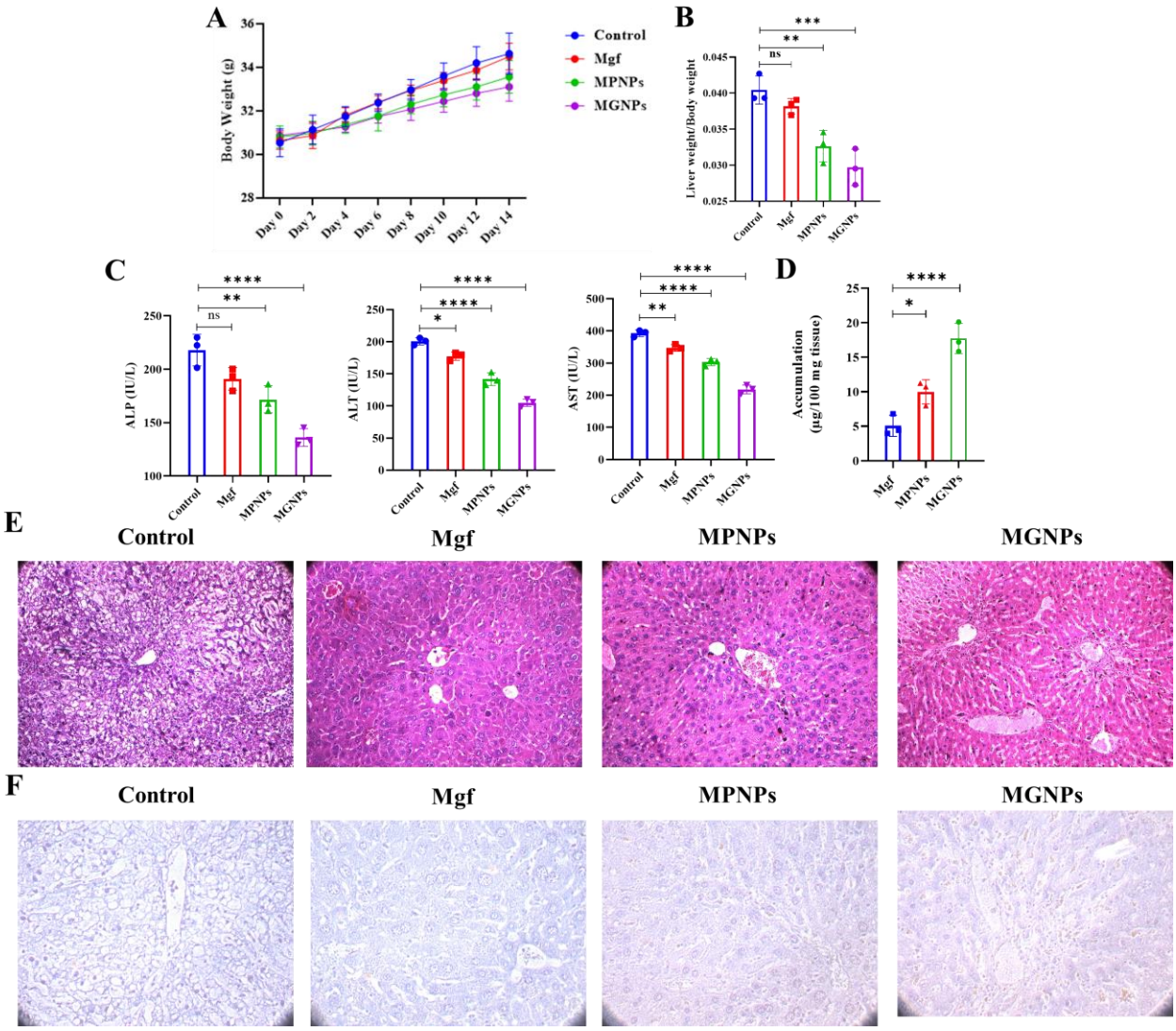

Figure 4.6. Anti-tumor effect of formulated nanoparticles on hepatocellular carcinoma-bearing mice. (A) Body weight of mice belonging to different groups during treatment duration, (B) liver weight to body weight ratios of experimental animals, (C) serum biochemical parameters regarding hepatic function, (D) tissue accumulation of Mgf in treatment groups, (E) H&E-stained histological sections of excised tissues and (F) Immunohistochemical detection of p53 expression in tumor tissue sections. Graphical data were expressed as mean ± SD (n = 3). *Values signify $p < 0.05$; **values signify $p < 0.01$; ***values signify $p < 0.001$; ****values signify $p < 0.0001$; ns, insignificant.

To further assess anti-tumor activity, dissected liver tissues from the experimental groups were stained with H&E and observed under a microscope (Figure 4.6E). In the control group, tumor tissue could be characterized by numerous micronuclei spread across the entire section,

dark-stained nucleoli and larger-sized nuclei accompanied by a highly irregular arrangement with torn/loosened stroma. In the Mgf-treated tissue section, the irregularities improved slightly. The MPNPs-treated group presented with somewhat tightly packed stroma, however, represented bigger nuclei, multiple dividing nuclei in cells, darkly stained nucleoli and appearance of micronuclei in the tissue section. Interestingly, the tissue section from the MGNPs-treated group presented with consistent nuclear sizes akin to those of healthy hepatocytes, along with a low appearance of micronuclei. It further shows hints of regaining the radial arrangement of hepatocytes, along with low to no appearance of either actively dividing nuclei in the cells or dark-stained nucleoli. Thus, the MGNPs-treated group represents the lowest tumor load among the groups (Martin-Filho et al., 2017). Immunohistochemical studies reassured the therapeutic impact of formulated nanoparticles on tumors (Figure 4.6F). The MGNPs-treated group exhibited the highest expression of tumor suppressor protein p53, indicating superior therapeutic activity of MGNPs. In line with the earlier findings, the immunohistochemical study also establishes the superior anti-tumor activity of MGNPs. Clearly, galactosylation-mediated hepatic targeting conferred chemotherapeutic efficacy to a greater extent compared to MPNPs.

4.3.8. Assessment of systemic toxicity in vivo

A balance between therapeutic and toxicological outcomes of any treatment module is a crucial parameter to evaluate its pharmacological applicability. Four groups of mice (not bearing hepatocellular carcinoma) were treated with PBS, Mgf, MPNPs and MGNPs, respectively. There was no notable variation in body weights across groups during the treatment period (Figure 4.7A). However, higher values of body weights and active movements throughout the entire study duration distinguish them from the groups administered with CCl_4 + DENA. In order to assess any probable systemic toxicities of the prepared nanoformulations at applied doses, levels of renal and hepatic biomarkers in blood were examined, as well as H&E-stained tissue sections of vital organs from experimental animals were also analyzed. Both hepatic and renal parameters, i.e., ALP, ALT, BUN and creatinine (Figure 4.7B), did not differ significantly across the four groups, hinting at the absence of hepatotoxicity and nephrotoxicity by formulated nanoparticles during the period of treatment. Hepatic tissues did not represent major alterations among experimental groups (Figure 4.7C). Renal and cardiac tissues also seem to remain unaffected, retaining more or less normal tissue characteristics across all the groups (Figure 4.7C). The findings indicate that the formulated nanoparticles do not initiate concerning systemic toxicity to mice compared to the control group. Therefore, the current study advocates for MGNPs as a safe tool for chemotherapy without concerning toxicities.

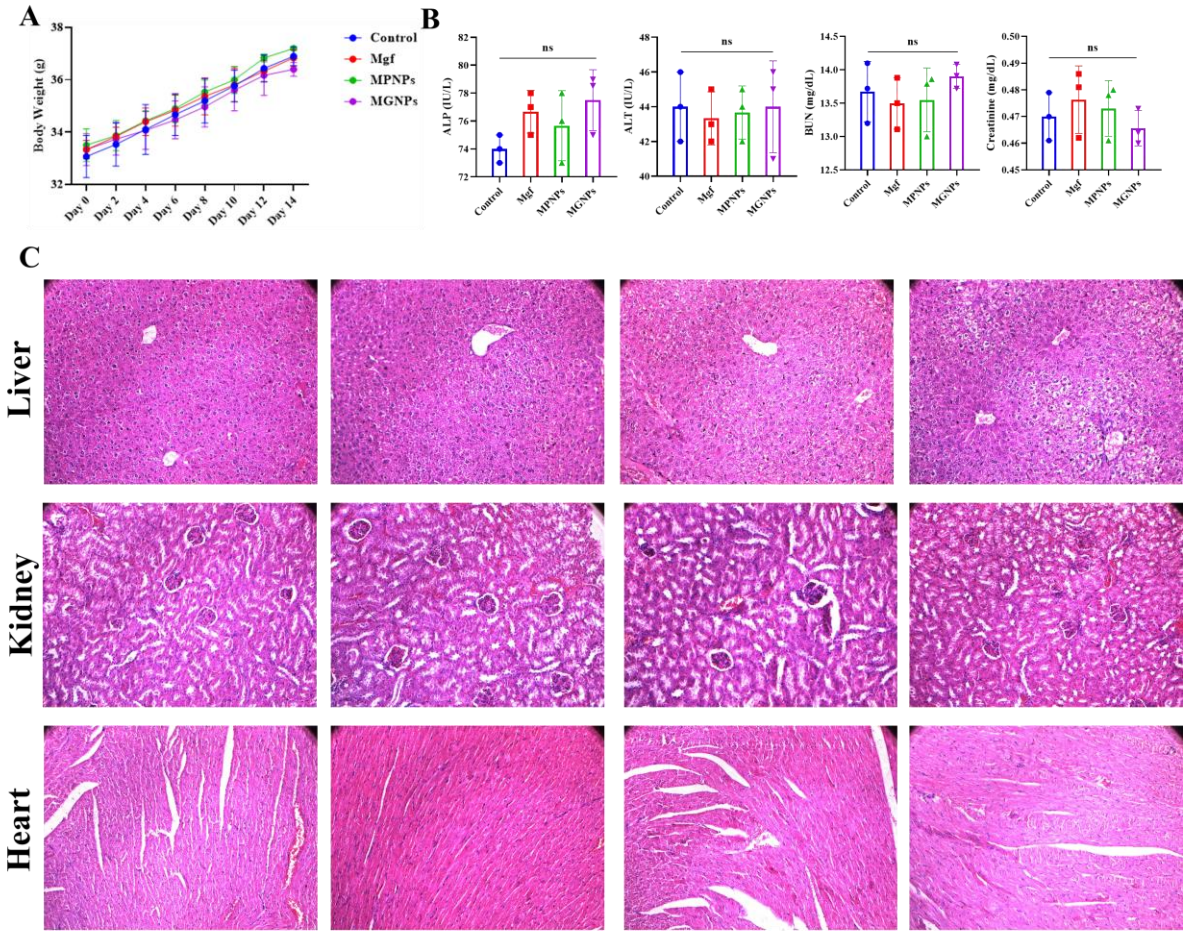

Figure 4.7. Safety profile of formulated nanoparticles. (A) Body weight of experimental mice during treatment duration, (B) serum biochemical parameters regarding hepatic and renal biomarkers of different experimental groups and (C) H&E-stained histological sections of liver, kidney and heart of different experimental groups. Graphical data were represented as mean ± SD (n = 3). ns, insignificant.

4.4. Concluding remarks

The current study produced well-characterized nanoparticles with substantial loading and a satisfactory release profile of Mgf. MGNPs displayed the best results regarding tumor alleviation by improving the accumulation of Mgf at the target site. In vitro assays established superior anticancer effects imparted by MGNPs, surpassing MPNPs and Mgf. In line with the findings, during in vivo preclinical assays, MGNPs could significantly minimize tumor load compared to native Mgf and MPNPs, accompanied by a promising safety profile of the nanoparticles. Therefore, galactose-mediated active targeting of hepatocellular carcinoma cells

(by recognizing asialoglycoprotein receptors) resulted in improved accumulation of Mgf in liver cancer cells, consequently leading to better anticancer activity (Figure 4.8).

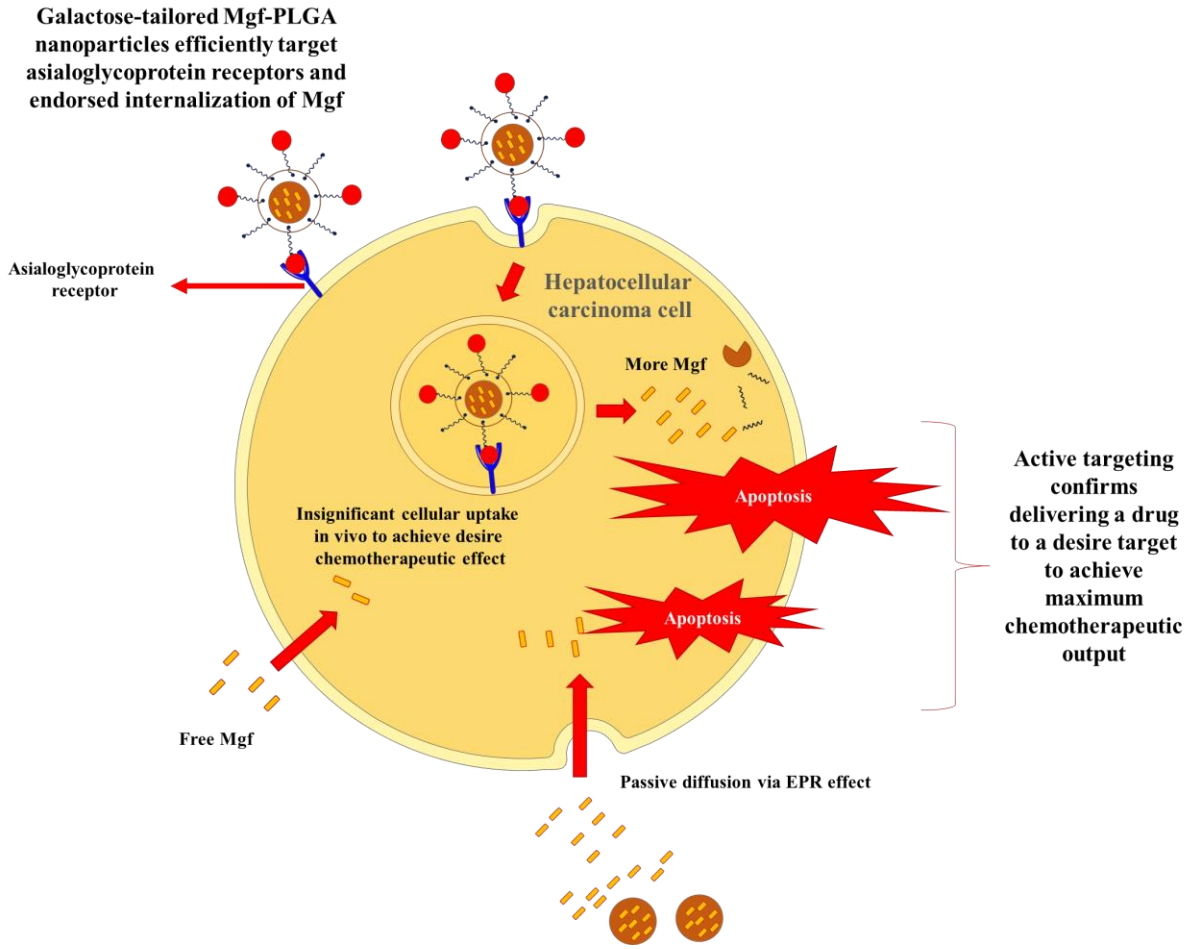

Figure 4.8. Schematic representation of active targeting of liver cancer cells endorsing higher internalization of Mgf, leading to better anticancer effects by utilizing galactose-tailored Mgf-PLGA nanoparticles. EPR, Enhanced permeability and retention; Mgf, Mangiferin. PLGA, poly (lactic-co-glycolic) acid.

Regarding systemic effects, in vivo assays did not reveal concerning toxicities. Thus, in addition to impressive anti-tumor potential, developed galactose-tailored polymeric nanoparticles also present with acceptable safety profile. Summarily, PLGA nanoparticles improve chemotherapeutic efficacy over free Mgf. overcoming biopharmaceutical concerns, and galactose-tailoring of the polymer further enhances therapeutic efficacy against hepatocellular carcinoma by virtue of active targeting. Active targeting aids in delivering Mgf predominantly at the desirable site of action. Asialoglycoprotein receptors, abundant on liver cancer cells, recognize the galactose-tailored polymeric nanoparticles for interactive binding, thereby boosting

intracellular accumulation of Mgf and subsequent anticancer activity. Therefore, the current study advocates for MGNPs as a novel, efficacious and safe drug delivery system with futuristic promise for active targeting-mediated chemotherapy of hepatocellular carcinoma using a nature-derived small molecule i.e. Mgf. MGNPs, therefore, present strong candidature for evaluation regarding possibility of future clinical translation.

Chapter 5

References

5. References

Acosta E. Bioavailability onoparticles in nutrient and nutraceutical delivery. Current opinion in colloid & interface science. 2009;14(1):3-15. doi: 10.1016/j.cocis.2008.01.002.

Acosta J, Sevilla I, Salomón S, Nuevas L, Romero A, Amaro D. Determination of mangiferin solubility in solvents used in the biopharmaceutical industry. J Pharm Pharmacogn Res. 2016;4(2):49-53.

Akhter MH, Kumar S, Nomani S. Sonication tailored enhance cytotoxicity of naringenin nanoparticle in pancreatic cancer: design, optimization, and *in vitro* studies. Drug Dev Ind Pharm. 2020;46(4):659-672. doi: 10.1080/03639045.2020.1747485.

Alharbi HM, Alqahtani T, Alamri AH, Kumarasamy V, Subramaniyan V, Babu KS. Nanotechnological synergy of mangiferin and curcumin in modulating PI3K/Akt/mTOR pathway: a novel front in ovarian cancer precision therapeutics. Front Pharmacol. 2024;14:1276209. doi: 10.3389/fphar.2023.1276209.

Ali SA, Zaitone SA, Moustafa YM. Boswellic acids synergize antitumor activity and protect against the cardiotoxicity of doxorubicin in mice bearing Ehrlich's carcinoma. Can J Physiol Pharmacol. 2015;93(8):695-708. doi: 10.1139/cjpp-2014-0524.

Aljabali AAA, Bashatwah RM, El-Tanani M, Tambuwala MM. Natural Anticancer Drugs: Efficacy, Safety, and Future Challenges. Curr Med Chem. 2025;12(1):201. doi: 10.2174/0109298673344501250109210447.

Alkhatib MH, Alkreathy HM, Al Omar MI, Balamash KS, Abdu F, Esmat A. Doxorubicin Supplemented with Pravastatin in Lipid Nanoemulsion Induces Antineoplastic Activity with Limited Hepatotoxicity and Cardiotoxicity in Tumor-Bearing Mice. Asian J Pharm Res Health Care 2021;13(1):17-29. doi: 10.18311/ajprhc/2021/26066.

Allen JD, Brinkhuis RF, van Deemter L, Wijnholds J, Schinkel AH. Extensive contribution of the multidrug transporters P-glycoprotein and Mrp1 to basal drug resistance. Cancer Res. 2000;60(20):5761-5766.

Alshehri SM, Shakeel F, Ibrahim MA, Elzayat EM, Altamimi M, Mohsin K, Almeanazel OT, Alkholief M, Alshetaili A, Alsulays B, Alanazi FK, Alsarra IA. Dissolution and bioavailability improvement of bioactive apigenin using solid dispersions prepared by different techniques. Saudi Pharm J. 2019;27(2):264-273. doi: 10.1016/j.jsps.2018.11.008.

Arnold M, Morgan E, Rumgay H, Mafra A, Singh D, Laversanne M, Vignat J, Gralow JR, Cardoso F, Siesling S, Soerjomataram I. Current and future burden of breast cancer:

global statis tics for 2020 and 2040. Breast 2022;66:15–23. Doi: 10.1016/j. breast.2022.08.010.

Assar DH, Mokhbatly AA, Ghazy EW, Ragab AE, Abou Asa S, Abdo W, Elbialy ZI, Mohamed NE, El-Far AH. Ameliorative Effects of *Aspergillus awamori* against the Initiation of Hepatocarcinogenesis Induced by Diethylnitrosamine in a Rat Model: Regulation of *Cyp19* and *p53* Gene Expression. Antioxidants (Basel). 2021;10(6):922. doi: 10.3390/antiox10060922.

Attia MF, Anton N, Wallyn J, Omran Z, Vandamme TF. An overview of active and passive targeting strategies to improve the nanocarriers efficiency to tumour sites. J Pharm Pharmacol. 2019;71(8):1185-1198. doi: 10.1111/jphp.13098.

Azizi M, Ghourchian H, Yazdian F, Bagherifam S, Bekhradnia S, Nyström B. Anti-cancerous effect of albumin coated silver nanoparticles on MDA-MB 231 human breast cancer cell line. Sci Rep. 2017;7(1):5178. doi: 10.1038/s41598-017-05461-3.

Badawi NM, Attia YM, El-Kersh DM, Hammam OA, Khalifa MKA. Investigating the Impact of Optimized Trans-Cinnamic Acid-Loaded PLGA Nanoparticles on Epithelial to Mesenchymal Transition in Breast Cancer. Int J Nanomed. 2022;17:733-750. doi: 10.2147/IJN.S345870.

Baghel M, Baghel I, Kumari P, Bharkatiya M, Joshi G, Sakure K, Badwaik H. Nano-delivery Systems and Therapeutic Applications of Phytodrug Mangiferin. Appl Biochem Biotechnol. 2024;196(10):7429-7463. doi: 10.1007/s12010-024-04906-6.

Bai X, Smith ZL, Wang Y, Butterworth S, Tirella A. Sustained Drug Release from Smart Nanoparticles in Cancer Therapy: A Comprehensive Review. Micromachines (Basel). 2022;13(10):1623. doi: 10.3390/mi13101623.

Bayda S, Adeel M, Tuccinardi T, Cordani M, Rizzolio F. The History of Nanoscience and Nanotechnology: From Chemical-Physical Applications to Nanomedicine. Molecules. 2019;25(1):112. doi: 10.3390/molecules25010112.

Beach MA, Nayanathara U, Gao Y, Zhang C, Xiong Y, Wang Y, Such GK. Polymeric Nanoparticles for Drug Delivery. Chem Rev. 2024;124(9):5505-5616. doi: 10.1021/acs.chemrev.3c00705.

Betancourt T, Brown B, Brannon-Peppas L. Doxorubicin-loaded PLGA nanoparticles by nanoprecipitation: preparation, characterization and in vitro evaluation. Nanomed. (Lond) 2007;2(2):219-232. doi: 10.2217/17435889.2.2.219.

Bhattacharya S, Ahir M, Patra P, Mukherjee S, Ghosh S, Mazumdar M, Chattopadhyay S, Das T, Chattopadhyay D, Adhikary A. PEGylated-thymoquinone-nanoparticle mediated retardation of breast cancer cell migration by deregulation of cytoskeletal actin polymerization through miR-34a. Biomaterials 2015;51:91-107. doi: 10.1016/j.biomaterials.2015.01.007.

Bhattacharya S, Mondal L, Mukherjee B, Dutta L, Ehsan I, Debnath MC, Gaonkar RH, Pal MM, Majumdar S. Apigenin loaded nanoparticle delayed development of hepatocellular carcinoma in rats. Nanomedicine. 2018;14(6):1905-1917. doi: 10.1016/j.nano.2018.05.011.

Bhattacharyya A, Mandal D, Lahiry L, Bhattacharyya S, Chattopadhyay S, Ghosh UK, Sa G, Das T. Black tea-induced amelioration of hepatic oxidative stress through antioxidative activity in EAC-bearing mice. J Environ Pathol Toxicol Oncol. 2007;26(4):245-254. doi: 10.1615/jenvironpatholtoxicoloncol.v26.i4.10.

Cao SJ, Xu S, Wang HM, Ling Y, Dong J, Xia RD, Sun XH. Nanoparticles: Oral Delivery for Protein and Peptide Drugs. AAPS PharmSciTech. 2019;20(5):190. doi: 10.1208/s12249-019-1325-z.

Chakraborty S, Dlie ZY, Chakraborty S, Roy S, Mukherjee B, Besra SE, Dewanjee S, Mukherjee A, Ojha PK, Kumar V, Sen R. Aptamer-Functionalized Drug Nanocarrier Improves Hepatocellular Carcinoma toward Normal by Targeting Neoplastic Hepatocytes. Mol Ther Nucleic Acids. 2020;20:34-49. doi: 10.1016/j.omtn.2020.01.034.

Chatterjee S, Chakraborty P, Dutta S, Karak S, Mahalanobis S, Ghosh N, Dewanjee S, Sil PC. Formulation of Carnosic-Acid-Loaded Polymeric Nanoparticles: An Attempt to Endorse the Bioavailability and Anticancer Efficacy of Carnosic Acid against Triple-Negative Breast Cancer. ACS Appl Bio Mater. 2024;7(3):1656-1670. doi: 10.1021/acsabm.3c01087.

Chaurasia S, Patel RR, Vure P, Mishra B. Potential of Cationic-Polymeric Nanoparticles for Oral Delivery of Naringenin: In Vitro and In Vivo Investigations. J Pharm Sci. 2018;107(2):706-716. doi: 10.1016/j.xphs.2017.10.006.

Chenthamara D, Subramaniam S, Ramakrishnan SG, Krishnaswamy S, Essa MM, Lin FH, Qoronfleh MW. Therapeutic efficacy of nanoparticles and routes of administration. Biomater Res. 2019;23:20. doi: 10.1186/s40824-019-0166-x.

Chhimwal J, Dhritlahre RK, Anand P, Ruchika, Patial V, Saneja A, Padwad YS. Amorphous solid dispersion augments the bioavailability of phloretin and its therapeutic efficacy via targeting mTOR/SREBP-1c axis in NAFLD mice. Biomater Adv. 2023;154:213627. doi: 10.1016/j.bioadv.2023.213627.

Chintamani, Singh JP, Mittal MK, Saxena S, Bansal A, Bhatia A, Kulshreshtha P. Role of p-glycoprotein expression in predicting response to neoadjuvant chemotherapy in breast cancer--a prospective clinical study. World J Surg Oncol. 2005;3:61. doi: 10.1186/1477-7819-3-61.

Colombo M, Figueiró F, de Fraga Dias A, Teixeira HF, Battastini AMO, Koester LS. Kaempferol-loaded mucoadhesive nanoemulsion for intranasal administration reduces glioma growth in vitro. Int J Pharm. 2018;543(1-2):214-223. doi: 10.1016/j.ijpharm.2018.03.055.

Cuccioloni M, Bonfili L, Mozzicafreddo M, Cecarini V, Scuri S, Cocchioni M, Nabissi M, Santoni G, Eleuteri AM, Angeletti M. Mangiferin blocks proliferation and induces apoptosis of breast cancer cells via suppression of the mevalonate pathway and by proteasome inhibition. Food Funct. 2016;7(10):4299-4309. doi: 10.1039/c6fo01037g.

de Oliveira Pedro R, Goycoolea FM, Pereira S, Schmitt CC, Neumann MG. Synergistic effect of quercetin and pH-responsive DEAE-chitosan carriers as drug delivery system for breast cancer treatment. Int J Biol Macromol. 2018;106:579-586. doi: 10.1016/j.ijbiomac.2017.08.056.

De R, Mahata MK, Kim KT. Structure-Based Varieties of Polymeric Nanocarriers and Influences of Their Physicochemical Properties on Drug Delivery Profiles. Adv Sci (Weinh). 2022;9(10):e2105373. doi: 10.1002/advs.202105373.

Dewanjee S, Chakraborty P, Bhattacharya H, Singh SK, Dua K, Dey A, Jha NK. Recent advances in flavonoid-based nanocarriers as an emerging drug delivery approach for cancer chemotherapy. Drug Discov Today. 2023;28(1):103409. doi: 10.1016/j.drudis.2022.103409.

Dewanjee S, Chakraborty P, Mukherjee B, De Feo V. Plant-Based Antidiabetic Nanoformulations: The Emerging Paradigm for Effective Therapy. Int J Mol Sci. 2020;21(6):2217. doi: 10.3390/ijms21062217.

Dey N, Kamatchi C, Vickram AS, Anbarasu K, Thanigaivel S, Palanivelu J, Pugazhendhi A, Ponnusamy VK. Role of nanomaterials in deactivating multiple drug resistance efflux pumps - A review. Environ Res. 2022;204(Pt A):111968. doi: 10.1016/j.envres.2021.111968.

Dey S, Hassan S, Pandey RK. Nanomedicine in Targeted Drug Delivery: Precision Therapeutics for Personalized Medicine. In: Nanomedicine 2024;179-231. Springer, Cham. doi: 10.1007/978-3-031-72467-1_8.

Dibaei M, Rouini MR, Sheikholeslami B, Gholami M, Dinarvand R. The effect of surface treatment on the brain delivery of curcumin nanosuspension: in vitro and in vivo studies. Int J Nanomedicine. 2019;14:5477-5490. doi: 10.2147/IJN.S199624.

Din FU, Aman W, Ullah I, Qureshi OS, Mustapha O, Shafique S, Zeb A. Effective use of nanocarriers as drug delivery systems for the treatment of selected tumors. Int J Nanomedicine. 2017;12:7291-7309. doi: 10.2147/IJN.S146315.

Dobrzynska M, Napierala M, Florek E. Flavonoid Nanoparticles: A Promising Approach for Cancer Therapy. Biomolecules. 2020;10(9):1268. doi: 10.3390/biom10091268.

Dong X. Current Strategies for Brain Drug Delivery. Theranostics. 2018;8(6):1481-1493. doi: 10.7150/thno.21254.

du Plessis-Stoman D, du Preez J, van de Venter M. Combination treatment with oxaliplatin and mangiferin causes increased apoptosis and downregulation of NFκB in cancer cell lines. Afr J Tradit Complement Altern Med. 2011;8(2):177-184. doi: 10.4314/ajtcam.v8i2.63206.

Du S, Liu H, Lei T, Xie X, Wang H, He X, Tong R, Wang Y. Mangiferin: An effective therapeutic agent against several disorders. Mol Med Rep. 2018;18(6):4775-4786. doi: 10.3892/mmr.2018.9529.

Dutta D, Chakraborty A, Mukherjee B, Gupta S. Aptamer-Conjugated Apigenin Nanoparticles To Target Colorectal Carcinoma: A Promising Safe Alternative of Colorectal Cancer Chemotherapy. ACS Appl Bio Mater. 2018;1(5):1538-1556. doi: 10.1021/acsabm.8b00441.

Dutta D, Paul B, Mukherjee B, Mondal L, Sen S, Chowdhury C, Debnath MC. Nanoencapsulated betulinic acid analogue distinctively improves colorectal carcinoma in vitro and in vivo. Sci Rep. 2019;9(1):11506. doi: 10.1038/s41598-019-47743-y.

Dutta S, Chakraborty P, Basak S, Ghosh S, Ghosh N, Chatterjee S, Dewanjee S, Sil PC. Synthesis, characterization, and evaluation of in vitro cytotoxicity and in vivo antitumor activity of asiatic acid-loaded poly lactic-co-glycolic acid nanoparticles: A strategy of treating breast cancer. Life Sci. 2022;307:120876. doi: 10.1016/j.lfs.2022.120876.

Dutta S, Sadhukhan P, Saha S, Sil PC. Regulation of oxidative stress by different naturally occurring polyphenolic compounds: an emerging anticancer therapeutic approach. React. Oxyg. Species. 2017;3:81-95. doi: 10.20455/ros.2017.815.

El-Ashmawy NE, Khedr EG, Khedr NF, El-Adawy SA. Suppression of epithelial-mesenchymal transition and SIRT1/AKT signaling pathway in breast cancer by montelukast. Int Immunopharmacol. 2023;119:110148. doi: 10.1016/j.intimp.2023.110148.

El-Masry TA, El-Nagar MMF, El Mahdy NA, Alherz FA, Taher R, Osman EY. Potential Antitumor Activity of Combined Lycopene and Sorafenib against Solid Ehrlich Carcinoma via Targeting Autophagy and Apoptosis and Suppressing Proliferation. Pharmaceuticals. (Basel) 2024;17(4):527. doi: 10.3390/ph17040527.

Elsabahy M, Heo GS, Lim SM, Sun G, Wooley KL. Polymeric Nanostructures for Imaging and Therapy. Chem Rev. 2015;115(19):10967-11011. doi: 10.1021/acs.chemrev.5b00135.

El-Sisi AE, Sokkar SS, Ibrahim HA, Hamed MF, Abu-Risha SE. Targeting MDR-1 gene expression, BAX/BCL2, caspase-3, and Ki-67 by nanoencapsulated imatinib and hesperidin to enhance anti-cancer activity and ameliorate cardiotoxicity. Fundam Clin Pharmacol. 2020;34(4):458-475. doi: 10.1111/fcp.12549.

Fabián RF, Mayra HM, Manuel ZV, Guadalupe SS, Alejandro PL, Alberto SJ. Characterization of Functionalized PLGA Nanoparticles Loaded with Mangiferin and Lupeol, and their Effect on BEAS-2B and HepG2 Cell Lines. Anticancer Agents Med Chem. 2023;23(10):1174-1183. doi: 10.2174/1871520622666220617101515.

Feng C, Yuan X, Chu K, Zhang H, Ji W, Rui M. Preparation and optimization of poly (lactic acid) nanoparticles loaded with fisetin to improve anti-cancer therapy. Int J Biol Macromol. 2019;125:700-710. doi: 10.1016/j.ijbiomac.2018.12.003.

Feng M, Wei S, Zhang S, Yang Y. Anti-Inflammation and Anti-Pyroptosis Activities of Mangiferin via Suppressing NF-κB/NLRP3/GSDMD Signaling Cascades. Int J Mol Sci. 2022;23(17):10124. doi: 10.3390/ijms231710124.

Fernando W, Rupasinghe HPV, Hoskin DW. Dietary phytochemicals with anti-oxidant and pro-oxidant activities: A double-edged sword in relation to adjuvant chemotherapy and radiotherapy? Cancer Lett. 2019;452:168-177. doi: 10.1016/j.canlet.2019.03.022.

Fessi HP, Puisieux F, Devissaguet JP, Ammoury N, Benita S. Nanocapsule formation by interfacial polymer deposition following solvent displacement. Int J Pharmaceutics 1989;55(1):R1-R4. doi: 10.1016/0378-5173(89)90281-0.

Ganguly S, Dewanjee S, Sen R, Chattopadhyay D, Ganguly S, Gaonkar R, Debnath MC. Apigenin-loaded galactose tailored PLGA nanoparticles: A possible strategy for liver targeting to treat hepatocellular carcinoma. Colloids Surf B Biointerfaces. 2021;204:111778. doi: 10.1016/j.colsurfb.2021.111778.

Gao S, Siddiqui N, Etim I, Du T, Zhang Y, Liang D. Developing nutritional component chrysin as a therapeutic agent: Bioavailability and pharmacokinetics consideration, and ADME mechanisms. Biomed Pharmacother. 2021;142:112080. doi: 10.1016/j.biopha.2021.112080.

Gaonkar RH, Ganguly S, Dewanjee S, Sinha S, Gupta A, Ganguly S, Chattopadhyay D, Chatterjee Debnath M. Garcinol loaded vitamin E TPGS emulsified PLGA nanoparticles: preparation, physicochemical characterization, in vitro and in vivo studies. Sci Rep. 2017;7(1):530. doi: 10.1038/s41598-017-00696-6.

Gautam AK, Kumar P, Kumar V, Singh A, Mahata T, Maity B, Yadav S, Kumar D, Singh S, Saha S, Vijayakumar MR. Preclinical evaluation of dalbergin loaded PLGA-galactose-modified nanoparticles against hepatocellular carcinoma via inhibition of the AKT/NF-κB signaling pathway. Int Immunopharmacol. 2024;140:112813. doi: 10.1016/j.intimp.2024.112813.

Gavas S, Quazi S, Karpiński TM. Nanoparticles for Cancer Therapy: Current Progress and Challenges. Nanoscale Res Lett. 2021;16(1):173. doi: 10.1186/s11671-021-03628-6.

Gera S, Talluri S, Rangaraj N, Sampathi S. Formulation and Evaluation of Naringenin Nanosuspensions for Bioavailability Enhancement. AAPS PharmSciTech. 2017;18(8):3151-3162. doi: 10.1208/s12249-017-0790-5.

Ghosh N, Kundu M, Ghosh S, Das AK, De S, Das J, Sil PC. pH-responsive and targeted delivery of chrysin via folic acid-functionalized mesoporous silica nanocarrier for breast cancer therapy. Int J Pharm. 2023;631:122555. doi: 10.1016/j.ijpharm.2022.122555.

Gold-Smith F, Fernandez A, Bishop K. Mangiferin and Cancer: Mechanisms of Action. Nutrients. 2016;8(7):396. doi: 10.3390/nu8070396.

Guruswamy DKM, Balaji KDS, Dharmappa KK, Jayarama S. Novel 3-(3, 5-difluoro-4-hydroxyphenyl)-1-(naphthalen-2-yl;prop-2-en-1-one as a potent inhibitor of MAP-kinase in HeLa cell lines and anti-angiogenic activity is mediated by HIF-1α in EAC animal model. Oncotarget 2020;11(50):4661-4676. doi: 10.18632/oncotarget.27836.

Haidar LL, Bilek M, Akhavan B. Surface Bio-engineered Polymeric Nanoparticles. Small. 2024;20(21):e2310876. doi: 10.1002/smll.202310876.

Haripriyaa M, Suthindhiran K. Pharmacokinetics of nanoparticles: current knowledge, future directions and its implications in drug delivery. Future Journal of Pharmaceutical Sciences. 2023;9(1):113. doi: 10.1186/s43094-023-00569-y.

Hogarth C, Arnold K, McLauchlin A, Rannard SP, Siccardi M, McDonald TO. Evaluating the impact of systematic hydrophobic modification of model drugs on the control, stability and loading of lipid-based nanoparticles. J Mater Chem B. 2021;9(48):9874-9884. doi: 10.1039/d1tb02297k.

Hompland T, Fjeldbo CS, Lyng H. Tumor Hypoxia as a Barrier in Cancer Therapy: Why Levels Matter. Cancers (Basel). 2021;13(3):499. doi: 10.3390/cancers13030499.

Huang T, Liu Y, Zhang C. Pharmacokinetics and Bioavailability Enhancement of Baicalin: A Review. Eur J Drug Metab Pharmacokinet. 2019;44(2):159-168. doi: 10.1007/s13318-018-0509-3.

Ioele G, Chieffallo M, Occhiuzzi MA, De Luca M, Garofalo A, Ragno G, Grande F. Anticancer Drugs: Recent Strategies to Improve Stability Profile, Pharmacokinetic and Pharmacodynamic Properties. Molecules. 2022;27(17):5436. doi: 10.3390/molecules27175436.

Iqbal H, Inam-Ur-Raheem M, Munir S, Rabail R, Kafeel S, Shahid A, Mousavi Khaneghah A, Aadil RM. Therapeutic potential of mangiferin in cancer: Unveiling regulatory pathways, mechanisms of action, and bioavailability enhancements - An updated review. Food Sci Nutr. 2023;12(3):1413-1429. doi: 10.1002/fsn3.3869.

Iureva AM, Nikitin PI, Tereshina ED, Nikitin MP, Shipunova VO. The influence of various polymer coatings on the in vitro and in vivo properties of PLGA nanoparticles: Comprehensive study. Eur J Pharm Biopharm. 2024;201:114366. doi: 10.1016/j.ejpb.2024.114366.

Jabbari S, Ghamkhari A, Javadzadeh Y, Salehi R, Davaran S. Doxorubicin and chrysin combination chemotherapy with novel pH-responsive poly [(lactide-co-glycolic acid)-block-methacrylic acid] nanoparticle. J Drug Deliv Sci Technol. 2018;46:129-137. doi: 10.1016/j.jddst.2018.05.006.

Javia A, Bardoliwala D, Patel M. Ligands and Receptors for Targeted Delivery of Nanoparticles: Recent Updates and Challenges. InDrug Delivery with Targeted Nanoparticles 2021;97-130. Jenny Stanford Publishing.

Jiang M, He K, Qiu T, Sun J, Liu Q, Zhang X, Zheng H. Tumor-targeted delivery of silibinin and IPI-549 synergistically inhibit breast cancer by remodeling the microenvironment. Int J Pharm. 2020;581:119239. doi: 10.1016/j.ijpharm.2020.119239.

Kadari A, Gudem S, Kulhari H, Bhandi MM, Borkar RM, Kolapalli VR, Sistla R. Enhanced oral bioavailability and anticancer efficacy of fisetin by encapsulating as inclusion complex with HPβCD in polymeric nanoparticles. Drug Deliv. 2017;24(1):224-232. doi: 10.1080/10717544.2016.1245366.

Kaminskas LM, Boyd BJ. Nanosized drug delivery vectors and the reticuloendothelial system. Intracellular Delivery: Fundamentals and Applications. 2011:155-178. doi: 10.1007/978-94-007-1248-5_6.

Kammalla AK, Ramasamy MK, Inampudi J, Dubey GP, Agrawal A, Kaliappan I. Comparative pharmacokinetic study of mangiferin after oral administration of pure mangiferin and US patented polyherbal formulation to rats. AAPS PharmSciTech. 2015;16(2):250-258. doi: 10.1208/s12249-014-0206-8.

Kandemir K, Tomas M, McClements DJ, Capanoglu E. Recent advances on the improvement of quercetin bioavailability. Trends in Food Science & Technology. 2022;119:192-200. doi: 10.1016/j.tifs.2021.11.032.

Kannan K, Jain SK. Oxidative stress and apoptosis. Pathophysiol. 2000;7(3):153-163. doi: 10.1016/s0928-4680(00)00053-5.

Kazi J, Sen R, Ganguly S, Jha T, Ganguly S, Chatterjee Debnath M. Folate decorated epigallocatechin-3-gallate (EGCG) loaded PLGA nanoparticles; in-vitro and in-vivo targeting efficacy against MDA-MB-231 tumor xenograft. Int J Pharm. 2020;585:119449. doi: 10.1016/j.ijpharm.2020.119449.

Khan H, Ullah H, Martorell M, Valdes SE, Belwal T, Tejada S, Sureda A, Kamal MA. Flavonoids nanoparticles in cancer: Treatment, prevention and clinical prospects. Semin Cancer Biol. 2021;69:200-211. doi: 10.1016/j.semcancer.2019.07.023.

Khan S, Baboota S, Ali J, Khan S, Narang RS, Narang JK. Nanostructured lipid carriers: An emerging platform for improving oral bioavailability of lipophilic drugs. Int J Pharm Investig. 2015;5(4):182-191. doi: 10.4103/2230-973X.167661.

Khan T, Gurav P. PhytoNanotechnology: Enhancing Delivery of Plant Based Anti-cancer Drugs. Front Pharmacol. 2018;8:1002. doi: 10.3389/fphar.2017.01002.

Khurana RK, Bansal AK, Beg S, Burrow AJ, Katare OP, Singh KK, Singh B. Enhancing biopharmaceutical attributes of phospholipid complex-loaded nanostructured lipidic carriers of mangiferin: Systematic development, characterization and evaluation. Int J Pharm. 2017;518(1-2):289-306. doi: 10.1016/j.ijpharm.2016.12.044.

Khurana RK, Gaspar BL, Welsby G, Katare OP, Singh KK, Singh B. Improving the biopharmaceutical attributes of mangiferin using vitamin E-TPGS co-loaded self-assembled phosholipidic nano-mixed micellar systems. Drug Deliv Transl Res. 2018;8(3):617-632. doi: 10.1007/s13346-018-0498-4.

Kim H, Kim H, Mosaddik A, Gyawali R, Ahn KS, Cho SK. Induction of apoptosis by ethanolic extract of mango peel and comparative analysis of the chemical constitutes of mango peel and flesh. Food Chem. 2012;133(2):416-422. doi: 10.1016/j.foodchem.2012.01.053.

Kopustinskiene DM, Jakstas V, Savickas A, Bernatoniene J. Flavonoids as Anticancer Agents. Nutrients. 2020 Feb 12;12(2):457. doi: 10.3390/nu12020457.

Kundu M, Sadhukhan P, Ghosh N, Chatterjee S, Manna P, Das J, Sil PC. pH-responsive and targeted delivery of curcumin via phenylboronic acid-functionalized ZnO nanoparticles for breast cancer therapy. J Adv Res. 2019;18:161-172. doi: 10.1016/j.jare.2019.02.036.

Kunjiappan S, Pavadai P, Vellaichamy S, Ram Kumar Pandian S, Ravishankar V, Palanisamy P, Govindaraj S, Srinivasan G, Premanand A, Sankaranarayanan M, Theivendren P. Surface receptor-mediated targeted drug delivery systems for enhanced cancer treatment: A state-of-the-art review. Drug Dev Res. 2021;82(3):309-340. doi: 10.1002/ddr.21758.

Li M, Ma H, Yang L, Li P. Mangiferin inhibition of proliferation and induction of apoptosis in human prostate cancer cells is correlated with downregulation of B-cell lymphoma-2 and upregulation of microRNA-182. Oncol Lett. 2016;11(1):817-822. doi: 10.3892/ol.2015.3924.

Li M, Zhang W, Wang B, Gao Y, Song Z, Zheng QC. Ligand-based targeted therapy: a novel strategy for hepatocellular carcinoma. Int J Nanomedicine. 2016a;11:5645-5669. doi: 10.2147/IJN.S115727.

Li M, Zhao G, Su WK, Shuai Q. Enzyme-Responsive Nanoparticles for Anti-tumor Drug Delivery. Front Chem. 2020;8:647. doi: 10.3389/fchem.2020.00647.

Lingling G, Yuan Z, Weigen L. Preparation, optimization, characterization and in vivo pharmacokinetic study of asiatic acid tromethamine salt-loaded solid lipid nanoparticles. Drug Dev Ind Pharm. 2016;42(8):1325-1333. doi: 10.3109/03639045.2015.1135934.

Liu XQ, Xiong MH, Shu XT, Tang RZ, Wang J. Therapeutic delivery of siRNA silencing HIF-1 alpha with micellar nanoparticles inhibits hypoxic tumor growth. Mol Pharm. 2012;9(10):2863-2874. doi: 10.1021/mp300193f.

Louisa M, Soediro TM, Suyatna FD. In vitro modulation of P-glycoprotein, MRP-1 and BCRP expression by mangiferin in doxorubicin-treated MCF-7 cells. Asian Pac J Cancer Prev. 2014;15(4):1639-1642. doi: 10.7314/apjcp.2014.15.4.1639.

Luo J, Sun J, Luo X, Wei Y, Zheng H, Mu C, Yao W. Low molecular weight chitosan-based conjugates for efficient Rhein oral delivery: synthesis, characterization, and pharmacokinetics. Drug Dev Ind Pharm. 2019;45(1):96-104. doi: 10.1080/03639045.2018.1522326.

Lv T, Yu T, Fang Y, Zhang S, Jiang M, Zhang H, Zhang Y, Li Z, Chen H, Gao Y. Role of generation on folic acid-modified poly(amidoamine) dendrimers for targeted delivery of baicalin to cancer cells. Mater Sci Eng C Mater Biol Appl. 2017;75:182-190. doi: 10.1016/j.msec.2016.12.134.

Lyu S, Zhang M, Zhang B, Zhu J, Gao L, Qiu Y, Yang L, Zhang Y. The value of radiomics model based on ultrasound image features in the differentiation between minimal breast

cancer and small benign breast masses. J Clin Ultrasound 2023;51(9):1536-1543. doi: 10.1002/jcu.23556.

Madureira AR, Nunes S, Campos DA, Fernandes JC, Marques C, Zuzarte M, Gullón B, Rodríguez-Alcalá LM, Calhau C, Sarmento B, Gomes AM, Pintado MM, Reis F. Safety profile of solid lipid nanoparticles loaded with rosmarinic acid for oral use: in vitro and animal approaches. Int J Nanomedicine. 2016;11:3621-3640. doi: 10.2147/IJN.S104623.

Maghsoudnia N, Eftekhari RB, Sohi AN, Zamzami A, Dorkoosh FA. Application of nano-based systems for drug delivery and targeting: a review. Journal of Nanoparticle Research. 2020;22:1-41. doi: 10.1007/s11051-020-04959-8.

Makadia HK, Siegel SJ. Poly Lactic-co-Glycolic Acid (PLGA) as Biodegradable Controlled Drug Delivery Carrier. Polymers (Basel). 2011;3(3):1377-1397. doi: 10.3390/polym3031377.

Man N, Wang Q, Li H, Adu-Frimpong M, Sun C, Zhang K, Yang Q, Wei Q, Ji H, Toreniyazov E, Yu J. Improved oral bioavailability of myricitrin by liquid self-microemulsifying drug delivery systems. Journal of drug delivery science and technology. 2019;52:597-606. doi: 10.1016/j.jddst.2019.05.003.

Manna P, Dewanjee S, Joardar S, Chakraborty P, Bhattacharya H, Bhanja S, Bhattacharyya C, Bhowmik M, Bhowmick S, Saha A, Das J, Sil PC. Carnosic acid attenuates doxorubicin-induced cardiotoxicity by decreasing oxidative stress and its concomitant pathological consequences. Food Chem Toxicol. 2022;166:113205. doi: 10.1016/j.fct.2022.113205.

Markeb AA, El-Maali NA, Sayed DM, Osama A, Abdel-Malek MA, Zaki AH,Elwanis ME, Driscoll JJ. Synthesis, Structural Characterization, and Preclinical Efficacy of a Novel Paclitaxel-Loaded Alginate Nanoparticle for Breast Cancer Treatment. Int J Breast Cancer 2016;2016:7549372. doi: 10.1155/2016/7549372.

Martins-Filho SN, Paiva C, Azevedo RS, Alves VAF. Histological Grading of Hepatocellular Carcinoma-A Systematic Review of Literature. Front Med (Lausanne). 2017;4:193. doi: 10.3389/fmed.2017.00193.

Mei S, Perumal M, Battino M, Kitts DD, Xiao J, Ma H, Chen X. Mangiferin: a review of dietary sources, absorption, metabolism, bioavailability, and safety. Crit Rev Food Sci Nutr. 2023;63(18):3046-3064. doi: 10.1080/10408398.2021.1983767.

Metzler M, Pfeiffer E, Schulz SI, Dempe JS. Curcumin uptake and metabolism. Biofactors. 2013;39(1):14-20. doi: 10.1002/biof.1042.

Mittal P, Vardhan H, Ajmal G, Bonde GV, Kapoor R, Mittal A, Mishra B. Formulation, optimization, hemocompatibility and pharmacokinetic evaluation of PLGA nanoparticles

containing paclitaxel. Drug Dev Ind Pharm 2019;45(3):365-378. doi: 10.1080/03639045.2018.1542706.

Moodley T, Singh M. Polymeric mesoporous silica nanoparticles for combination drug delivery in vitro. Biointerface Res Appl Chem. 2020;11:11905-11919. doi: 10.33263/BRIAC114.1190511919.

Murthy SS, Narsaiah TB. Cytotoxic Effect of Bromelain on HepG2 Hepatocellular Carcinoma Cell Line. Appl Biochem Biotechnol. 2021;193(6):1873-1897. doi: 10.1007/s12010-021-03505-z.

Natarajan JV, Nugraha C, Ng XW, Venkatraman S. Sustained-release from nanocarriers: a review. J Control Release. 2014;193:122-138. doi: 10.1016/j.jconrel.2014.05.029.

Naveen P, Lingaraju HB, Prasad KS. Rapid Development and Validation of Improved Reversed-Phase High-performance Liquid Chromatography Method for the Quantification of Mangiferin, a Polyphenol Xanthone Glycoside in Mangifera indica. Pharmacognosy Res 2017;9(2):215-219. doi: 10.4103/0974-8490.204652.

Németh Z, Csóka I, Semnani Jazani R, Sipos B, Haspel H, Kozma G, Kónya Z, Dobó DG. Quality by Design-Driven Zeta Potential Optimisation Study of Liposomes with Charge Imparting Membrane Additives. Pharmaceutics 2022;14(9):1798. doi: 10.3390/pharmaceutics14091798.

Nguyen TT, Duong VA, Maeng HJ. Pharmaceutical Formulations with P-Glycoprotein Inhibitory Effect as Promising Approaches for Enhancing Oral Drug Absorption and Bioavailability. Pharmaceutics. 2021;13(7):1103. doi: 10.3390/pharmaceutics13071103.

Nirgude S, Mahadeva R, Koroth J, Kumar S, Kumar KSS, Gopalakrishnan V, S Karki SS, Choudhary B. ST09, A Novel Curcumin Derivative, Blocks Cell Migration by Inhibiting Matrix Metalloproteases in Breast Cancer Cells and Inhibits Tumor Progression in EAC Mouse Tumor Models. Molecules 2020;25(19):4499. doi: 10.3390/molecules25194499.

Núñez Selles AJ, Daglia M, Rastrelli L. The potential role of mangiferin in cancer treatment through its immunomodulatory, anti-angiogenic, apoptopic, and gene regulatory effects. Biofactors. 2016;42(5):475-491. doi: 10.1002/biof.1299.

Padera TP, Meijer EF, Munn LL. The Lymphatic System in Disease Processes and Cancer Progression. Annu Rev Biomed Eng. 2016;18:125-158. doi: 10.1146/annurev-bioeng-112315-031200.

Padera TP, Stoll BR, Tooredman JB, Capen D, di Tomaso E, Jain RK. Pathology: cancer cells compress intratumour vessels. Nature. 2004;427(6976):695. doi: 10.1038/427695a.

Pan LL, Wang AY, Huang YQ, Luo Y, Ling M. Mangiferin induces apoptosis by regulating Bcl-2 and Bax expression in the CNE2 nasopharyngeal carcinoma cell line. Asian Pac J Cancer Prev. 2014;15(17):7065-7068. doi: 10.7314/apjcp.2014.15.17.7065.

Pan W, Gu F, Yan X, Huang J, Liao H, Niu F. Biomacromolecular carriers based hydrophobic natural products for potential cancer therapy. Int J Biol Macromol. 2024;269(Pt 2):132274. doi: 10.1016/j.ijbiomac.2024.132274.

Pandey P, Rahman M, Bhatt PC, Beg S, Paul B, Hafeez A, Al-Abbasi FA, Nadeem MS, Baothman O, Anwar F, Kumar V. Implication of nano-antioxidant therapy for treatment of hepatocellular carcinoma using PLGA nanoparticles of rutin. Nanomedicine (Lond). 2018;13(8):849-870. doi: 10.2217/nnm-2017-0306.

Panwar R, Raghuwanshi N, Srivastava AK, Sharma AK, Pruthi V. In-vivo sustained release of nanoencapsulated ferulic acid and its impact in induced diabetes. Mater Sci Eng C Mater Biol Appl. 2018;92:381-392. doi: 10.1016/j.msec.2018.06.055.

Parashar P, Rathor M, Dwivedi M, Saraf SA. Hyaluronic Acid Decorated Naringenin Nanoparticles: Appraisal of Chemopreventive and Curative Potential for Lung Cancer. Pharmaceutics. 2018;10(1):33. doi: 10.3390/pharmaceutics10010033.

Patra JK, Das G, Fraceto LF, Campos EVR, Rodriguez-Torres MDP, Acosta-Torres LS, Diaz-Torres LA, Grillo R, Swamy MK, Sharma S, Habtemariam S, Shin HS. J Nanobiotechnol. 2018;16(1):71. doi: 10.1186/s12951-018-0392-8.

Paul P, Mandal S, Dua TK, Mandal D, Deepa RM. Smart multifunctional nanosystem: Next-generation drug delivery platform for drug-resistant breast cancer. In: Multifunctional Theranostic Nanomedicines in Cancer 2021;177-199. Academic Press. doi: 10.1016/B978-0-12-821712-2.00012-8.

Pelicano H, Martin DS, Xu RH, Huang P. Glycolysis inhibition for anticancer treatment. Oncogene. 2006;25(34):4633-4646. doi: 10.1038/sj.onc.1209597.

Peñalva R, Morales J, González-Navarro CJ, Larrañeta E, Quincoces G, Peñuelas I, Irache JM. Increased Oral Bioavailability of Resveratrol by Its Encapsulation in Casein Nanoparticles. Int J Mol Sci. 2018;19(9):2816. doi: 10.3390/ijms19092816.

Peng ZG, Yao YB, Yang J, Tang YL, Huang X. Mangiferin induces cell cycle arrest at G2/M phase through ATR-Chk1 pathway in HL-60 leukemia cells. Genet Mol Res. 2015;14(2):4989-5002. doi: 10.4238/2015.May.12.2.

Pinto TV, Silva CA, Siquenique S, Learmonth DA. Micro-and nanocarriers for encapsulation of biological plant protection agents: A systematic literature review. ACS Agricultural Science & Technology. 2022;2(5):838-857. doi: 10.1021/acsagscitech.2c00113.

Prabha S, Labhasetwar V. Nanoparticle-mediated wild-type p53 gene delivery results in sustained antiproliferative activity in breast cancer cells. Mol Pharm. 2004;1(3):211-219. doi: 10.1021/mp049970+.

Rahim MA, Jan N, Khan S, Shah H, Madni A, Khan A, Jabar A, Khan S, Elhissi A, Hussain Z, Aziz HC, Sohail M, Khan M, Thu HE. Recent Advancements in Stimuli Responsive Drug Delivery Platforms for Active and Passive Cancer Targeting. Cancers (Basel). 2021;13(4):670. doi: 10.3390/cancers13040670.

Rahmani AH, Almatroudi A, Allemailem KS, Alharbi HOA, Alwanian WM, Alhunayhani BA, Algahtani M, Theyab A, Almansour NM, Algefary AN, Aldeghaim SSA, Khan AA. Role of Mangiferin in Management of Cancers through Modulation of Signal Transduction Pathways. Biomedicines. 2023;11(12):3205. doi: 10.3390/biomedicines11123205.

Raposo CD, Costa R, Petrova KT, Brito C, Scotti MT, Cardoso MM. Development of Novel Galactosylated PLGA Nanoparticles for Hepatocyte Targeting Using Molecular Modelling. Polymers (Basel). 2020;12(1):94. doi: 10.3390/polym12010094.

Ratan C, Arian AM, Rajendran R, Jayakumar R, Masson M, Mangalathillam S. Nano-based formulations of curcumin: elucidating the potential benefits and future prospects in skin cancer. Biomed Mater. 2023;18(5). doi: 10.1088/1748-605X/acf0af.

Ray M, Al Hoque A, Chatterjee S, Adhikary S, Paul S, Mukherjee B, Bhattacharya A. Clofarabine-loaded aptamer-conjugated biodegradable nanoparticle successfully targeted CD117 overexpressed HL60 cells and potentially induced apoptosis. Heliyon. 2025;11(4):e42450. doi: 10.1016/j.heliyon.2025.e42450.

Ren KW, Li YH, Wu G, Ren JZ, Lu HB, Li ZM, Han XW. Quercetin nanoparticles display antitumor activity via proliferation inhibition and apoptosis induction in liver cancer cells. Int J Oncol. 2017;50(4):1299-1311. doi: 10.3892/ijo.2017.3886.

Rezk AI, Hwang TI, Kim JY, Lee JY, Park CH, Kim CS. Functional composite nanofibers loaded with β-TCP and SIM as a control drug delivery system. Materials Lett. 2019;240:25-29. doi: 10.1016/j.matlet.2018.12.107.

Rodriguez-Ruiz V, Salatti-Dorado JÁ, Barzegari A, Nicolas-Boluda A, Houaoui A, Caballo C, Caballero-Casero N, Sicilia D, Bastias Venegas J, Pauthe E, Omidi Y, Letourneur D, Rubio S, Gueguen V, Pavon-Djavid G. Astaxanthin-Loaded Nanostructured Lipid Carriers for

Preservation of Antioxidant Activity. Molecules. 2018;23(10):2601. doi: 10.3390/molecules23102601.

Sabourian P, Yazdani G, Ashraf SS, Frounchi M, Mashayekhan S, Kiani S, Kakkar A. Effect of Physico-Chemical Properties of Nanoparticles on Their Intracellular Uptake. Int J Mol Sci. 2020;21(21):8019. doi: 10.3390/ijms21218019.

Sadhukhan P, Kundu M, Chatterjee S, Ghosh N, Manna P, Das J, Sil PC. Targeted delivery of quercetin via pH-responsive zinc oxide nanoparticles for breast cancer therapy. Mater Sci Eng C Mater Biol Appl. 2019;100:129-140. doi: 10.1016/j.ms50ec.2019.02.096.

Samadarsi R, Dutta D. Design and characterization of mangiferin nanoparticles for oral delivery. Journal of Food Engineering. 2019;247:80-94. doi: 10.1016/j.jfoodeng.2018.11.020.

Sanna V, Singh CK, Jashari R, Adhami VM, Chamcheu JC, Rady I, Sechi M, Mukhtar H, Siddiqui IA. Targeted nanoparticles encapsulating (-)-epigallocatechin-3-gallate for prostate cancer prevention and therapy. Sci Rep. 2017;7:41573. doi: 10.1038/srep41573.

Sarkar S, Das AK, Bhattacharya S, Gachhui R, Sil PC. Isorhamnetin exerts anti-tumor activity in DEN + CCl_4-induced HCC mice. Med Oncol. 2023;40(7):188. doi: 10.1007/s12032-023-02050-5.

Sarwar AR, Iqbal FM, Jamil MA, Abbas K. Nanocrystals of Mangiferin Using Design Expert: Preparation, Characterization, and Pharmacokinetic Evaluation. Molecules. 2023;28(15):5918. doi: 10.3390/molecules28155918.

Selc M, Macova R, Babelova A. Novel Strategies Enhancing Bioavailability and Therapeutical Potential of Silibinin for Treatment of Liver Disorders. Drug Des Devel Ther. 2024;18:4629-4659. doi: 10.2147/DDDT.S483140.

Semwal R, Joshi SK, Semwal RB, Semwal DK. Health benefits and limitations of rutin-A natural flavonoid with high nutraceutical value. Phytochemistry Letters. 2021;46:119-128. doi: 10.1016/j.phytol.2021.10.006.

Sen R, Ganguly S, Ganguly S, Debnath MC, Chakraborty S, Mukherjee B, Chattopadhyay D. Apigenin-Loaded PLGA-DMSA Nanoparticles: A Novel Strategy to Treat Melanoma Lung Metastasis. Mol Pharm. 2021;18(5):1920-1938. doi: 10.1021/acs.molpharmaceut.0c00977.

Senapati S, Mahanta AK, Kumar S, Maiti P. Controlled drug delivery vehicles for cancer treatment and their performance. Signal Transduct Target Ther. 2018;3:7. doi: 10.1038/s41392-017-0004-3.

Shaker SA, Alshufta SM, Gowayed MA, El-Salamouni NS, Bassam SM, Megahed MA, El-Tahan RA. Propolis-loaded nanostructured lipid carriers halt breast cancer progression

through miRNA-223 related pathways: an in-vitro/in-vivo experiment. Sci Rep. 2023;13(1):15752. doi: 10.1038/s41598-023-42709-7.

Sharma M, Sharma R, Jain DK. Nanotechnology Based Approaches for Enhancing Oral Bioavailability of Poorly Water Soluble Antihypertensive Drugs. Scientifica (Cairo). 2016;2016:8525679. doi: 10.1155/2016/8525679.

Shavi GV, Nayak UY, Maliyakkal N, Deshpande PB, Raghavendra R, Kumar AR, Reddya MS, Udupa N, Shrawan B. Nanomedicine of anastrozole for breast cancer: Physicochemical evaluation, in vitro cytotoxicity on BT-549 and MCF-7 cell lines and preclinical study on rat model. Life Sci. 2015;141:143-155. doi: 10.1016/j.lfs.2015.09.021.

Shehatta NH, Okda TM, Omran GA, Abd-Alhaseeb MM. Baicalin; a promising chemopreventive agent, enhances the antitumor effect of 5-FU against breast cancer and inhibits tumor growth and angiogenesis in Ehrlich solid tumor. Biomed Pharmacother 2022;146:112599. doi: 10.1016/j.biopha.2021.112599.

Siepmann J, Peppas NA. Modeling of drug release from delivery systems based on hydroxypropyl methylcellulose. HPMC). Adv Drug Deliv Rev. 2001;48(2-3):139-157. doi: 10.1016/s0169-409x(01)00112-0.

Singh P, Singh RK. Emerging Nano-Phytochemicals-Based Sustained Drug Delivery System for Cancer Therapeutics. In: Nano-formulation of Dietary Phytochemicals for Cancer Management 2025;375-400. Singapore: Springer Nature Singapore. doi: 10.1007/978-981-97-8005-1_14.

Singh S, Singha P. Effect of Modifications in Poly (Lactide-co-Glycolide) (PLGA) on Drug Release and Degradation Characteristics: A Mini Review. Curr Drug Deliv. 2021;18(10):1378-1390. doi: 10.2174/1567201818666210510165938.

Sohail M, Guo W, Li Z, Xu H, Zhao F, Chen D, Fu F. Nanocarrier-based Drug Delivery System for Cancer Therapeutics: A Review of the Last Decade. Curr Med Chem. 2021;28(19):3753-3772. doi: 10.2174/0929867327666201005111722.

Su S, Kang PM. Systemic Review of Biodegradable Nanomaterials in Nanomedicine. Nanomaterials (Basel). 2020;10(4):656. doi: 10.3390/nano10040656.

Subhan MA, Yalamarty SSK, Filipczak N, Parveen F, Torchilin VP. Recent Advances in Tumor Targeting via EPR Effect for Cancer Treatment. J Pers Med. 2021;11(6):571. doi: 10.3390/jpm11060571.

Sun L, Liu H, Ye Y, Lei Y, Islam R, Tan S, Tong R, Miao YB, Cai L. Smart nanoparticles for cancer therapy. Signal Transduct Target Ther. 2023;8(1):418. doi: 10.1038/s41392-023-01642-x.

Sun X, Xu Y, Zhao L, Yan H, Wang S, Wang D. The stability and bioaccessibility of fucoxanthin in spray-dried microcapsules based on various biopolymers. RSC Adv. 2018;8(61):35139-35149. doi: 10.1039/c8ra05621h.

Sur S, Pal D, Mandal S, Roy A, Panda CK. Tea polyphenols epigallocatechin gallete and theaflavin restrict mouse liver carcinogenesis through modulation of self-renewal Wnt and hedgehog pathways. J Nutr Biochem. 2016;27:32-42. doi: 10.1016/j.jnutbio.2015.08.016.

Sutradhar KB, Amin ML. Nanotechnology in cancer drug delivery and selective targeting. International scholarly research notices. 2014;2014(1):939378. doi: 10.1155/2014/939378.

Tabanelli R, Brogi S, Calderone V. Improving Curcumin Bioavailability: Current Strategies and Future Perspectives. Pharmaceutics. 2021;13(10):1715. doi: 10.3390/pharmaceutics13101715.

Taghipour YD, Hajialyani M, Naseri R, Hesari M, Mohammadi P, Stefanucci A, Mollica A, Farzaei MH, Abdollahi M. Nanoformulations of natural products for management of metabolic syndrome. Int J Nanomedicine. 2019;14:5303-5321. doi: 10.2147/IJN.S213831.

Talevi A, Ruiz ME. Drug Dissolution: Fundamental Theoretic Models. InThe ADME Encyclopedia: A Comprehensive Guide on Biopharmacy and Pharmacokinetics 2022;341-349. Cham: Springer International Publishing. doi: 10.1007/978-3-030-84860-6_29.

Tang SH, Li R, Tan J, Wang Y, Jiang ZT. One pot synthesis of water-soluble quercetin derived multifunctional nanoparticles with photothermal and antioxidation capabilities. Colloids Surf B Biointerfaces. 2019;183:110429. doi: 10.1016/j.colsurfb.2019.110429.

Tessiri C, Channarong S, Wongtrakul P. Development of aqueous formulation containing the extracted mangiferin. Key Engg Mater. 2021;901:40-47. doi: 10.4028/www.scientific.net/KEM.901.40.

Toragall V, Srirangam P, Jayapala N, Baskaran V. Lutein encapsulated oleic-linoleic acid nanoemulsion boosts oral bioavailability of the eye protective carotenoid lutein in rat model. Materials Today Communications. 2021;28:102522. doi: 10.1016/j.mtcomm.2021.102522.

Trachootham D, Alexandre J, Huang P. Targeting cancer cells by ROS-mediated mechanisms: a radical therapeutic approach? Nat Rev Drug Discov. 2009;8(7):579-591. doi: 10.1038/nrd2803.

Upponi JR, Torchilin VP. Passive vs. active targeting: an update of the epr role in drug delivery to tumors. In: Nano-Oncologicals: New Targeting and Delivery Approaches 2014;3-45. Cham: Springer International Publishing. doi: 10.1007/978-3-319-08084-0_1.

Van Thoai D, Nguyen DT, Dang LH, Nguyen NH, Nguyen VT, Doan P, Nguyen BT, Le Van Thu, Tung NN, Quyen TN. Lipophilic effect of various pluronic-grafted gelatin copolymers on the quercetin delivery efficiency in these self-assembly nanogels. J Polymer Res. 2020;27:1-2. doi: 10.1007/s10965-020-02216-z.

Wang Y, Pi C, Feng X, Hou Y, Zhao L, Wei Y. The Influence of Nanoparticle Properties on Oral Bioavailability of Drugs. Int J Nanomedicine. 2020;15:6295-6310. doi: 10.2147/IJN.S257269.

Wei QY, He KM, Chen JL, Xu YM, Lau ATY. Phytofabrication of Nanoparticles as Novel Drugs for Anticancer Applications. Molecules. 2019;24(23):4246. doi: 10.3390/molecules24234246.

Wu W, Pu Y, Shi J. Nanomedicine-enabled chemotherapy-based synergetic cancer treatments. J Nanobiotechnol. 2022;20(1):4. doi: 10.1186/s12951-021-01181-z.

Xu QT, Zhang WX, Xu HX, Zhang QF. Fabrication of Luteolin Loaded Zein-Caseinate Nanoparticles and its Bioavailability Enhancement in Rats. J Pharm Sci. 2023;112(12):3056-3066. doi: 10.1016/j.xphs.2023.06.010.

Yameen B, Choi WI, Vilos C, Swami A, Shi J, Farokhzad OC. Insight into nanoparticle cellular uptake and intracellular targeting. J Control Release. 2014;190:485-499. doi: 10.1016/j.jconrel.2014.06.038.

Yao Y, Zhou Y, Liu L, Xu Y, Chen Q, Wang Y, Wu S, Deng Y, Zhang J, Shao A. Nanoparticle-Based Drug Delivery in Cancer Therapy and Its Role in Overcoming Drug Resistance. Front Mol Biosci. 2020;7:193. doi: 10.3389/fmolb.2020.00193.

Yetisgin AA, Cetinel S, Zuvin M, Kosar A, Kutlu O. Therapeutic Nanoparticles and Their Targeted Delivery Applications. Molecules. 2020;25(9):2193. doi: 10.3390/molecules25092193.

Yoo J, Park C, Yi G, Lee D, Koo H. Active Targeting Strategies Using Biological Ligands for Nanoparticle Drug Delivery Systems. Cancers (Basel). 2019;11(5):640. doi: 10.3390/cancers11050640.

Yuan Y, Cai T, Xia X, Zhang R, Chiba P, Cai Y. Nanoparticle delivery of anticancer drugs overcomes multidrug resistance in breast cancer. Drug Deliv. 2016;23(9):3350-3357. doi: 10.1080/10717544.2016.1178825.

Zheng H, Wijaya W, Zhang H, Feng K, Liu Q, Zheng T, Yin Z, Cao Y, Huang Q. Improving the bioaccessibility and bioavailability of carnosic acid using a lecithin-based nanoemulsion: complementary *in vitro* and *in vivo* studies. Food Funct. 2020;11(9):8141-8149. doi: 10.1039/d0fo01098g.

Zhou Q, Hou K, Fu Z. Transferrin-Modified Mangiferin-Loaded SLNs: Preparation, Characterization, and Application in A549 Lung Cancer Cell. Drug Des Devel Ther. 2022;16:1767-1778. doi: 10.2147/DDDT.S366531.

Zhu Y, Liao L. Applications of Nanoparticles for Anticancer Drug Delivery: A Review. J Nanosci Nanotechnol. 2015;15(7):4753-4773. doi: 10.1166/jnn.2015.10298.

Zi Y, Yang K, He J, Wu Z, Liu J, Zhang W. Strategies to enhance drug delivery to solid tumors by harnessing the EPR effects and alternative targeting mechanisms. Adv Drug Deliv Rev. 2022;188:114449. doi: 10.1016/j.addr.2022.114449.

Naunyn-Schmiedeberg's Archives of Pharmacology
https://doi.org/10.1007/s00210-025-04068-0

RESEARCH

Formulation and evaluation of polymeric nanoparticles to improve in vivo chemotherapeutic efficacy of mangiferin against breast cancer

Pratik Chakraborty[1] · Ananya Das[2] · Sharmistha Chatterjee[3] · Aparajita Bairagi[2] · Hiranmoy Bhattacharya[1] · Chiranjib Bhattacharyya[1] · Nabanita Chatterjee[2] · Parames C. Sil[3] · Saikat Dewanjee[1]

Received: 20 November 2024 / Accepted: 17 March 2025

Abstract

Mangiferin (Mgf), a naturally occurring polyphenol, can act as an apoptosis inducer for various cancer cells. Thus, it is holding the prospect of being a promising chemotherapeutic agent. However, a discrepancy between the in vitro results and in vivo observations seems to exist that apprehends its potential usefulness. The in vivo chemotherapeutic capacity of Mgf is greatly challenged because of the unfavorable pharmacokinetic credentials. The present study aims to overcome the biopharmaceutical limitations and improve the chemotherapeutic efficacy by incorporating it within nano-scale delivery system. Stable and sphere-shaped Mgf-loaded poly(lactic-co-glycolic) acid (PLGA) nanoparticles (MNPs) were formulated using the nanoprecipitation method and characterized. Further, MNPs were assessed through multiple in vitro and in vivo preclinical evaluations for their chemotherapeutic efficacy, with an ambition to improve the performance in the biological system. Sphere-shaped MNPs exhibited satisfactory drug loading and release profile. The Mgf-loaded nanoformulation also exhibited better cytotoxic potential against breast cancer cells compared to native Mgf owing to its better penetrability into cancer cells. MNPs were also found to confer superior in vivo chemotherapeutic efficacy in breast cancer-bearing mice evidenced by the reduction of tumor load. Improved anti-cancer potential of MNPs over free Mgf was also established through different bioassays. Moreover, the nanoparticles did not confer systemic toxicity to levels of concern. To conclude, the current study pleads for MNPs as a safe and efficacious tool in the fight against breast cancer for futuristic translations.

Keywords Breast cancer · Chemotherapeutic efficacy · Mangiferin · Plant-derived small molecule · Polymeric nanoparticles

Introduction

Breast cancer has currently become one of the most common malignancies in women globally (Lyu et al. 2023). Cases of breast cancer are predicted to go beyond 3 million by 2040 globally, leading to nearly 1 million deaths per annum (Arnold et al. 2022). The heterogeneity associated with breast cancer poses additional challenges towards its therapeutic management. Conventional chemotherapeutic modalities mostly suffer from burdensome non-specific toxicities (Wu et al. 2022). Thus, there is an alarming requirement for newer approaches for the efficient management of cancers including breast cancer. Nature-derived chemotherapeutic agents against different cancer types have been gaining scientific attraction throughout the past decades (Przystupski et al. 2019).

Mangiferin (Mgf), a naturally occurring polyphenol, exhibits promising apoptosis induction capacity in diverse types of cancer cells including breast cancer cells (Pan et al. 2014; Cuccioloni et al. 2016; Li et al. 2016; Núñez Selles et al. 2016). Thus, Mgf holds promise to serve as a potential therapeutic agent for breast cancer chemotherapy. Mgf imparts death to cancer cells by elevating oxidative stress

✉ Nabanita Chatterjee
nabanita.chatterje@yahoo.com

✉ Parames C. Sil
parames_95@yahoo.co.in

✉ Saikat Dewanjee
saikat.dewanjee@jadavpuruniversity.in

[1] Advanced Pharmacognosy Research Laboratory, Department of Pharmaceutical Technology, Jadavpur University, Kolkata 700032, India

[2] Chittaranjan National Cancer Institute, Kolkata 700026, India

[3] Division of Molecular Medicine, Bose Institute, Kolkata 700054, India

Published online: 28 March 2025

and promoting apoptosis, as well as modulating mitochondrial membrane potential (MMP) (Dutta et al. 2017; Du et al. 2018). To exert anti-tumor activity, Mgf mainly targets tumor growth factors, apoptotic pathways, and angiogenesis. Mgf downregulates inflammation and cellular proliferation in breast cancer. Further, it is associated with upregulation of proapoptotic signals (Cuccioloni et al. 2016; Wang et al. 2021; Rahmani et al. 2023). Mgf can even improve the sensitivity of breast cancer cells to other anti-cancer drugs, in a concentration-dependent manner (Louisa et al. 2014; Iqbal et al. 2023). However, the in vitro therapeutic promise is somewhat compromised within biological system in vivo, which apprehends its clinical usefulness (Khurana et al. 2018; Dewanjee et al. 2020). Poor aqueous solubility, poor bioavailability, rapid metabolism, and considerable P-gp efflux can be attributed to its in vivo incompetence (Nguyen et al. 2021; Mei et al. 2023; Baghel et al. 2024; Iqbal et al. 2023). Decades of research have attempted to resolve this issue via different approaches. Formulation of Mgf within a suitable drug delivery system could be a potential pharmaceutical approach to eradicate its pharmacokinetic incompetence and recover its chemotherapeutic efficacy.

Nanostructured delivery systems have displayed exciting promise to recuperate biopharmaceutical and pharmacokinetic limitations of a potential therapeutic candidate (Aminu et al. 2020). Polymeric nanoparticles, owing to their good tissue penetrability, sustained release effect, low toxicity, and easy moldability have emerged as popular tool in cancer therapeutics (Mughees and Wajid 2021; Gautam et al. 2022). Poly(lactic-co-glycolic) acid (PLGA), a biocompatible polymer with low to no toxicity, is approved by the European Medical Association for parenteral administration and the United States Food and Drug Administration for utilization in drug delivery systems. Poorly soluble chemotherapeutic moieties can be effectively encapsulated within PLGA nanoshells, that, in turn, extravasate through tumor vasculature by virtue of enhanced permeability and retention (EPR) effect (Zi et al. 2022). PLGA nanoshells contain lipophilic moieties on the inside and polar groups on the outside, thus enabling efficient encapsulation of drugs and/or chemotherapeutic agents, as well as the release of the loaded agent in the desired medium.

Nano-scale carriers of Mgf are emerging as potentially useful chemotherapeutic tools against different types of cancers. In this context, ZnO and PLGA-matrix nanoparticles carrying lupeol and Mgf have exhibited promising anti-cancer potential against prostate cancer (Fabián et al. 2023). Liposomal delivery of Mgf with curcumin offers remarkable therapeutic advances against ovarian cancer (Alharbi et al. 2024). Transferrin-modified solid-lipid nanoparticles loaded with Mgf efficiently suppressed the progress of lung cancer in vivo (Zhou et al. 2022). As an exemplary clinical translation, Mgf-supplementation has reduced serum triglycerides and free fatty acids in hyperlipidemic patients in a double-blind clinical trial (Na et al. 2015). A recent clinical study has established *Mangifera indica* extract, standardized to Mgf to confer significant benefits regarding cognition and memory (Jeyakodi et al. 2024). With regard to cancer chemotherapy with Mgf, the transition from preclinical investigations to clinical trials would mark a significant milestone. Establishing safety and efficacy in human subjects will be critical for the broad-scale utilization of nano-scale carriers of Mgf. Such improvements might also aid in planning and execution of clinical trials using a phytodrug for a specific disease. More preclinical and clinical investigations are needed to unleash the full potential of Mgf, which may serve as a therapeutic alternative for a number of different types of cancer, including breast cancer.

The current study aimed to formulate Mgf-containing PLGA-based nanoparticles (MNPs) utilizing vitamin E tocopheryl polyethylene glycol succinate (TPGS) as an emulsifier, employing nanoprecipitation method to enhance the pharmacokinetic attributes and, subsequently, improve the chemotherapeutic effectiveness of Mgf against breast cancer. Developed nanoparticles have been characterized for particle size distribution, shape, surface properties, and in vitro release profile. Further, we detailed the therapeutic efficacy and safety profile of MNPs and compared them with native Mgf employing substantial preclinical assays. The current study bears an ambition to showcase the encapsulation of potential chemotherapeutic molecules from plant sources within nano-sized polymeric delivery system, as an effective tool to reciprocate the pharmacokinetic incompetence and reclaim their chemotherapeutic attributes in biological system for probable advanced therapeutic translations.

Materials and methods

Materials

Mgf (CAS No, 4773–96-0), PLGA (L/G molar ratio 50:50, MW 38,000–54,000, acid-terminated), and vitamin E-TPGS were purchased from Sigma-Aldrich, St. Louis, USA. MDA-MB-231 cells and MCF-7 cells were obtained from the National Centre for Cell Science, Pune, India. Culture media and 3-[4,5-dimethylthiazol-2-yl]−2,5 diphenyl tetrazolium bromide (MTT) were purchased from HiMedia Laboratories, Mumbai, India. Bovine serum albumin (BSA) was procured from Sisco Research Laboratories, Mumbai, India. Serum assay kits were obtained from Transasia Bio-medicals Limited, Solan, India, and Span Diagnostics Limited, Mumbai, India. The protein assay kit (Pierce BCA protein assay kit) was obtained from Thermo Fisher Scientific, MA, USA. Annexin V-FITC/PI Apoptosis Kit (E-CK-A211) was

purchased from Elabscience, Houston, USA. Primary antibodies were obtained from Biobharati LifeScience, Kolkata, India (p53, #BB-AB0100), and Elabscience, Houston, USA (caspase 3, #E-AB-13815). Immunohistochemistry kit was purchased from Abcam, MA, USA.

Preparation of nanoparticles

Mgf-loaded nanoparticles were formulated following the nanoprecipitation method (Fessi et al. 1989). In brief, Mgf and PLGA were first dissolved in a non-aqueous solvent system (acetone:ethanol = 4:1). A drug:polymer ratio of 1:10 has been chosen based on earlier studies by our group whereby this ratio exhibited best-suited results regarding drug encapsulation (Gaonkar et al. 2017; Chatterjee et al. 2024). The solution containing Mgf and PLGA was added dropwise to an aqueous phase containing vitamin E-TPGS (0.03%; w/v), under continuous stirring. The resultant dispersion loses its transparency owing to the formation of nanoparticles. Evaporation of the non-aqueous solvent was allowed overnight. The aqueous dispersion underwent filtration to remove the unwanted particles. Nanoparticles were recovered by centrifugation (Hermle refrigerated centrifuge, Wehingen, Germany) at 16,000 rpm for 50 min at 4 °C. Upon centrifugation, the supernatant was disposed of, and the pellet was washed 2–3 times with water and lyophilized (LaboGene Scanvac Coolsafe, Bjarkesvej, Denmark) to obtain a free-flowing powder. Following a similar protocol, blank nanoparticles were also synthesized. For fluorescent nanoparticles, an alcoholic solution of FITC (0.4%; w/v) was included in the non-aqueous phase, and a similar protocol was followed for the rest of the steps. However, fluorescent nanoparticles were protected from light during preparation and storage.

Characterization of nanoparticles

Particle size, size distribution, and surface charge

Average particle size and polydispersity index (PDI) were determined using Malvern Zetasizer Nano-ZS (Malvern Instruments, Malvern, Worcestershire, UK), according to the concept of dynamic light scattering (DLS). Briefly, nanoparticle suspension (1 mg/mL) was prepared in MilliQ water. Ten microliters of this dispersion was diluted to 1 mL with MilliQ water and analyzed. Using the same instrument, zeta potential of properly diluted samples was measured at 25 °C.

Shape, morphology, and surface characters

The shape and surface morphology of the prepared nanoparticles were examined in a field emission scanning electron microscope (FESEM, JEOL JSM-7600F, Tokyo, Japan). Particle structure was evaluated in a transmission electron microscope (TEM, JEOL JEM-2100Plus, Tokyo, Japan). Atomic force microscopy (AFM; MFP-3D Origin, Asylum Research, Oxford Instruments, CA, USA) was undertaken to observe the surface topography of the nanoparticles. The specific surface area was determined with a BET surface area analyzer (Micromeritics Gemini VII 2390t, GA, USA).

Physicochemical characterization of nanoparticles

Physicochemical compatibility between Mgf and other formulation ingredients was evaluated using Fourier transform infrared (FTIR) spectroscopy (IR Prestige-21, Shimadzu, Kyoto, Japan), X-ray diffraction (XRD; Ultima III, Rigaku, Japan), and differential scanning calorimetry (DSC; DSC STARe System, Mettler Toledo, USA). Drug loading capacity and entrapment efficiency were determined utilizing a spectrophotometric technique with the help of a JASCO V-550 double beam UV–visible spectrophotometer (OK, USA).

Solubility

To compare the aqueous solubility of Mgf before and after PLGA modification, saturation solubility was determined at room temperature. Samples in excessive amount were dispersed individually in 10 mL of water and incubated at 200 rpm for 24 h. Following incubation, samples were taken out and filtered (0.45 µ), and each filtrate was subjected to spectroscopic analysis (JASCO V-550 double beam UV–visible spectrophotometer, OK, USA).

In vitro drug release kinetics

In vitro release pattern of Mgf from the MNPs was evaluated in phosphate-buffered saline (PBS) of pH 7.4 as per the protocol described by Gaonkar and co-workers (2017). To elaborate, MNPs were dissolved in PBS (1 mg/mL) and stirred continuously at 100 rpm maintaining a temperature of 37 °C. At predetermined intervals, 2 mL release media was taken out from the system and centrifuged, and the supernatant was collected for spectroscopic analysis. Meanwhile, the pellet (nanoparticles with unreleased Mgf) was redissolved in an equal volume of fresh PBS and was transferred back in order to continue the process, maintaining sink condition. The collected supernatant was analyzed spectrophotometrically (JASCO V-550 double beam UV–visible spectrophotometer, OK, USA) at 258 nm to measure the released Mgf from the nanoshells. The procedure was performed in triplicate. Diverse mathematical models were utilized to anticipate the manner/mechanism of release of Mgf from the nanoformulation. Obtained data were fitted into various

kinetic equations to explore the mechanistic pattern regarding the release of Mgf from the polymeric matrix.

Stability study

To assess the long-term stability of prepared MNPs, lyophilized nanoparticles were preserved at ~4 °C for 90 days and evaluated for FTIR spectrum, drug loading, particle size, and surface charge.

Assessment of protein adsorption

The extent of protein adsorption onto the surface of MNPs was estimated by studying the adsorption of BSA. Initially, an aqueous solution of BSA was prepared at a concentration of 0.6 mg/mL. Then, separately, PLGA and freshly prepared MNPs were dissolved in PBS (2.0 mg/mL). The resultant PBS suspensions were separately added dropwise to 5 mL BSA solution. After 4 h, the clear solutions from the top layers were collected following centrifugation at 135 rpm for 4 h at 37 °C. For each sample, the concentration of BSA was evaluated using Pierce™ BCA protein assay kit following the manufacturer's protocol.

In vitro cytotoxicity assay

MDA-MB-231 cells were maintained in Roswell Park Memorial Institute (RPMI) medium or RPMI 1640 supplemented with 10% fetal bovine serum (FBS) and 1% penicillin–streptomycin, incubated at 37 °C in a humidified condition of 5% CO_2. To perform cytotoxicity assay, ~5000 cells/well were seeded in a 96-well plate (Corning Costar, Fisher Scientific, NY, USA) and incubated for 24 h to allow the cells to adhere. The cells were then incubated with Mgf and MNPs in a concentration gradient of 0–50 µg/mL for 24 h. After the treatment, cells were subjected to 20 µL of MTT (5 mg/mL, in PBS) and incubated for 4 h. Finally, the insoluble formazan was solubilized in dimethyl sulfoxide (DMSO), and the absorbance was measured at 450 nm. Cytotoxicity of MNPs to MCF-7 cells and NKE cells was also assayed following a similar protocol.

In vitro cellular uptake

To evaluate the intracellular uptake, FITC-tagged nanoparticles were given in MDA-MB-231 cells followed by incubation of 6 h. The cells were then trypsinized and uptake assessed by flow cytometry (BD LSRFortessa, BD Biosciences, NJ, USA), and the percentage of cellular uptake was calculated with control cells.

To evaluate the comparative cellular internalization of Mgf, MDA-MB-231 cells were treated with native Mgf and MNPs, individually. Subsequently, cells were lysed followed by spectroscopic analysis of cell homogenates, to discover the Mgf present in the cells.

Assessment of therapeutic effects of MNPs in vitro

To assess the apoptosis-inducing ability of Mgf and MNPs at their respective IC_{50} concentrations obtained from cytotoxicity assay, MDA-MB-231 cells were seeded in 6-well plates ($\sim 15 \times 10^4$ cells/well) followed by overnight incubation. Treatment of Mgf and MNPs were given at respective IC_{50} doses calculated from the MTT assay for 24 h. Cells were then harvested, stained with FITC Annexin V, and incubated for 15 min. Finally, the cells were stained with propidium iodide (PI). Cells were acquired in a flow cytometer (BD LSRFortessa, BD Biosciences, NJ, USA).

To evaluate reactive oxygen species (ROS) production by MNPs at effective concentration, MDA-MB-231 cells were plated in 35-mm culture plates ($\sim 2 \times 10^5$ cells/mL). After 24 h of incubation following treatment with Mgf and MNPs, respectively, the cells were washed and stained with diluted DCFDA solution for 45 min at 37 °C in darkness. Intracellular ROS was evaluated by flow cytometry (BD LSRFortessa, BD Biosciences, NJ, USA).

In order to assess the effect of MNPs on MMP, MDA-MB-231 cells were plated in 35-mm culture plates ($\sim 2 \times 10^5$ cells/mL). After incubation of 24 h following treatment with Mgf and MNPs, respectively, the medium was removed followed by washing with PBS, and JC-1 solution was included further. The plates were incubated in the dark for 20 min, and expression was measured using flow cytometric technique (BD LSRFortessa, BD Biosciences, NJ, USA).

Animals

In the study, 2–3-week-old female Balb/c mice were used. Animals were acclimatized for 14 days in 12-h light/dark cycles and provided with water and food ad libitum. The study has been carried out according to the guidelines of the Institutional Animal Ethics Committee (IAEC) of Jadavpur University (registration no. 1805/GO/Re/F/15/CPCSEA) vide certificate proposal no. JU/IAEC-22/31.

Hemolysis assay

Freshly collected mouse blood was taken in EDTA-coated tubes and centrifuged at 2000 rpm for 5 min at 4 °C. After discarding the supernatant, the erythrocyte pellet was washed with PBS. Two hundred microliters of aliquots were utilized for the hemolysis study. To determine the hemolytic effect and predict biocompatibility, 200 µL of MNPs dispersion (containing MNPs at intended dose amount) was added to the PBS dispersion. The mixture thus obtained was incubated at 37 °C for 1 h under shaking conditions, followed

by centrifugation at 2000 rpm for 5 min. To calculate the hemolysis percentage, optical density of the supernatant was measured at 570 nm. Triton X-100 and PBS served as controls, positive and negative, respectively.

In vivo evaluation of anti-tumor efficacy

In order to evaluate the in vivo effect of the developed MNPs, an Ehrlich ascites carcinoma (EAC)–based solid mammary tumor-bearing mouse model was undertaken (Badawi et al. 2022; Shehatta et al. 2022; El-Ashmawy et al. 2023; Shaker et al. 2023; El-Masry et al. 2024). Briefly, 15 Balb/c mice were randomly divided into five groups. Groups I and V received subcutaneous injections of PBS in mammary pads. The rest of the animals received subcutaneous injection of EAC cells (~10^7 cells/50 µL for each mouse) (Kundu et al. 2019). Ehrlich tumor, a spontaneous murine mammary adenocarcinoma, is undifferentiated, rapidly proliferating, malignant, and easy to grow and transplant. Ehrlich tumors have been used in tumor biology since many years to study carcinogenesis and evaluate anti-tumor effects of different agents (Shehatta et al. 2022). After inoculation, animals were monitored for about 2 weeks to allow the growth of solid tumors. Then, the animals were treated with PBS (groups I and II), Mgf (5 mg/kg, group III), and nanoparticles (equivalent to 5 mg/kg of Mgf, group IV; and group V) through intravenous route for 14 days every alternate day. After completion of the treatment period, animals were sacrificed after collecting blood samples, and tumors and organs were removed. After determining tumor mass and tumor volume (ellipsoidal volume equation), they were stored for further analyses (Bhattacharya et al. 2015).

Tumor histology

The tumor tissues isolated from experimental animals were fixed in 10% formalin and processed for paraffin sectioning. Subsequently, paraffin-embedded sections were stained with hematoxylin and eosin (H&E) to study the histological changes using a bright field light microscope (Leica Microsystems, Wetzlar, Germany).

Mgf accumulation in tumor tissues

The extent of accumulation of Mgf within tumor tissues was evaluated quantitatively by HPLC (Dionex Ultimate 3000, Dionex, Idstein, Germany) utilizing a C-18 column (250 × 4.6 mm, particle size 5 µ; Thermo Scientific™ Hypersil GOLD™, MA, USA) and UV detector. Accurately weighed tissue samples from each tumor-bearing group were homogenized individually in a solution containing methanol (75%) and DMSO (0.05%). The mixture was then centrifuged at 10,000 rpm for 15 min. Supernatant was collected, filtered (0.45 µ), and analyzed chromatographically. Aliquots of the filtrate (injection volume 20 µL) were eluted with an isocratic mobile phase comprising of 0.1% formic acid and acetonitrile at a ratio of 87:13, with a flow rate of 1.5 mL/min and detection wavelength set at 258 nm (Naveen et al. 2017). The Mgf concentration in the tissues was determined following the standard curve method.

Assessment of antioxidant and redox markers in tumor tissues

To measure the alterations in the enzymatic and non-enzymatic antioxidant activity levels in the tumor tissues upon different treatments, activities of catalase (CAT), superoxide dismutase (SOD), and reduced glutathione (GSH) were estimated following established protocols of our laboratory (Manna et al. 2022). The extent of protein carbonylation was assessed as an oxidative stress marker according to standard protocol.

Immunohistochemical study

Sections of tumor tissues were subjected to immunohistochemical staining in order to assess the localized expression profile of p53 and caspase 3. Following standard protocol, tissue sections on charged slides were incubated with anti-p53 antibody (Biobharati LifeScience, Kolkata, India, #BB-AB0100) and anti-caspase 3 antibody (Elabscience, Houston, USA, #E-AB-13815), respectively, at appropriate dilutions. Slides were then exposed to HRP-conjugated secondary antibody. Diaminobenzidine (DAB) was introduced to serve as a substrate of HRP. Hematoxylin served as a counterstain in the experiment to aid in visualizing the nuclei. Slides were mounted in DPX prior to observing in a bright field light microscope (Leica Microsystems, Wetzlar, Germany).

In vivo assessment of systemic toxicity

The levels of ALT and ALP in serum were evaluated as hepatic toxicity markers for all five groups. Further, levels of blood urea nitrogen (BUN) and creatinine in sera were examined as renal toxicity markers. All serum markers were analyzed using commercially available kits following respective manufacturer protocols. The histological sections (H&E-stained) of the liver, kidney, heart, and spleen of different experimental groups were also analyzed for the estimation of systemic toxicity using a bright field microscope (Leica Microsystems, Wetzlar, Germany).

Data analyses

Experiments were performed in triplicate, and data were expressed as mean ± SD. Statistical analyses of experimental data were conducted using GraphPad Prism 10.0.2. Statistical analyses involved one-way analysis of variance (ANOVA) followed by Dunnett's test and *t*-test; statistical significance was designated as p-value < 0.05.

Result and discussion

Preparation and characterization of nanoparticles

Mgf-containing nanoparticles were prepared to increase the solubility and bioavailability of Mgf to improve therapeutic efficacy against breast cancer. Blank and Mgf-loaded polymeric nanoparticles were prepared according to the nanoprecipitation process utilizing vitamin E-TPGS as emulsifier. The highest aqueous solubility achieved for native Mgf was 0.12 ± 0.02 mg/mL, which jumped to a value corresponding to 3.29 ± 0.33 mg/mL MNPs on PLGA modification. Clearly, solubility was increased nearly 27 times (Fig. S1A) by polymeric modification. MNPs with average hydrodynamic diameter of ~162.5 nm were produced (Fig. 1A) exhibiting 5.08 ± 0.49% loading and encapsulation efficiency of 55.89 ± 5.39%. A low PDI value of 0.103 indicated narrow size distribution, i.e., nearly uniform-sized particles. Regarding surface charge, high absolute values impart colloidal stability and monodispersity to the nanoparticles (Nemeth et al. 2022). On the other hand, negative surface charge value tends to reduce the possibility of interaction of nanoparticles with cellular membrane (negatively charged) with increasing absolute value. To strike an acceptable balance between stability and biological interaction is desirable. In the current study, surface charge of – 34.9 mV (Fig. 1B) was satisfactory for stable nanoparticles with low chances of agglomeration to each other in the dispersed phase as well as for imparting acceptable effectiveness (Betancourt et al. 2007; Shavi et al. 2015; Markeb et al. 2016; Németh et al. 2022). Such monodisperse particles with a loading efficiency of about ~5% have been evinced as potential candidates for good biological activity against cancer (Betancourt et al. 2007; Ganguly et al. 2021; Sen et al. 2021).

The FESEM image (Fig. 1C) exhibited a thick distribution of more or less uniform-sized nanospheres with smooth exteriors. TEM-based image (Fig. 1D) revealed discrete spherical delineation of the nanoparticles. Smooth, sphere-shaped particles devoid of aggregation were further ascertained by AFM images (Fig. 1E). The three-dimensional view also revealed a more or less homogeneous size distribution of particles, with smooth topography (Fig. 1F). BET analysis revealed a specific surface area of ~157.51 m^2/g. Specific surface value on the higher side is expected to facilitate the dissolution of loaded Mgf from polymeric nanoparticles in the release medium since a large proportion of molecules are expected to be present on the surface (Liu et al. 2008; Mallakpour and Behranvand 2016).

Physicochemical characterization and compatibility

FTIR spectroscopic investigations provided information regarding the compatibility and/or stability of Mgf with other formulation ingredients. FTIR spectra were documented for Mgf, PLGA, vitamin E-TPGS, their physical mixture, blank nanoparticles, and MNPs (Fig. 2A).

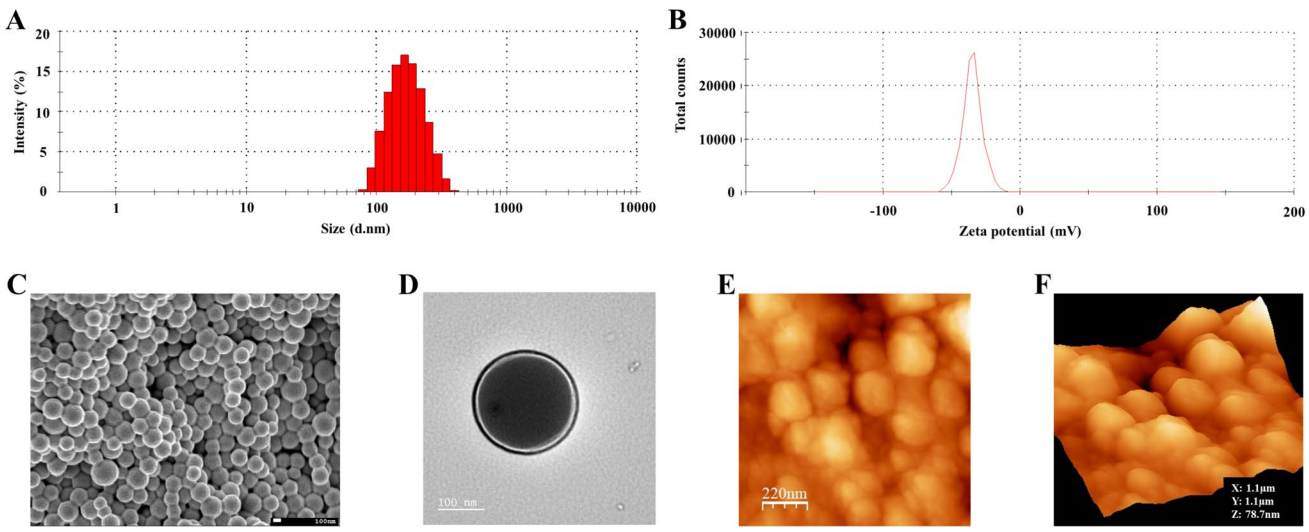

Fig. 1 Characterization of prepared MNPs in terms of particle size distribution (**A**), surface charge (**B**), FESEM image (**C**), TEM image (**D**), and AFM image, both 2D (**E**) and 3D (**F**) view

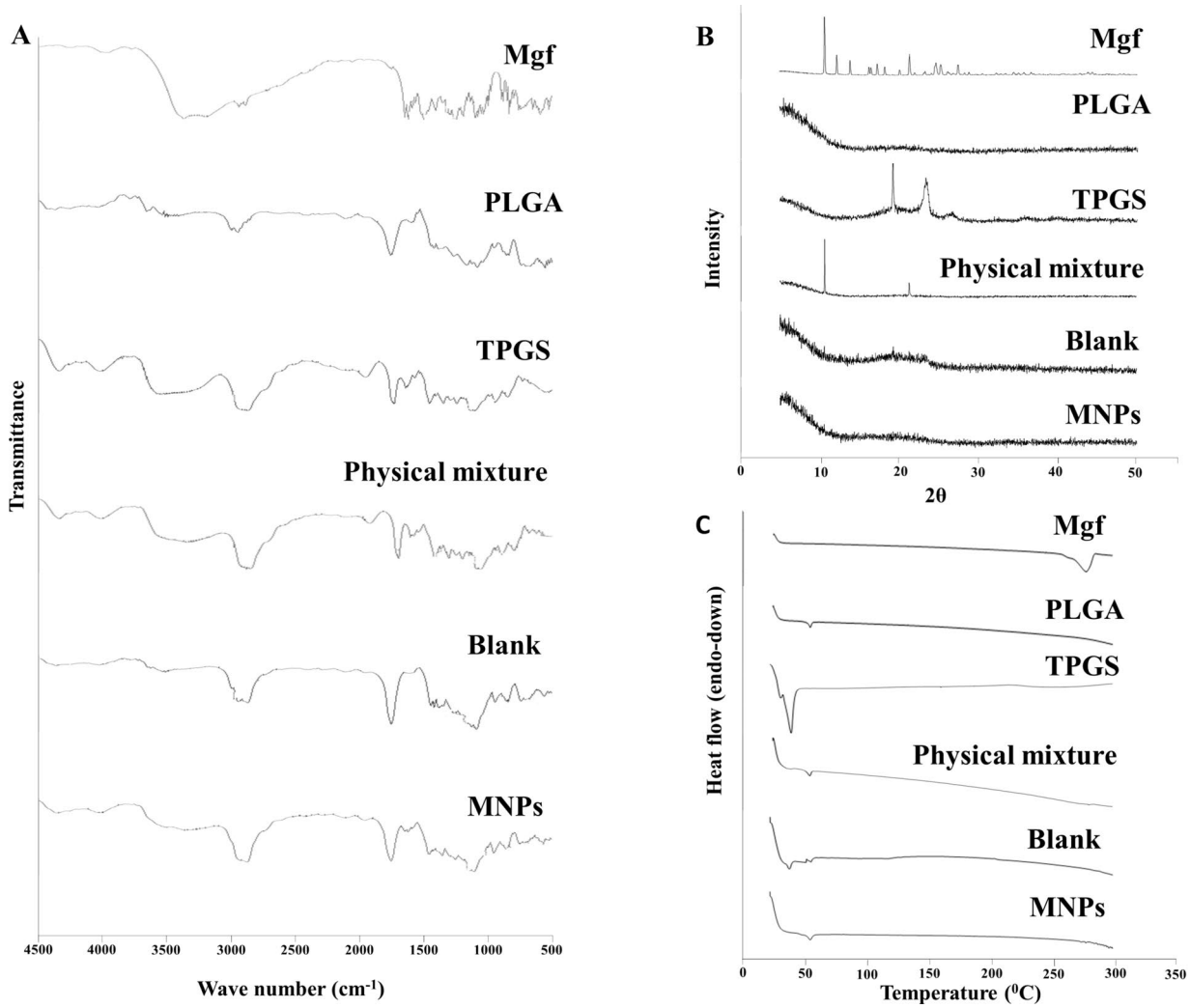

Fig. 2 Physicochemical characterization of MNPs concerning FTIR spectra (**A**), XRD diffractograms (**B**), and DSC thermograms (**C**)

The spectra showed the characteristic peaks for Mgf at 3365 cm^{-1} due to OH-stretching of secondary hydroxyl groups, peak at 2939 cm^{-1} due to C-H stretching, and peak at 1651 cm^{-1} corresponding to conjugated carbonyl stretching. Peaks at 1620 cm^{-1}, 1492 cm^{-1}, and 1406 cm^{-1} indicate aromatic C = C ring-stretching; peak at 1253 cm^{-1} correlates to ether-stretching while peak at 1097 cm^{-1} indicates C–O–C-stretching. FTIR spectrum of PLGA revealed the characteristic peaks at 3000–2947 cm^{-1} for C-H stretching bands and 1764 cm^{-1} for C-O stretching band of ester. Peak at 1049 cm^{-1} corresponds to –OH bending vibrations. In the spectrum representing vitamin E-TPGS, peaks at 3415 cm^{-1} and 2868 cm^{-1} indicate terminal –OH function and –CH function stretching, respectively. The carbonyl band of vitamin E-TPGS appears at 1732 cm^{-1}. Majority of the important peaks of Mgf, PLGA, and vitamin E-TPGS are featured in the FTIR spectrum of the physical mixture, exhibiting only minor shifts. Certain physical interactions such as dipole–dipole interaction, hydrogen bond formation, and Vander-Waals force acting between the functional groups of Mgf and excipients might have led to the minor shifting of the peaks. The spectrum of blank nanoparticles exhibits major characteristic peaks of PLGA and vitamin E-TPGS. Similarly, appearance of typical peaks of Mgf and excipients in the spectrum of prepared MNPs indicate the presence of Mgf without any major chemical interactions.

XRD analysis detects the presence of crystalline properties of samples. Amorphous materials, like polymers, do not produce any sharp peaks, whereas sharp peaks with high intensity are observed with crystalline materials. XRD patterns of Mgf, PLGA, vitamin E-TPGS, their physical mixture, blank nanoparticles, and MNPs are depicted in Fig. 2B. The XRD pattern for native Mgf displays distinct peaks free of distortions indicating crystalline nature. The lack of sharp peaks in the diffractogram of PLGA confirms its amorphous nature. Interestingly,

the diffractogram corresponding to the physical mixture exhibited some distinct peaks; their positions suggested minimum to no interaction of Mgf with other components. The characteristic peaks of Mgf disappeared in the XRD pattern of MNPs, which might indicate transformation from crystalline to amorphous state while encapsulation during nanoparticle formation (Gaonkar et al. 2017). The DSC thermograms of Mgf, PLGA, vitamin E-TPGS, their physical mixture, excipient mixture (blank), and MNPs are depicted in Fig. 2C. All of Mgf, polymer, and vitamin E-TPGS exhibited sharp endothermic peaks in their respective spectra at characteristic positions. The disappearance of the characteristic melting peak of Mgf in the DSC pattern of MNPs hints at the possibility of transformation of Mgf from crystalline to an amorphous disordered state during nanoencapsulation, thus promoting the stability of the formulation by inhibiting crystal growth (Ganguly et al. 2021). Findings from DSC studies in this regard conform to the observation from XRD analysis. Also, in the thermogram for MNPs, the endothermic peak is close to that of the native polymer, hinting that the polymer is not degraded during nanoparticulate formation.

In vitro release kinetics

In vitro release was studied to investigate the release pattern of Mgf from MNPs in PBS (Fig. 3A). PBS is an isotonic physiologic solution utilized to mimic extracellular fluid (Susa et al. 2017; Ibarra and Foresto 2023). It imitates the pH, osmolarity, and ionic concentrations of blood to a large extent. This study observed an initial rapid release of $38.13 \pm 0.41\%$ within the initial 6 h. The release rate was moderate up to 24 h, followed by a sustained release of Mgf up to 5 days, after which no noteworthy increment in cumulative release of Mgf was noticed. Over the period of 5 days, $82.61 \pm 1.51\%$ Mgf was released. The early burst might be attributed to Mgf loosely attached onto the surface and/or embedded within the surface layer of the polymeric matrix. Again, the persistent sustained release seems to result from diffusion of Mgf from the polymer shell possibly by virtue of either or more of erosion, swelling, and degradation of the polymer matrix (Gaonkar et al. 2017; Jabbari et al. 2018; Ghosh et al. 2023). Interestingly, the phasic behavior regarding release pattern potentially allows the formulated MNPs for fast onset of action besides serving as drug depot (Chatterjee et al. 2024).

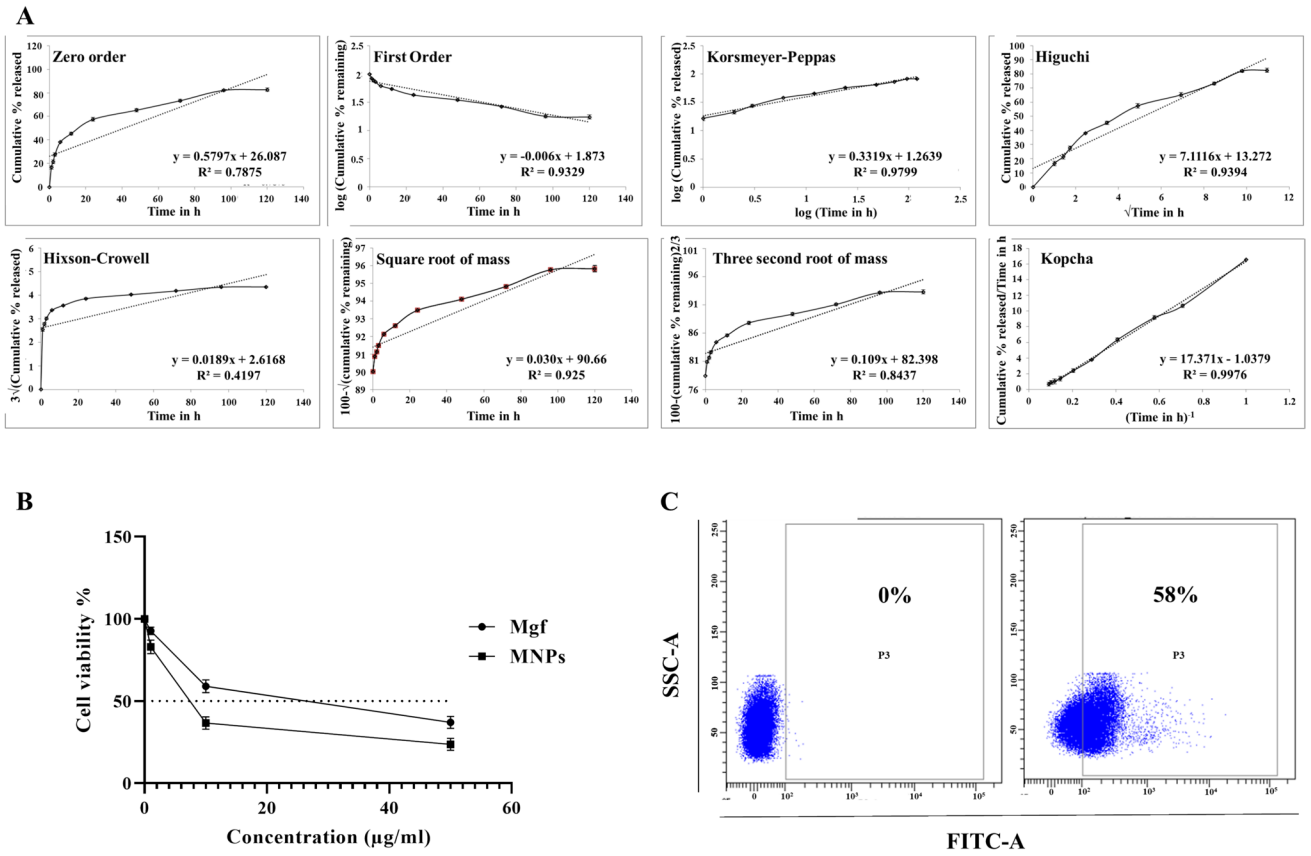

Fig. 3 In vitro drug release pattern from MNPs (**A**), the effect of nanoencapsulation of Mgf on in vitro cell viability of MDA-MB-231 cells (**B**), and cellular uptake of MNPs to MDA-MB-231 cells (**C**). The values were expressed as mean ± SD ($n = 3$)

The in vitro release data obtained experimentally were fitted to mathematical models in order to examine the mechanistic pattern of Mgf release (Fig. 3A). According to regression co-efficient (R^2) values, the Kopcha model emerged as the best fit, followed by Korsmeyer-Peppas release kinetics. Kopcha plot computes the contribution of diffusion and erosion to the release pattern. Absolute values of diffusion and erosion constants suggested that diffusion dominates over erosion in the drug release (Rezk et al. 2019). Supporting this, the Korsmeyer-Peppas release exponent also hinted at Fickian diffusion to be the principal mechanism for Mgf release (Siepmann and Peppas 2001; Moodley and Singh 2020).

Stability studies

The free-flowing powder of MNPs was stored at ~4 °C for 90 days. Prepared nanoparticles represented no major alterations in particle size and surface charge on storage (Table S1). Drug loading did not vary significantly (Table S1) between fresh and stored formulations indicating stable nanoshells without leakage. Also, the FTIR spectrum (Fig. S1B) did not exhibit any major changes from that of freshly prepared MNPs hinting at decent stability of MNPs on storage.

BSA binding of MNPs

The formation of polymeric nanoconjugates has decreased the adsorption of BSA (Fig. S1C). The nanoparticle formation has lowered the binding of BSA from 1.46 ± 0.02 mg BSA/mg PLGA to 0.86 ± 0.03 mg BSA/mg MNPs. BSA actually functions as transporter of biologically active molecules. The availability of physiologically active molecules is inversely related to their binding to serum albumin (Yallur et al. 2019). Herein, upon nanoparticle formation, binding of BSA with sample is significantly weaker; hence, the availability of MNPs in the blood is expected to increase. Lower adsorption of BSA ensures higher stability of MNPs, as well as increased circulation time within the system. Since native Mgf is known to form a stable complex with BSA, the enhanced circulation time and availability of MNPs can be expected to contribute to higher therapeutic efficacy of MNPs compared to free Mgf (Lin et al. 2009).

Effect on hemolysis

Hematocompatibility is an important parameter for injectables, especially for intravenous route. In the present study, formulated MNPs exhibited negligible (Fig. S1D) hemolytic activity ($0.51 \pm 0.03\%$) upon 1-h incubation. Results indicated that the formulated MNPs could be used safely in biological system (Mittal et al. 2019).

Anti-cancer effects

MNPs improve therapeutic efficacy in vitro

Cytotoxic potential is a primary feature of an anti-cancer candidate for chemotherapy. While evaluating the percentage viability of breast cancer cells, MTT analysis revealed dose-dependent cytotoxicity on MDA-MB-231 cells. IC_{50} value of MNPs was found to be ~ 7.53 µg/mL while that of free Mgf was found to be ~ 27.03 µg/mL (Fig. 3B). Clearly, MNPs exhibited better inhibition compared to free Mgf on cancer cells. Comparable IC_{50} values of MNPs were obtained for both types of breast cancer cells, i.e., MDA-MB-231 cells and MCF-7 cells (Table S2). Cell viability of NKE cells remained above 50% at the experimental concentration range of MNPs, hinting at lower inhibition to normal cells.

Several studies claimed that Mgf induces the death of cancer cells by elevating oxidative stress and promoting apoptosis (Li et al. 2016; Du et al. 2018). The apoptotic potential of free Mgf and MNPs at equivalent effective concentrations was examined to reveal whether the nanoformulation development would impart any change in the cell death mechanism. MDA-MB-231 cells were treated with Mgf and MNPs at their respective IC_{50} concentrations. Cells exhibited a similar pattern of death induction (Fig. S2A). However, the effectiveness of MNPs was achieved at much lower concentrations, which hints at improved apoptosis induction efficacy of nano-scale formulation containing Mgf. Treatment groups exhibited comparable intracellular ROS production in breast cancer cells (Fig. S2B) indicating induction of oxidative stress as a primary mechanism for inducing cell death. Comparable intracellular ROS production achieved with nearly 1/4th concentration of chemotherapeutic agent hints at superior efficacy of the nano-scale delivery system. Regarding MMP, MNPs enhanced the FITC-positive cells which indicates increased depolarized mitochondria percentage and simultaneously decreased PE-positive cells (Fig. S2C). Combining the observations, MNPs induce mitochondria-dependent apoptosis by virtue of elevating ROS production in breast cancer cells, which also conforms to earlier findings regarding the mechanism of action of Mgf (Li et al. 2016; Dutta et al. 2017). The superior efficacy of MNPs could well be associated with impressive cellular internalization of the nanoformulation (Fig. 3C) such that an elevated amount of Mgf becomes available in the intracellular microenvironment (Fig. S2D) to confer activities.

In vivo anti-tumor efficacy

MDA-MB-231 cells are considered among the most aggressive breast cancer cell lines (Azizi et al. 2017; Nirgude et al. 2020). Thus, it can be expected that a formulation displaying

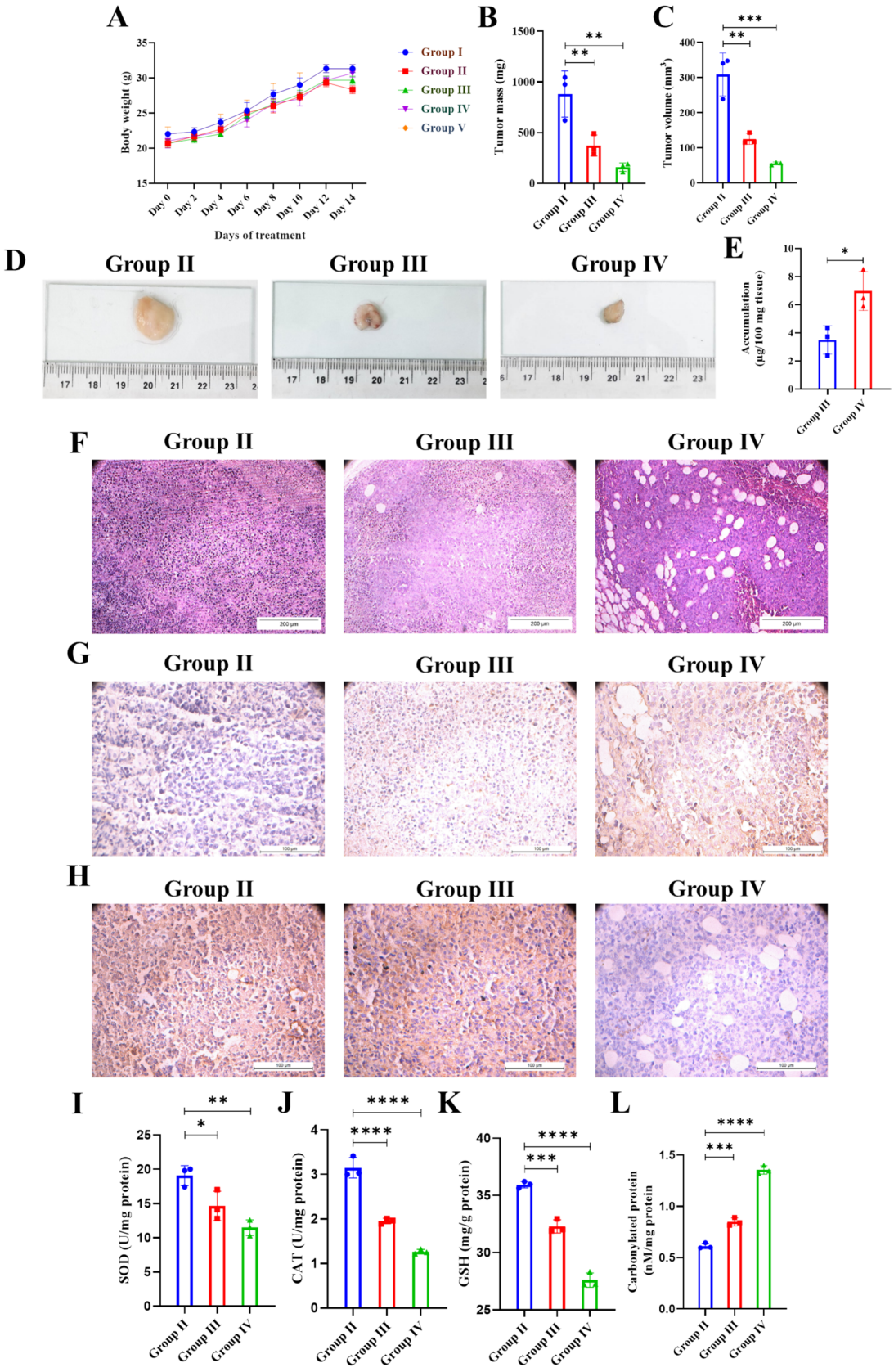
A
Body weight (g)
Days of treatment
Day 0
Day 2
Day 4
Day 6
Day 8
Day 10
Day 12
Day 14
Group I
Group II
Group III
Group IV
Group V
B
Tumor mass (mg)
C
Tumor volume (mm³)
D
Group II
Group III
Group IV
E
Accumulation (μg/100 mg tissue)
F
Group II
Group III
Group IV
G
Group II
Group III
Group IV
H
Group II
Group III
Group IV
I
SOD (U/mg protein)
J
CAT (U/mg protein)
K
GSH (mg/g protein)
L
Carbonylated protein (nM/mg protein)

◂**Fig. 4** Anti-tumor effects of MNPs on breast tumor-bearing mice. **A** Body weight of mice belonging to different groups during treatment duration. **B** Tumor mass and **C** tumor volume of different tumor-bearing groups. **D** Representative images of mammary pad tumors dissected from experimental tumor-bearing mice. **E** Tissue accumulation of Mgf in treatment groups. **F** H&E-stained histological sections of tumor tissues. **G** Immunohistochemical detection of p53 expression in tumor tissue sections. **H** Immunohistochemical detection of caspase 3 expression in tumor tissue sections and the effects on tumor tissues receiving different treatments regarding endogenous antioxidant parameters, e.g., **I** SOD, **J** CAT, and **K** GSH, and **L** protein carbonylation. Graphical data were expressed as mean ± SD ($n = 3$). *Values signify $p < 0.05$; **values signify $p < 0.01$; ***values signify $p < 0.001$; ****values signify $p < 0.0001$

efficacy against these cells would be effective against breast cancer. In vitro assays served to gather some mechanistic insight regarding the efficacy of MNPs against breast cancer. The undifferentiated EAC cells (used in the current study to induce breast cancer in mice) offer a rapid growth rate, good transplantation capability, and high malignancy and virulence making it suitable for chemotherapy-based assays (Ali et al. 2015).

Experimental mice belonging to diverse groups did not represent a notable variation regarding normal movement throughout. In tumor-bearing groups, induction of tumor was confirmed by visual inspection (Fig. S3A). Throughout the treatment duration, the body weights of all the mice were observed every alternate day, whereby group II animals displayed the lowest body weight in contrast to higher body weights of other groups, especially groups I and V (Fig. 4A). This difference might arise from lowered food intake as a consequence of tumor load in the body and allied discomfort. Upon sacrificing the animals, mammary pad tumors were isolated and examined for volume and mass. MNPs clearly exhibited superior anti-tumor activity evinced by the lowest tumor mass and volume in the animals of group IV among the tumor-bearing groups, followed by group III (free Mgf), whereas group II animals presented with the highest tumor load with regard to mass and volume (Fig. 4B–D). Images of all three sets of isolated tumors have been included in the supporting supplementary document (Fig. S3B) for better understanding. Accumulation of Mgf in tumor tissues also corroborates with the findings since group IV exhibits significantly higher accumulation from MNPs, compared to that in group III (Fig. 4E). Thus, the lowest tumor load of group IV among tumor-bearing groups can be attributed to the highest accumulation of Mgf within tumor tissues ((Fig. 4E, Fig. S4).

To further assess anti-tumor activity, dissected tumor tissues from tumor-bearing groups were stained with H&E and observed under a microscope (Fig. 4F). In disease control mice (group II), tumor tissue could be characterized by numerous micronuclei spread across the entire section, accompanied by an irregular tissue arrangement. The high cellular intensity and compactness signify uncontrolled cell division, a typical characteristic of tumor tissue. In the Mgf-treated group, nuclear intensity was lessened compared to the control group. Though dense packing of cells persisted to some extent, void spaces indicative of cellular death have started to appear. In group IV (treated with MNPs), the nuclear intensity was even lesser than in group III mouse tumor. The packing density of cells loosened up further, aided by a higher abundance of void spaces. Cells in group IV showed more distinctive outlines compared to the disease-control group, and the tissue showed hints of regaining normalcy of breast tissue architecture. Immunohistochemical studies reassured the therapeutic impact of MNPs on tumors (Fig. 4G, H). Group IV tumors exhibited the highest expression of tumor suppressor protein p53, indicating superior therapeutic activity of MNPs. In line with the observation, the MNPs-treated group exhibited decreased expression of caspase 3 in the tumor as compared to the tumor control group (group II), represented by the lesser intensity of DAB (brown dots) in the MNPs-treated section. Lower expression of whole caspase 3 in the treated groups indicated induction of cellular apoptosis characterized by the lessening of whole caspase 3 by cleavage to form cleaved fragments (Alkhalaf et al. 2008; Silva et al. 2022). In line with the earlier findings, the immunohistochemical study also establishes the superior anti-tumor activity of MNPs via inducing caspase-mediated apoptosis. Infliction of oxidative stress is reassured by evaluating antioxidant markers in tumor tissues. MNPs significantly augmented the inhibitory effects on both SOD and CAT activities while downregulating GSH (Fig. 4I–K), thereby indicating pro-oxidant actions, inducing oxidative stress (likely to lead to subsequent apoptotic death) in tumor tissues (Kannan and Jain 2000). In addition, the highest level of carbonylated protein was found in group IV tissues (Fig. 4L), reinstating the previous findings regarding the infliction of oxidative stress. Thus, clearly, formulation of MNPs improves the in vivo efficacy of Mgf against breast cancer.

Effects on systemic toxicity

A proper balance between therapeutic and toxicological outcomes of any treatment module is a crucial parameter to evaluate its applicability towards pharmacological utilization. In order to assess any probable systemic toxicities of the prepared nanoformulation at applied dose, levels of renal and hepatic biomarkers in blood were examined, as well as H&E-stained tissue sections of vital organs from experimental animals were also analyzed. Figure 5A clearly indicates that induction of tumor leads to hepatic abnormality characterized by sharp increments in ALP and ALT values of group II animals compared to normal controls. The levels of hepatic biomarkers seem to reduce among

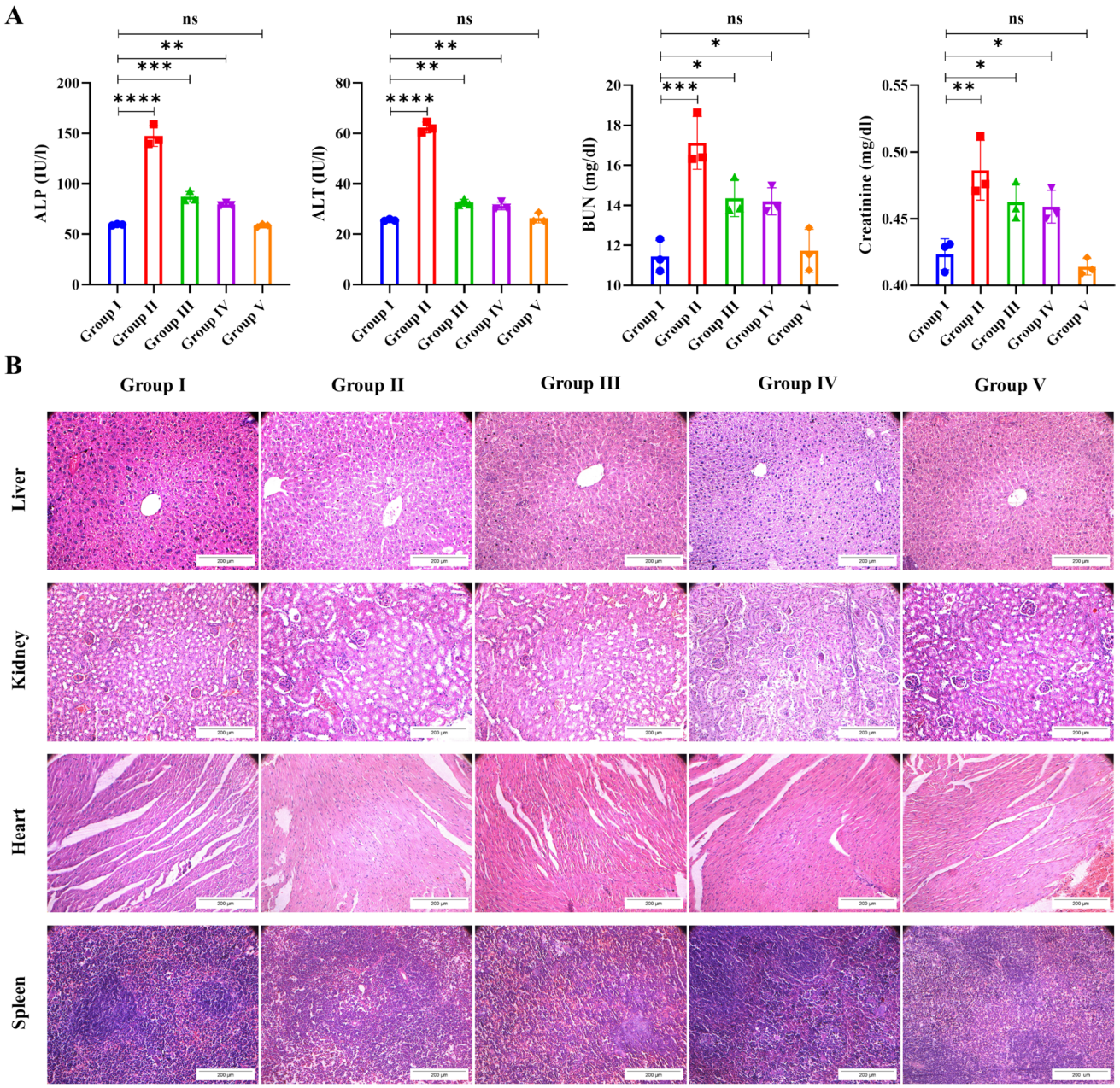

Fig. 5 Safety profile of formulated MNPs. **A** Serum biochemical parameters regarding hepatic and renal biomarkers of different experimental groups and **B** H&E-stained histological sections of the liver, kidney, heart, and spleen of different experimental groups. Graphical data were expressed as mean ± SD ($n = 3$). *Values signify $p < 0.05$; **values signify $p < 0.01$; ***values signify $p < 0.001$; ****values signify $p < 0.0001$; ns, insignificant

different treatment groups, thus indicating no additional toxicity and/or side effects to the liver arising from experimental chemotherapeutic regimens (Guruswamy et al. 2020). Both hepatic and renal parameters, i.e., ALP, ALT, BUN, and creatinine (Fig. 5A) did not differ significantly between group I and group V, hinting at the absence of hepatotoxicity and nephrotoxicity imposed by nanoparticles during the period of treatment. Tumor induction and progress seem to disrupt the normalcy of liver tissue, as indicated by the elongation of the portal vein and vacuolated cytoplasm in group II (Fig. 5B). This is probably a result of the EAC-induced generation of ROS, as well as the downregulation of antioxidants. However, hepatic tissue gradually displays lower abnormality along with gradual reduction of tumor load among different experimental groups. Anti-tumor therapy might well have replenished the antioxidant defense system, consequently reducing ROS production and leading to hepatoprotection (Bhattacharyya et al. 2007). Renal

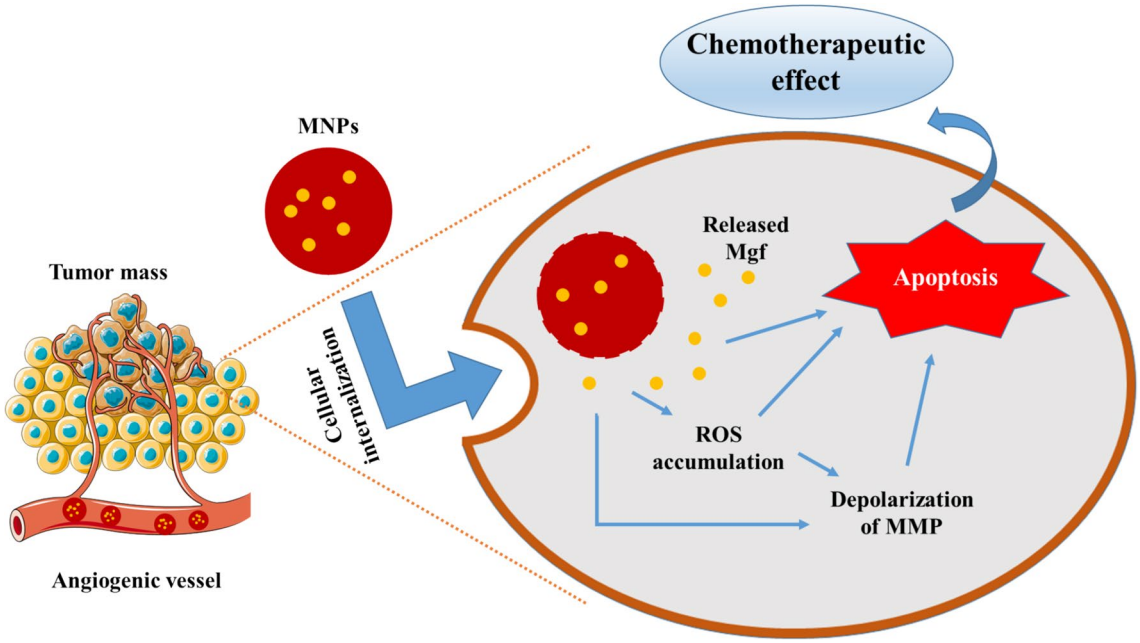

Fig. 6 Schematic representation of anti-tumor potential of MNPs

tissues did not represent major alterations among experimental groups (Fig. 5B). Cardiac tissues seem to remain unaffected by tumor induction and by nanoparticle treatment, retaining normal tissue characteristics across all the groups (Fig. 5B). These observations are in line with earlier findings in this regard (Ali et al. 2015; El-Sisi et al. 2020; Alkhatib et al. 2021). Tumor load seems to affect splenic tissue to some extent; however, the spleen images represent reduced abnormality correlating with a reduction in tumor load by means of anti-tumor therapy in treatment groups (Fig. 5B) (Sadhukhan et al. 2019; Guruswamy et al. 2020). The apparent absence of MNPs-induced apoptotic cascade might also hint at insignificant localization in tissues other than tumor tissues. Interestingly, the fact that none of the organs exhibits any abnormality in tissue architecture of group V animals further supports the prepared nanoparticles somewhat as a safe choice for chemotherapy.

Conclusion

The current study produced stable, well-characterized nanoparticles with substantial loading and satisfactory release profile of Mgf. MNPs conferred anti-cancer effects on breast cancer in vitro as well as in vivo. Mgf imparts death to cancer cells by elevating oxidative stress and promoting apoptosis, along with modulating MMP. MNPs inflicted comparable anti-cancer effects in vitro at nearly 1/4th concentration than free Mgf. Hence, MNPs can be attributed for improving chemotherapeutic efficacy against breast cancer cells. PLGA nanoparticles tend to ensure improved cancer cell penetration, making it possible to achieve a similar cytotoxic effect at much lower concentration. In vivo observations ascertain that MNPs retain efficacy in animal systems also, thus igniting the possibilities of utilization of Mgf in cancer therapeutics overcoming its unfavorable biopharmaceutical attributes. EPR effect can be attributed to the localization of MNPs at tumor vicinity; upon cellular internalization, they release Mgf in the intracellular microenvironment (Fig. 6). Therapeutic effect, i.e., reduction in tumor load is achieved by induction of apoptotic death.

MNPs significantly endorsed tumor reduction by improving the accumulation of Mgf within tumor tissue as well as by elevating the cellular uptake in breast cancer cells. During in vivo preclinical assays, MNPs could significantly minimize tumor load compared to native Mgf along with a promising safety profile. Hence, MNPs might well lead to an answer to the limitations regarding futuristic therapeutic translation of plant-derived small molecule, i.e., Mgf, as well as to the search for a safe and efficacious chemotherapeutic modality against breast cancer. However, more detailed in vitro-in vivo correlation studies, e.g., in vivo pharmacokinetic profile in biological system, comparative localization of Mgf in tumor tissue and other vital organs, etc., can be intriguing segments for research before probable translation from preclinical to clinical stage in future.

Supplementary information The online version contains supplementary material available at https://doi.org/10.1007/s00210-025-04068-0.

Acknowledgements The authors are thankful to Jadavpur University, Kolkata, India, Chittaranjan National Cancer Institute, Kolkata, India, and Bose Institute, Kolkata, India for providing the necessary facilities.

Author contribution PC: Investigations—formulation development, characterization, pharmaceutical assays, in vivo experiments, pharmacological and biochemical assays and Writing- original draft. AD: Investigations—in vitro pharmacological assays, and Writing- original draft. SC: Investigations – pharmacological and biochemical assays. AB: Investigations—in vitro pharmacological assays, and Writing-original draft. HB: Investigations—formulation development, characterization, pharmaceutical assays. CB: Investigations – pharmacological and biochemical assays. NC: Supervision, and Editing – original draft. PCS: Supervision, and Editing – original draft. SD: Conceptualization, Methodology, Resources, Supervision, and Editing – original draft. The authors declare that all data were generated in-house and that no paper mill was used.

Funding Jadavpur University, Kolkata, India (State Government Research Fellowship Scheme, Ref no: R-11/13/20 dated 22.01.2020).

Data availability All source data for this work (or generated in this study) are available upon reasonable request.

Declarations

Competing interests The authors declare no competing interests.

References

Alharbi HM, Alqahtani T, Alamri AH, Kumarasamy V, Subramaniyan V, Babu KS (2024) Nanotechnological synergy of mangiferin and curcumin in modulating PI3K/Akt/mTOR pathway: a novel front in ovarian cancer precision therapeutics. Front Pharmacol 14. https://doi.org/10.3389/fphar.2023.1276209

Ali SA, Zaitone SA, Moustafa YM (2015) Boswellic acids synergize antitumor activity and protect against the cardiotoxicity of doxorubicin in mice bearing Ehrlich's carcinoma. Can J Physiol Pharmacol 93(8):695–708. https://doi.org/10.1139/cjpp-2014-0524

Alkhalaf M, El-Mowafy A, Renno W, Rachid O, Ali A, Al-Attyiah R (2008) Resveratrol-induced apoptosis in human breast cancer cells is mediated primarily through the caspase-3-dependent pathway. Arch Med Res 39(2):162–168. https://doi.org/10.1016/j.arcmed.2007.09.003

Alkhatib MH, Alkreathy HM, Al Omar MI, Balamash KS, Abdu F, Esmat A (2021) Doxorubicin supplemented with pravastatin in lipid nanoemulsion induces antineoplastic activity with limited hepatotoxicity and cardiotoxicity in tumor-bearing mice. Asian J Pharm Res Health Care 13(1):17–29. https://doi.org/10.18311/ajprhc/2021/26066

Aminu N, Bello I, Umar NM, Tanko N, Aminu A, Audu MM (2020) The influence of nanoparticulate drug delivery systems in drug therapy. J Drug Deliv Sci Technol 60. https://doi.org/10.1016/j.jddst.2020.101961

Arnold M, Morgan E, Rumgay H, Mafra A, Singh D, Laversanne M, Vignat J, Gralow JR, Cardoso F, Siesling S, Soerjomataram I (2022) Current and future burden of breast cancer: global statistics for 2020 and 2040. Breast 66:15–23. https://doi.org/10.1016/j.breast.2022.08.010

Azizi M, Ghourchian H, Yazdian F, Bagherifam S, Bekhradnia S, Nyström B (2017) Anti-cancerous effect of albumin coated silver nanoparticles on MDA-MB 231 human breast cancer cell line. Sci Rep 7(1):5178. https://doi.org/10.1038/s41598-017-05461-3

Badawi NM, Attia YM, El-Kersh DM, Hammam OA, Khalifa MKA (2022) Investigating the impact of optimized trans-cinnamic acid-loaded PLGA nanoparticles on epithelial to mesenchymal transition in breast cancer. Int J Nanomed 17:733–750. https://doi.org/10.2147/IJN.S345870

Baghel M, Baghel I, Kumari P, Bharkatiya M, Joshi G, Sakure K, Badwaik H (2024) Nano-delivery systems and therapeutic applications of phytodrug mangiferin. Appl Biochem Biotechnol 196(10):7429–7463. https://doi.org/10.1007/s12010-024-04906-6

Betancourt T, Brown B, Brannon-Peppas L (2007) Doxorubicin-loaded PLGA nanoparticles by nanoprecipitation: preparation, characterization and in vitro evaluation. Nanomed (Lond) 2(2):219–232. https://doi.org/10.2217/17435889.2.2.219

Bhattacharya S, Ahir M, Patra P, Mukherjee S, Ghosh S, Mazumdar M, Chattopadhyay S, Das T, Chattopadhyay D, Adhikary A (2015) PEGylated-thymoquinone-nanoparticle mediated retardation of breast cancer cell migration by deregulation of cytoskeletal actin polymerization through miR-34a. Biomaterials 51:91–107. https://doi.org/10.1016/j.biomaterials.2015.01.007

Bhattacharyya A, Mandal D, Lahiry L, Bhattacharyya S, Chattopadhyay S, Ghosh UK, Sa G, Das T (2007) Black tea-induced amelioration of hepatic oxidative stress through antioxidative activity in EAC-bearing mice. J Environ Pathol Toxicol Oncol 26(4):245–254. https://doi.org/10.1615/jenvironpatholtoxicoloncol.v26.i4.10

Chatterjee S, Chakraborty P, Dutta S, Karak S, Mahalanobis S, Ghosh N, Dewanjee S, Sil PC (2024) Formulation of carnosic-acid-loaded polymeric nanoparticles: an attempt to endorse the bioavailability and anticancer efficacy of carnosic acid against triple-negative breast cancer. ACS Appl Bio Mater 7(3):1656–1670. https://doi.org/10.1021/acsabm.3c01087

Cuccioloni M, Bonfili L, Mozzicafreddo M, Cecarini V, Scuri S, Cocchioni M, Nabissi M, Santoni G, Eleuteri AM, Angeletti M (2016) Mangiferin blocks proliferation and induces apoptosis of breast cancer cells via suppression of the mevalonate pathway and by proteasome inhibition. Food Funct 7(10):4299–4309. https://doi.org/10.1039/c6fo01037g

Dewanjee S, Chakraborty P, Mukherjee B, De Feo V (2020) Plant-based antidiabetic nanoformulations: the emerging paradigm for effective therapy. Int J Mol Sci 21(6). https://doi.org/10.3390/ijms21062217

Du S, Liu H, Lei T, Xie X, Wang H, He X, Tong R, Wang Y (2018) Mangiferin: an effective therapeutic agent against several disorders. Mol Med Rep 18(6):4775–4786. https://doi.org/10.3892/mmr.2018.9529

Dutta S, Sadhukhan P, Saha S, Sil PC (2017) Regulation of oxidative stress by different naturally occurring polyphenolic compounds: an emerging anticancer therapeutic approach. React Oxyg Species 3:81–95. https://doi.org/10.20455/ros.2017.815

El-Ashmawy NE, Khedr EG, Khedr NF, El-Adawy SA (2023) Suppression of epithelial-mesenchymal transition and SIRT1/AKT signaling pathway in breast cancer by montelukast. Int Immunopharmacol 119. https://doi.org/10.1016/j.intimp.2023.110148

El-Masry TA, El-Nagar MMF, El Mahdy NA, Alherz FA, Taher R, Osman EY (2024) Potential antitumor activity of combined lycopene and sorafenib against solid Ehrlich carcinoma via targeting autophagy and apoptosis and suppressing proliferation. Pharmaceuticals (Basel) 17(4). https://doi.org/10.3390/ph17040527

El-Sisi AE, Sokkar SS, Ibrahim HA, Hamed MF, Abu-Risha SE (2020) Targeting MDR-1 gene expression, BAX/BCL2, caspase-3, and Ki-67 by nanoencapsulated imatinib and hesperidin to enhance anti-cancer activity and ameliorate cardiotoxicity. Fundam Clin Pharmacol 34(4):458–475. https://doi.org/10.1111/fcp.12549

Fabián RF, Mayra HM, Manuel ZV, Guadalupe SS, Alejandro PL, Alberto SJ (2023) Characterization of functionalized PLGA nanoparticles loaded with mangiferin and lupeol, and their effect on BEAS-2B and HepG2 cell lines. Anticancer Agents Med Chem

23(10):1174–1183. https://doi.org/10.2174/1871520622666220617101515

Fessi HP, Puisieux F, Devissaguet JP, Ammoury N, Benita S (1989) Nanocapsule formation by interfacial polymer deposition following solvent displacement. Int J Pharmaceutics 55(1):R1–R4. https://doi.org/10.1016/0378-5173(89)90281-0

Ganguly S, Dewanjee S, Sen R, Chattopadhyay D, Ganguly S, Gaonkar R, Debnath MC (2021) Apigenin-loaded galactose tailored PLGA nanoparticles: a possible strategy for liver targeting to treat hepatocellular carcinoma. Colloids Surf B Biointerfaces 204. https://doi.org/10.1016/j.colsurfb.2021.111778

Gaonkar RH, Ganguly S, Dewanjee S, Sinha S, Gupta A, Ganguly S, Chattopadhyay D, Chatterjee Debnath M (2017) Garcinol loaded vitamin E TPGS emulsified PLGA nanoparticles: preparation, physicochemical characterization, in vitro and in vivo studies. Sci Rep 7(1):530. https://doi.org/10.1038/s41598-017-00696-6

Gautam L, Thakur PS, Goel I, Sankar M, Jain A, Shrivastava P, Vyas S, Vyas SP (2022) Polymeric nanoparticles as theranostics for targeting solid tumors. In: Padhi, S., Behera, A., Lichtfouse, E. (eds) Polymeric nanoparticles for the treatment of solid tumors. Environmental Chemistry for a Sustainable World, vol 71. Springer, Cham. https://doi.org/10.1007/978-3-031-14848-4_10

Ghosh N, Kundu M, Ghosh S, Das AK, De S, Das J, Sil PC (2023) pH-responsive and targeted delivery of chrysin via folic acid-functionalized mesoporous silica nanocarrier for breast cancer therapy. Int J Pharm 631. https://doi.org/10.1016/j.ijpharm.2022.122555

Guruswamy DKM, Balaji KDS, Dharmappa KK, Jayarama S (2020) Novel 3-(3, 5-difluoro-4-hydroxyphenyl)-1-(naphthalen-2-yl) prop-2-en-1-one as a potent inhibitor of MAP-kinase in HeLa cell lines and anti-angiogenic activity is mediated by HIF-1α in EAC animal model. Oncotarget 11(50):4661–4676. https://doi.org/10.18632/oncotarget.27836

Ibarra LE, Foresto E (2023) An experimental approach to evaluate osmosis and tonicity on white blood cells by flow cytometry for biomedical physiology students. J Biologic Education 57(3):678–691. https://doi.org/10.1080/00219266.2021.1941188

Iqbal H, Inam-Ur-Raheem M, Munir S, Rabail R, Kafeel S, Shahid A, Mousavi Khaneghah A, Aadil RM (2023) Therapeutic potential of mangiferin in cancer: unveiling regulatory pathways, mechanisms of action, and bioavailability enhancements - an updated review. Food Sci Nutr 12(3):1413–1429. https://doi.org/10.1002/fsn3.3869

Jabbari S, Ghamkhari A, Javadzadeh Y, Salehi R, Davaran S (2018) Doxorubicin and chrysin combination chemotherapy with novel pH-responsive poly [(lactide-co-glycolic acid)-block-methacrylic acid] nanoparticle. J Drug Deliv Sci Technol 46:129–137. https://doi.org/10.1016/j.jddst.2018.05.006

Jeyakodi S, Krishnakumar A, Dalal M, Shetty BS (2024) Assessment of efficacy and safety of Mangifera indica extract (Stadice®) for cognitive function: a randomized, double-blind, placebo-controlled study. Cureus 16(7). https://doi.org/10.7759/cureus.65751

Kannan K, Jain SK (2000) Oxidative stress and apoptosis. Pathophysiol 7(3):153–163. https://doi.org/10.1016/s0928-4680(00)00053-5

Khurana RK, Gaspar BL, Welsby G, Katare OP, Singh KK, Singh B (2018) Improving the biopharmaceutical attributes of mangiferin using vitamin E-TPGS co-loaded self-assembled phosholipidic nano-mixed micellar systems. Drug Deliv Transl Res 8(3):617–632. https://doi.org/10.1007/s13346-018-0498-4

Kundu M, Sadhukhan P, Ghosh N, Chatterjee S, Manna P, Das J, Sil PC (2019) pH-responsive and targeted delivery of curcumin via phenylboronic acid-functionalized ZnO nanoparticles for breast cancer therapy. J Adv Res 18:161–172. https://doi.org/10.1016/j.jare.2019.02.036

Li M, Ma H, Yang L, Li P (2016) Mangiferin inhibition of proliferation and induction of apoptosis in human prostate cancer cells is correlated with downregulation of B-cell lymphoma-2 and upregulation of microRNA-182. Oncol Lett 11(1):817–822. https://doi.org/10.3892/ol.2015.3924

Lin H, Lan J, Guan M, Sheng F, Zhang H (2009) Spectroscopic investigation of interaction between mangiferin and bovine serum albumin. Spectrochim Acta A Mol Biomol Spectrosc 73(5):936–941. https://doi.org/10.1016/j.saa.2009.04.025

Liu M, Li H, Luo G, Liu Q, Wang Y (2008) Pharmacokinetics and biodistribution of surface modification polymeric nanoparticles. Arch Pharm Res 31(4):547–554. https://doi.org/10.1007/s12272-001-1191-8

Louisa M, Soediro TM, Suyatna FD (2014) In vitro modulation of P-glycoprotein, MRP-1 and BCRP expression by mangiferin in doxorubicin-treated MCF-7 cells. Asian Pac J Cancer Prev 15(4):1639–1642. https://doi.org/10.7314/apjcp.2014.15.4.1639

Lyu S, Zhang M, Zhang B, Zhu J, Gao L, Qiu Y, Yang L, Zhang Y (2023) The value of radiomics model based on ultrasound image features in the differentiation between minimal breast cancer and small benign breast masses. J Clin Ultrasound 51(9):1536–1543. https://doi.org/10.1002/jcu.23556

Mallakpour S, Behranvand VJ (2016) Polymeric nanoparticles: recent development in synthesis and application. Express Polymer Lett 10(11):895. https://doi.org/10.3144/expresspolymlett.2016.84

Manna P, Dewanjee S, Joardar S, Chakraborty P, Bhattacharya H, Bhanja S, Bhattacharyya C, Bhowmik M, Bhowmick S, Saha A, Das J, Sil PC (2022) Carnosic acid attenuates doxorubicin-induced cardiotoxicity by decreasing oxidative stress and its concomitant pathological consequences. Food Chem Toxicol 166. https://doi.org/10.1016/j.fct.2022.113205

Markeb AA, El-Maali NA, Sayed DM, Osama A, Abdel-Malek MA, Zaki AH, Elwanis ME, Driscoll JJ (2016) Synthesis, structural characterization, and preclinical efficacy of a novel paclitaxel-loaded alginate nanoparticle for breast cancer treatment. Int J Breast Cancer 2016. https://doi.org/10.1155/2016/7549372

Mei S, Perumal M, Battino M, Kitts DD, Xiao J, Ma H, Chen X (2023) Mangiferin: a review of dietary sources, absorption, metabolism, bioavailability, and safety. Crit Rev Food Sci Nutr 63(18):3046–3064. https://doi.org/10.1080/10408398.2021.1983767

Mittal P, Vardhan H, Ajmal G, Bonde GV, Kapoor R, Mittal A, Mishra B (2019) Formulation, optimization, hemocompatibility and pharmacokinetic evaluation of PLGA nanoparticles containing paclitaxel. Drug Dev Ind Pharm 45(3):365–378. https://doi.org/10.1080/03639045.2018.1542706

Moodley T, Singh M (2020) Polymeric mesoporous silica nanoparticles for combination drug delivery in vitro. Biointerface Res Appl Chem 11:11905–11919. https://doi.org/10.33263/BRIAC114.1190511919

Mughees M, Wajid S (2021) Herbal based polymeric nanoparticles as a therapeutic remedy for breast cancer. Anti-Cancer Agents Med Chem 21(4):433–444. https://doi.org/10.2174/1871520620666200619171616

Na L, Zhang Q, Jiang S, Du S, Zhang W, Li Y, Sun C, Niu Y (2015) Mangiferin supplementation improves serum lipid profiles in overweight patients with hyperlipidemia: a double-blind randomized controlled trial. Sci Rep 5. https://doi.org/10.1038/srep10344

Naveen P, Lingaraju HB, Prasad KS (2017) Rapid development and validation of improved reversed-phase high-performance liquid chromatography method for the quantification of mangiferin, a polyphenol xanthone glycoside in Mangifera indica. Pharmacognosy Res 9(2):215–219. https://doi.org/10.4103/0974-8490.204652

Németh Z, Csóka I, Semnani Jazani R, Sipos B, Haspel H, Kozma G, Kónya Z, Dobó DG (2022) Quality by design-driven zeta potential optimisation study of liposomes with charge imparting membrane additives. Pharmaceutics 14(9). https://doi.org/10.3390/pharmaceutics14091798

Nguyen TT, Duong VA, Maeng HJ (2021) Pharmaceutical formulations with P-glycoprotein inhibitory effect as promising approaches for enhancing oral drug absorption and bioavailability. Pharmaceutics 13(7). https://doi.org/10.3390/pharmaceutics13071103

Nirgude S, Mahadeva R, Koroth J, Kumar S, Kumar KSS, Gopalakrishnan V, Karki SS, Choudhary B, (2020) ST09, A novel curcumin derivative, blocks cell migration by inhibiting matrix metalloproteases in breast cancer cells and inhibits tumor progression in EAC mouse tumor models. Molecules 25(19):4499. https://doi.org/10.3390/molecules25194499

Núñez Selles AJ, Daglia M, Rastrelli L (2016) The potential role of mangiferin in cancer treatment through its immunomodulatory, anti-angiogenic, apoptopic, and gene regulatory effects. BioFactors 42(5):475–491. https://doi.org/10.1002/biof.1299

Pan LL, Wang AY, Huang YQ, Luo Y, Ling M (2014) Mangiferin induces apoptosis by regulating Bcl-2 and Bax expression in the CNE2 nasopharyngeal carcinoma cell line. Asian Pac J Cancer Prev 15(17):7065–7068. https://doi.org/10.7314/apjcp.2014.15.17.7065

Przystupski D, Niemczura MJ, Górska A, Supplitt S, Kotowski K, Wawryka P, Rozborska P, Woźniak K, Michel O, Kiełbik A, Bartosik W, Saczko J, Kulbacka J (2019) In search of panacea-review of recent studies concerning nature-derived anti-cancer agents. Nutrients 11(6). https://doi.org/10.3390/nu11061426

Rahmani AH, Almatroudi A, Allemailem KS, Alharbi HOA, Alwanian WM, Alhunayhani BA, Algahtani M, Theyab A, Almansour NM, Algefary AN, Aldeghaim SSA, Khan AA (2023) Role of mangiferin in management of cancers through modulation of signal transduction pathways. Biomedicines 11(12). https://doi.org/10.3390/biomedicines11123205

Rezk AI, Hwang TI, Kim JY, Lee JY, Park CH, Kim CS (2019) Functional composite nanofibers loaded with β-TCP and SIM as a control drug delivery system. Materials Lett 240:25–29. https://doi.org/10.1016/j.matlet.2018.12.107

Sadhukhan P, Kundu M, Chatterjee S, Ghosh N, Manna P, Das J, Sil PC (2019) Targeted delivery of quercetin via pH-responsive zinc oxide nanoparticles for breast cancer therapy. Mater Sci Eng C Mater Biol Appl 100:129–140. https://doi.org/10.1016/j.ms50ec.2019.02.096

Sen R, Ganguly S, Ganguly S, Debnath MC, Chakraborty S, Mukherjee B, Chattopadhyay D (2021) Apigenin-loaded PLGA-DMSA nanoparticles: a novel strategy to treat melanoma lung metastasis. Mol Pharmaceutics 18(5):1920–1938. https://doi.org/10.1021/acs.molpharmaceut.0c00977

Shaker SA, Alshufta SM, Gowayed MA, El-Salamouni NS, Bassam SM, Megahed MA, El-Tahan RA (2023) Propolis-loaded nanostructured lipid carriers halt breast cancer progression through miRNA-223 related pathways: an in-vitro/in-vivo experiment. Sci Rep 13(1):15752. https://doi.org/10.1038/s41598-023-42709-7

Shavi GV, Nayak UY, Maliyakkal N, Deshpande PB, Raghavendra R, Kumar AR, Reddya MS, Udupa N, Shrawan B (2015) Nanomedicine of anastrozole for breast cancer: physicochemical evaluation, in vitro cytotoxicity on BT-549 and MCF-7 cell lines and preclinical study on rat model. Life Sci 141:143–155. https://doi.org/10.1016/j.lfs.2015.09.021

Shehatta NH, Okda TM, Omran GA, Abd-Alhaseeb MM (2022) Baicalin; a promising chemopreventive agent, enhances the antitumor effect of 5-FU against breast cancer and inhibits tumor growth and angiogenesis in Ehrlich solid tumor. Biomed Pharmacother 146. https://doi.org/10.1016/j.biopha.2021.112599

Siepmann J, Peppas NA (2001) Modeling of drug release from delivery systems based on hydroxypropyl methylcellulose (HPMC). Adv Drug Deliv Rev 48(2–3):139–157. https://doi.org/10.1016/s0169-409x(01)00112-0

Silva FFVE, Padín-Iruegas ME, Caponio VCA, Lorenzo-Pouso AI, Saavedra-Nieves P, Chamorro-Petronacci CM, Suaréz-Peñaranda J, Pérez-Sayáns M (2022) Caspase 3 and cleaved caspase 3 expression in tumorogenesis and its correlations with prognosis in head and neck cancer: a systematic review and meta-analysis. Int J Mol Sci 23(19). https://doi.org/10.3390/ijms231911937

Susa AC, Xia Z, Williams ER (2017) Native mass spectrometry from common buffers with salts that mimic the extracellular environment. Angew Chem Int Ed Engl 56(27):7912–7915. https://doi.org/10.1002/anie.201702330

Wang X, Yuwen T, Yanqin T (2021) Mangiferin inhibits inflammation and cell proliferation, and activates proapoptotic events via NF-κB inhibition in DMBA-induced mammary carcinogenesis in rats. J Environ Pathol Toxicol Oncol 40(2):1–9. https://doi.org/10.1615/JEnvironPatholToxicolOncol.2021036057

Wu W, Pu Y, Shi J (2022) Nanomedicine-enabled chemotherapy-based synergetic cancer treatments. J Nanobiotechnol 20(1):4. https://doi.org/10.1186/s12951-021-01181-z

Yallur BC, Katrahalli U, Krishna PM, Hadagali MD (2019) BSA binding and antibacterial studies of newly synthesized 5,6-dihydroimidazo[2,1-b]thiazole-2-carbaldehyde. Spectrochim Acta A Mol Biomol Spectrosc 222. https://doi.org/10.1016/j.saa.2019.117192

Zhou Q, Hou K, Fu Z (2022) Transferrin-modified mangiferin-loaded SLNs: preparation, characterization, and application in A549 lung cancer cell. Drug Des Devel Ther 16:1767–1778. https://doi.org/10.2147/DDDT.S366531

Zi Y, Yang K, He J, Wu Z, Liu J, Zhang W (2022) Strategies to enhance drug delivery to solid tumors by harnessing the EPR effects and alternative targeting mechanisms. Adv Drug Deliv Rev 188. https://doi.org/10.1016/j.addr.2022.114449

INVERTIS
UNIVERSITY BAREILLY

8th INTERNATIONAL CONFERENCE

Theme : RECENT ADVANCES IN SCIENCE

In collaboration with :

International Association of Advanced Materials, Sweden and Indian Chemical Society, Kolkata India

CERTIFICATE OF PRESENTATION

It is certified that

Dr./Mr./Ms. Pratik Chakraborty from Jadavpur University, has presented a paper in ***Oral/Poster*** Session in the 8th International Conference on Recent Advances in Science ***(ICRAS-2024)*** held on March 14-15, 2024 at Invertis University, Bareilly (UP), India.

His/Her topic of presentation was "Formulation of Polymeric Nanoparticles with Nature-Derived small molecule Improves Therapeutic Efficiency Against Breast Cancer"

Prof. P. P. Singh
Dean, Faculty of Science

Dr. Kuldeep Chauhan
Convenor

Dr. Suchita Gupta
Co-Convenor

Organized by

FACULTY OF SCIENCE INVERTIS UNIVERSITY BAREILLY

Association of Pharmaceutical Scientists & Educators (APSE)

2nd International Conference on Healthy Aging & Research

(2nd ICHAR-2022)

Certificate

This is certify that **Mr. PRATIK CHAKRABORTY** from Jadavpur University has presented a paper entitled ***Polymeric Nanoformulation Loaded with Natural Polyphenol Shows Promise against Hepatocellular Carcinoma (Poster)*** in this TWO days conference

Organized by Association of Pharmaceutical Scientists & Educators (APSE), **Mysuru, India.**

On **21st** and **22nd March 2022.**

Dr. Arunachalam Muthuraman
Organizing secretary,
APSE Vice President

Prof. Milind Parle
President, APSE

Dr. Hanumanthachar Joshi
Secretary, APSE

ICTRHR-2022

2nd International Conference on

"Transforming Ripples in Healthcare Research: Obstacles, Sustenance & Cutting-edge Innovations"

Organized by School of Medical Sciences, Adamas University, Kolkata, India

Sponsored by Science and Engineering Research Board, Department of Science and Technology, Government of India

In collaboration with Central Ayurveda Research Institute (CARI), CCRAS, Ministry of Ayush, Govt. of India

Media Partner Pharmatutor

CERTIFICATE OF PRESENTATION

This is to certify that

Prof / Dr / Mr / Ms Pratik Chakraborty

from Jadavpur University

has presented a paper in oral/poster session on the topic

Formulation and characterization of nano-carrier based delivery system with mangiferin, an attempt to glorify its therapeutic usefulness

"Transforming Ripples in Healthcare Research: Obstacles, Sustenance & Cutting-edge Innovations" (ICTRHR-2022), organized by School of Medical Sciences, Adamas University, Kolkata, India on 10th – 11th February, 2022

Dr. Sajal Kumar Jha
(Associate Dean, SOMS)
Chairman, ICTRHR

Dr. Partha Roy
(Associate Professor, SOMS)
Convener, ICTRHR

Dr. Tanmoy Guria
(Associate Professor, SOMS)
Co-Convener, ICTRHR

Pratik Chakraborty
22.05.25